SIAM REVIEW
Vol. 59, No. 2, pp. 225–292

The Period Adding and Incrementing Bifurcations: From Rotation Theory to Applications*

Albert Granados†
Lluís Alsedà‡
Maciej Krupa§

Abstract. This survey article is concerned with the study of bifurcations of discontinuous piecewise-smooth maps, with a special focus on the one-dimensional case. We review the literature on circle maps and quasi-contractions and provide paths through this literature to prove sufficient conditions for the occurrence of two types of bifurcation scenarios involving rich dynamics. The first scenario consists of the appearance of periodic orbits whose symbolic sequences and "rotation" numbers follow a Farey tree structure; the periods of the periodic orbits are given by consecutive addition. This is called the *period adding* bifurcation, and the proof of its existence relies on results for maps on the circle. In the second scenario, symbolic sequences are obtained by consecutive attachment of a given symbolic block, and the periods of periodic orbits are incremented by a constant term. This is called the *period incrementing* bifurcation, and its proof relies on results for maps on the interval. We also discuss the expanding cases, as some of the partial results found in the literature also hold when these maps lose contractiveness. The higher-dimensional case is also discussed by means of *quasi-contractions*. We provide applied examples in control theory, power electronics, and neuroscience, where these results can be used to obtain precise descriptions of their dynamics.

Key words. piecewise-smooth maps, discontinuous circle maps, period adding, devil's staircase, Farey tree, period incrementing

AMS subject classifications. 37E05, 37E10, 37G15, 37N25, 37N35

DOI. 10.1137/140996598

Contents

*Received by the editors November 24, 2014; accepted for publication (in revised form) July 15, 2016; published electronically May 5, 2017.
http://www.siam.org/journals/sirev/59-2/99659.html
Funding: The work of the first author was partially supported by MINECO-FEDER MTM2012-31714 and MINECO MTM2015-65715-P Spanish grants. The work of the second author was partially supported by MINECO MTM2011-26995-C02-01 and MINECO MTM2014-52209-C2-1-P Spanish grants.

†Department of Applied Mathematics and Computer Science, Technical University of Denmark, Building 303B, 2800 Kgns. Lyngby, Denmark (algr@dtu.dk).
‡Department of Mathematics, Edifici Cc, Universitat Autònoma de Barcelona, 08193 Cerdanyola del Vallès, Spain.
§NeuroMathComp Project-Team, Inria Sophia-Antipolis Research Center, 2004 route des Lucioles, BP93, 06902 Sophia Antipolis cedex, France.

1. Introduction. Piecewise-smooth (piecewise-defined or nonsmooth) systems are nonregular or discontinuous systems induced by dynamics associated with sharp changes in position, velocity, or other magnitudes undergoing a jump in value. This type of system provides more natural and simple models in many applications, such as switching systems in power electronics [31, 135, 53, 16], sliding-mode techniques in control theory [132, 43, 52, 47], hybrid systems with resets in neuroscience [35, 83, 103, 74], or impact systems in mechanics [79, 71, 72]. Using nonsmooth modeling can reduce the dimension of the system, but may result in more complicated dynamics.

As a consequence of its broad field of application, the interest in such systems has grown considerably in the last decade (see [101] for a recent general survey). In particular, piecewise-smooth maps have captured the attention of many researchers, who have studied them from very different perspectives. One of the most reported dynamical aspects is the different bifurcation scenarios that they may exhibit, which turn out to be extraordinarily rich. Seduced by their graphical beauty and mainly supported by computations, many authors have recurrently observed and reported these bifurcation phenomena. However, although they resemble many well-known results on circle maps, they have been considered to be new and exclusive to piecewise-smooth maps.

In this review article we show that many of the well-known results for circle maps developed in the 1980s and early 1990s can be used to obtain rigorous proofs of general results that can be applied systematically to one-dimensional piecewise-smooth contracting maps. Moreover, we also show how many of these results scattered in the literature are valid not only for piecewise-smooth expanding maps, but also for higher-dimensional ones.

In the general setting for the one-dimensional case we consider a piecewise-smooth map undergoing a discontinuity at $x = 0$, and consider as parameters the two lateral images at this point. To our knowledge, such a map was first studied by Leonov [95], and was later obtained as an approximation of a Poincaré map of smooth flow near a homoclinic bifurcation of the figure eight and butterfly types [122, 80] (see sections 2.2 and 7.1.1 for more references).

Depending on the signs and magnitude of the slopes of the map on each side of the discontinuity, the bifurcation scenario in this two-dimensional parameter space may be very different. These signs are determined by the number of twists exhibited by the invariant manifolds (their orientability) involved in the homoclinic bifurcation [66, 80]. When the map is contracting on both sides of the discontinuity and both slopes have different sign, the so-called *period incrementing* scenario occurs. This bifurcation was reported in [80], and the details of the proof corresponding to this case were given in [18]. However, if both slopes are positive, then the so-called *period adding* scenario occurs.

Although this latter scenario has been widely reported (see section 2.2), corresponding proof is scattered throughout the literature in the form of partial results using different approaches. In the late 1980s, Gambaudo et al. [61, 60, 63] provided strong rigorous results in this direction by means of the *maximin* approach (see section 6). They provide very precise information on the symbolic sequences. Moreover, they were stated for maps in metric spaces of arbitrary dimension, which permits us to adapt them to provide results for piecewise-smooth maps in $\mathbb{R}^n$. However, they do not allow one to distinguish straightforwardly between the two bifurcation scenarios mentioned above.

In order to prove the bifurcation scenario for the increasing-increasing case, we propose to reduce the piecewise-smooth map to a discontinuous circle map. We then assemble and adapt many well-known results from rotation theory to the discontinuous case which provides the straightest path to proving the period adding bifurcation scenario. The main advantage over the maximin approach is the fact that this method does not require the map to be contracting, but relies only on its invertibility, and hence requires weaker assumptions. However, the maximin approach, although it requires a lot of contractiveness, obtains results that are valid in higher dimensions.

Other approaches suggest proceeding with renormalization arguments [62, 113, 68, 134, 80, 81] to prove the occurrence of the period adding bifurcation scenario.

Beyond their relation to homoclinic bifurcations for flows, such types of bifurcation scenarios have been observed in more applied contexts modeled by both one- and n-dimensional piecewise-smooth maps. Examples of such applications where these bifurcation scenarios appear are power electronics [45, 29, 114, 67, 138, 7, 85, 136], control theory [46, 58, 51, 135, 137, 50, 51], economics [128], and neuroscience [57, 74, 84, 89, 103, 121, 124, 117, 126, 127, 125].

Typically, these bifurcation scenarios are observed numerically in two-dimensional parameter space near codimension-two bifurcation points. Such points involve the emergence of an infinite number of bifurcation curves and were called *big bang* bifurcations by the nonsmooth community [22].

In this survey we also provide an illustration of how rotation theory can be applied to provide a rigorous basis to analyzing bifurcations of piecewise-smooth maps in four different applied contexts: nonsmooth dynamics, control theory, mathematical neuroscience, and power electronics. We first study (section 7.1.1) bifurcation scenarios around codimension-two bifurcation points given by the collision of two periodic orbits with the boundary (big bang bifurcations). In the second example (section 7.1.2) we consider a nonlinear system subject to sliding-mode control in order to stabilize it around a desired "equilibrium" point. In the third example (section 7.1.3), we consider a periodically forced integrate-and-fire model, a hybrid system widely used in neuroscience. For these two last examples we show how the period adding bifurcation scenario explains the dynamics of the systems and how the symbolic dynamics help to obtain relevant properties from the applied point of view. We finally provide two more examples leading to period–adding-like bifurcations for planar piecewise-smooth maps: a higher order system subject to sliding-mode control with relays (section 7.2.1) and a DC-DC boost converter controlled with the so-called ZAD strategy (section 7.2.2).

This work is organized as follows. In section 2 we provide basic definitions and a detailed statement of the results for the one-dimensional case. In section 3 we review and extend results for circle maps to provide a proof of the period adding bifurcation scenario (increasing-increasing or orientation preserving case). A detailed summary of the proof is given in section 3.2. In section 4 we revisit the proof provided in [18] for the period incrementing bifurcation scenario (increasing-decreasing or nonorientable case). In section 5 we emphasize the extent to which the results of section 3 are also valid in the presence of expansiveness. In section 6 we review the maximin approach and show how it can be applied to obtain results for piecewise-smooth maps in $\mathbb{R}^n$. Section 7 is dedicated to illustrating how these results can be used in different applied fields using five examples. Finally, we conclude in section 8 with some discussion and proposals for future directions.

2. Basic Definitions and Overview of Results.

2.1. System Definition and Properties. Let us consider a piecewise-smooth map

$$f(x) = \begin{cases} \mu_{\mathcal{L}} + f_{\mathcal{L}}(x) & \text{if } x < 0, \\ -\mu_{\mathcal{R}} + f_{\mathcal{R}}(x) & \text{if } x > 0, \end{cases} \tag{2.1}$$

with $x \in \mathbb{R}$ and $f_{\mathcal{L}}, f_{\mathcal{R}}$ smooth functions satisfying

h.1. $f_{\mathcal{L}}(0) = f_{\mathcal{R}}(0) = 0$,
h.2. $0 < (f_{\mathcal{L}}(x))' < 1$, $x \in (-\infty, 0)$,
h.3. $0 < |(f_{\mathcal{R}}(x))'| < 1$, $x \in (0, \infty)$.

We wish to describe the possible bifurcation structures obtained when parameters $\mu_{\mathcal{L}}$ and $\mu_{\mathcal{R}}$ are varied.

REMARK 1. *The global contractiveness of the maps $f_{\mathcal{L}}$ and $f_{\mathcal{R}}$ is assumed for simplicity. This allows us to state results on bifurcations for arbitrarily large values of $\mu_{\mathcal{L}}$ and $\mu_{\mathcal{R}}$. However, if contractiveness holds only locally at the origin, then all the results presented here are still valid for values of these parameters close enough to the origin. Their validity when contractiveness is lost is discussed in section* 5.

REMARK 2. *For convenience, we do not define at this point the map f at $x = 0$. Roughly speaking, the only difference made by the selection of the value of f at $x = 0$ concerns the existence or not of fixed points and periodic orbits at their bifurcation values. We remark that one cannot consider the value of f at $x = 0$ only by choosing one lateral image, but also can consider either both images or neither of them. We will focus on this question whenever it becomes relevant.*

Due to condition h.1, the map (2.1) is discontinuous at $x = 0$ if $\mu_{\mathcal{L}} \neq \mu_{\mathcal{R}}$. As we will show, this discontinuity introduces exclusive dynamical phenomena which are not possible in smooth (C^1) one-dimensional systems. As discussed in the introduction, one observes similar phenomena (the bifurcation scenarios described below) in smooth flows of dimension three near homoclinic bifurcations. They are also observed in smooth maps, when restricted to the circle instead of $\mathbb{R}$.

This discontinuity represents a boundary in the state space abruptly separating two different dynamics: those given by the maps $f_{\mathcal{L}}$ and $f_{\mathcal{R}}$. These dynamics will depend strongly on the sign of $f'_{\mathcal{R}}(x)$ on $(0, \infty)$, leading to completely different families of periodic orbits. Note that the cases when $f_{\mathcal{L}}(x)$ and $f_{\mathcal{R}}(x)$ have different slopes in their respective domains are conjugate through the symmetry $x \longleftrightarrow -x$. Moreover, as will be shown below, when both $f_{\mathcal{L}}(x)$ and $f_{\mathcal{R}}(x)$ are decreasing functions in their respective domains, the possible dynamics will be easy. Therefore, we can restrict our attention to the case that $f_{\mathcal{L}}(x)$ is an increasing function in $(-\infty, 0)$, as stated in *h*.2.

One of the differences between the families of periodic orbits that one can find depending on the sign of $f'_{\mathcal{R}}(x)$ in $(0, \infty)$ can be given by the sequence of steps that periodic orbits perform at each side of the boundary $x = 0$. Therefore, we introduce the symbolic dynamics given by the following symbolic encoding: Given a point $x \in \mathbb{R}$, we associate to its trajectory by f, $(x, f(x), f^2(x), \dots)$, a symbolic sequence given by

$$I_f(x) = \left(a(x), a\left(f(x)\right), a\left(f^2(x)\right), \dots\right), \tag{2.2}$$

where

$$a(x) = \begin{cases} \mathcal{R} & \text{if } x > 0, \\ \mathcal{L} & \text{if } x < 0. \end{cases} \tag{2.3}$$

Since $a(x)$ provides a symbol of length one ($\mathcal{L}$ or $\mathcal{R}$), one can omit the commas separating the symbols in (2.2) without introducing any imprecision.

We call this sequence the *itinerary* of x by f or the *symbolic sequence* associated with the trajectory of x by f.

Let us now consider the shift operator acting on symbolic sequences,

$$\sigma\left(\mathbf{x}_1\mathbf{x}_2\mathbf{x}_3\cdots\right) = \left(\mathbf{x}_2\mathbf{x}_3\cdots\right), \tag{2.4}$$

where $\mathbf{x}_i \in \{\mathcal{L}, \mathcal{R}\}$.

Clearly, the shift operator satisfies

$$\sigma\left(I_f(x)\right) = I_f\left(f\left(x\right)\right). \tag{2.5}$$

Of special interest will be the symbolic sequences associated with periodic orbits. In this case, the symbolic sequences will be also periodic and we will represent them by the repetition of the generating symbolic block. For example, let (x_1, x_2) be a periodic orbit such that

$$f(x_1) = x_2,$$
$$f(x_2) = x_1,$$

and assume $x_1 < 0$ and $x_2 > 0$. Then the symbolic sequences associated with x_1 and x_2 are

$$I_f(x_1) = (\mathcal{LRLR}\cdots) := (\mathcal{LR})^\infty,$$
$$I_f(x_2) = (\mathcal{RLRL}\cdots) := (\mathcal{RL})^\infty,$$

where ∞ indicates infinite repetition.

Due to property (2.5), the shift operator acts on the generating blocks as a cyclic permutation of offset 1, as it moves the first symbol to the last position. More precisely, if $(x_1, \ldots, x_n)$, $x_i \in \mathbb{R}$, is a periodic orbit of f and $(\mathbf{x}_1 \cdots \mathbf{x}_n)^\infty$, $\mathbf{x}_i \in \{\mathcal{L}, \mathcal{R}\}$, is the symbolic sequence associated with the periodic trajectory of x_1, then

$$\sigma(I_f(x_1)) = \left(\mathbf{x}_2\mathbf{x}_3 \cdots \mathbf{x}_n\mathbf{x}_1\right)^\infty.$$

Hence, a periodic orbit of length n can be represented by n different symbolic sequences obtained by cyclic permutations, one from each other.

DEFINITION 3. *Symbolic sequences can be ordered by lexicographical order induced by $\mathcal{L} < \mathcal{R}$. That is,*

$$(\mathbf{x}_1\mathbf{x}_2\cdots) < (\mathbf{y}_1\mathbf{y}_2\cdots)$$

if and only if $\mathbf{x}_1 = \mathcal{L}$ and $\mathbf{y}_1 = \mathcal{R}$ or $\mathbf{x}_1 = \mathbf{y}_1$ and there exists some $j > 1$ such that

$$\mathbf{x}_i = \mathbf{y}_i \text{ for all } i < j,$$
$$\mathbf{x}_j = \mathcal{L},$$
$$\mathbf{y}_j = \mathcal{R}.$$

EXAMPLE 4. *The sequences $(\mathbf{x}_1, \mathbf{x}_2, \mathbf{x}_3, \mathbf{x}_4)^\infty = (\mathcal{L}^2, \mathcal{R}, \mathcal{L})^\infty$ and $(\mathbf{y}_1, \mathbf{y}_2, \mathbf{y}_3, \mathbf{y}_4)^\infty = (\mathcal{L}^2, \mathcal{R}^2)^\infty$ satisfy*

$$(\mathcal{L}^2, \mathcal{R}, \mathcal{L})^\infty < (\mathcal{L}^2, \mathcal{R}^2)^\infty,$$

as $x_4 = \mathcal{L}$ and $\mathbf{y}_4 = \mathcal{R}$ and $\mathbf{x}_i = \mathbf{y}_i$ for $1 \le i \le 3$.

DEFINITION 5. *Given a periodic symbolic sequence $\mathbf{x} = (\mathbf{x}_1 \cdots \mathbf{x}_q)^\infty$, we say that it is minimal if*

$$\mathbf{x} = \min_{0 \le k < q} \sigma^k(\mathbf{x}),$$

and similarly for a maximal symbolic sequence.

Note that the min and max operators act on sequences following the order given in Definition 3, and hence its output is also a sequence.

EXAMPLE 6. *The sequence* $(\mathcal{L}^2,\mathcal{R})^\infty$ *is minimal, whereas* $(\mathcal{R},\mathcal{L}^2)^\infty$ *is maximal, as we find*

$$(\mathcal{L}^2,\mathcal{R})^\infty = \min\left\{(\mathcal{L}^2,\mathcal{R})^\infty,(\mathcal{L},\mathcal{R},\mathcal{L})^\infty,(\mathcal{R},\mathcal{L}^2)^\infty\right\},$$
$$(\mathcal{R},\mathcal{L}^2)^\infty = \max\left\{(\mathcal{L}^2,\mathcal{R})^\infty,(\mathcal{L},\mathcal{R},\mathcal{L})^\infty,(\mathcal{R},\mathcal{L}^2)^\infty\right\}.$$

DEFINITION 7. *We say that a periodic orbit of length* n *is an* $(\mathbf{x}_1\cdots\mathbf{x}_n)$*-periodic orbit,* $\mathbf{x}_i\in\{\mathcal{L},\mathcal{R}\}$*, if there exists some point of this periodic orbit,* $x_i\in\mathbb{R}$*, such that*

$$I_f(x_i) = (\mathbf{x}_1\cdots\mathbf{x}_n)^\infty.$$

EXAMPLE 8. *The periodic orbit* $(-1,-0.5,1,-2)$*, satisfying*

$$f(-1)=-0.5,\quad f(-0.5)=1,\quad f(1)=-2,\quad f(-2)=-1,$$

is an $\mathcal{L}^2\mathcal{R}\mathcal{L}$*-,* $\mathcal{L}\mathcal{R}\mathcal{L}^2$*-,* $\mathcal{R}\mathcal{L}^3$*-, and* $\mathcal{L}^3\mathcal{R}$*-periodic orbit, since*

$$I_f(-1) = (\mathcal{L}^2\mathcal{R}\mathcal{L})^\infty,$$
$$I_f(-0.5) = (\mathcal{L}\mathcal{R}\mathcal{L}^2)^\infty,$$
$$I_f(1) = (\mathcal{R}\mathcal{L}^3)^\infty,$$
$$I_f(-2) = (\mathcal{L}^3\mathcal{R})^\infty.$$

Usually, in order to represent the symbolic sequence of a periodic orbit we choose its minimal representative. For example, assume $(x_1,\ldots,x_5)$ is a 5-periodic orbit such that $I_f(x_1)=(\mathcal{L}\mathcal{R}\mathcal{L}\mathcal{L}\mathcal{R})^\infty$. Then we say that $(x_1,\ldots,x_5)$ is an $\mathcal{L}^2\mathcal{R}\mathcal{L}\mathcal{R}$-periodic orbit or a periodic orbit of type $\mathcal{L}^2\mathcal{R}\mathcal{L}\mathcal{R}$, where the superindex 2 means that there are two consecutive symbols $\mathcal{L}$.

Given a periodic orbit, besides its period, one important characteristic associated with its symbolic sequence is the number of symbols $\mathcal{R}$ and $\mathcal{L}$ and how they are distributed along the sequence. The latter will be explained in detail below. For the former we need the following definition.

DEFINITION 9. *We call* $W_{p,q}$ *the set of periodic symbolic sequences generated by a symbolic block of length* q *containing* p *symbols* $\mathcal{R}$*:*

$$W_{p,q} = \left\{\mathbf{y}\in\{\mathcal{L},\mathcal{R}\}^{\mathbb{N}} \mid \mathbf{y}=\mathbf{x}^\infty,\ \mathbf{x}\in\{\mathcal{L},\mathcal{R}\}^q,\ \textit{and } \mathbf{x} \textit{ contains } p \textit{ symbols } \mathcal{R}\right\}.$$

EXAMPLE 10. *The sets* $W_{2,7}$ *and* $W_{3,7}$ *become*

$$W_{2,7} = \left\{(\mathcal{L}^5,\mathcal{R}^2)^\infty,(\mathcal{L}^4,\mathcal{R},\mathcal{L})^\infty\right\}$$

and

$$W_{3,7} = \left\{(\mathcal{L}^4,\mathcal{R}^3)^\infty,(\mathcal{L}^3,\mathcal{R}^2,\mathcal{L},\mathcal{R})^\infty,(\mathcal{L}^2,\mathcal{R},\mathcal{L},\mathcal{R},\mathcal{L},\mathcal{R})^\infty\right\}.$$

Now let W be the set of all periodic symbolic sequences,

$$W = \bigcup_{(p,q)=1} W_{p,q},$$

where $(\cdot,\cdot)$ refers to the greatest common divisor.

We next define the η-number associated with a periodic symbolic sequence.

DEFINITION 11. *Let* $\mathbf{x} = (\mathbf{x}_1 \cdots \mathbf{x}_q) \in \{\mathcal{L}, \mathcal{R}\}^q$ *be a symbolic sequence, and let* p *be the number of symbols* $\mathcal{R}$ *contained in* $\mathbf{x}$. *We then define the* η*-number of* $\mathbf{x}$ *as*

$$\eta : \begin{array}{ccc} W & \longrightarrow & \mathbb{Q}, \\ \mathbf{x}^\infty & \longmapsto & \frac{p}{q} \end{array} \tag{2.6}$$

if $\mathbf{x} \in W_{p,q}$, $(p, q) = 1$.

EXAMPLE 12. *The* η*-numbers of the sequences* $(\mathcal{R}^3, \mathcal{L})^\infty$ *and* $(\mathcal{L}^2, \mathcal{R}, \mathcal{L}, \mathcal{R})^\infty$ *become*

$$\eta\left((\mathcal{R}^3, \mathcal{L})^\infty\right) = \frac{3}{4}$$

and

$$\eta\left((\mathcal{L}^2, \mathcal{R}, \mathcal{L}, \mathcal{R})^\infty\right) = \frac{2}{5}.$$

As is detailed below (see section 3.1, Remark 18), under certain conditions, the piecewise-smooth map (2.1) becomes a circle map with *rotation number* the η-number. Hence, the η-number as defined above is frequently referred to as rotation number in the context of piecewise-smooth maps, even when those conditions are not satisfied (see, for example, [63, 60]).

We now focus on the question, for a map f of type (2.1) satisfying h.1–h.3, of what are the possible periodic orbits, their symbolic sequences, and their bifurcations in the parameter space given by the offsets, $\mu_\mathcal{L} \times \mu_\mathcal{R}$. To this end, we first note that if $\mu_\mathcal{L}, \mu_\mathcal{R} < 0$, as the maps $f_\mathcal{L}$ and $f_\mathcal{R}$ are contracting, then f possesses two attracting coexisting $\mathcal{L}$ and $\mathcal{R}$ fixed points $x_\mathcal{L} < 0$ and $x_\mathcal{R} > 0$:

$$f_\mathcal{L}(x_\mathcal{L}) = x_\mathcal{L},$$
$$f_\mathcal{R}(x_\mathcal{R}) = x_\mathcal{R}.$$

The domains of attraction are separated by the boundary $x = 0$. Indeed, if both $f_\mathcal{L}$ and $f_\mathcal{R}$ are increasing maps, then these domains become $(-\infty, 0)$ and $(0, \infty)$, respectively. Note that, although $x = 0$ is not an invariant point (an equilibrium), it acts as a separatrix between these domains of attraction.

If one of these two parameters vanishes and becomes positive (for example, $\mu_\mathcal{L}$), the fixed point $x_\mathcal{L}$ collides with the boundary $x = 0$ and undergoes a border collision bifurcation. Depending on how the map f given in (2.1) is defined at $x = 0$, at the moment of the bifurcation this fixed point may or may not still exist. Just after this bifurcation, $x_\mathcal{L}$ no longer exists, and the fixed point $x_\mathcal{R}$ becomes the unique global attractor. As will be discussed below, this fixed point may coexist with a two-periodic orbit. A similar situation occurs when the parameter $\mu_\mathcal{R}$ crosses 0, replacing $x_\mathcal{L}$ by $x_\mathcal{R}$ in the previous argument. Hence, the origin of this parameter space consists of a codimension-two bifurcation point. But then the question arises: what exists when both parameters are positive and both fixed points disappear in border collision bifurcations? The answer to this question (summarized in sections 2.2 and 2.3) depends on the signs of the slopes of the maps $f_\mathcal{L}$ and $f_\mathcal{R}$ for $x < 0$ and $x > 0$, respectively. Recalling that the increasing-decreasing and decreasing-increasing cases are conjugate, we will only distinguish between two cases: increasing-increasing and increasing-decreasing. These are also typically referred to as orientation preserving and nonorientable cases.

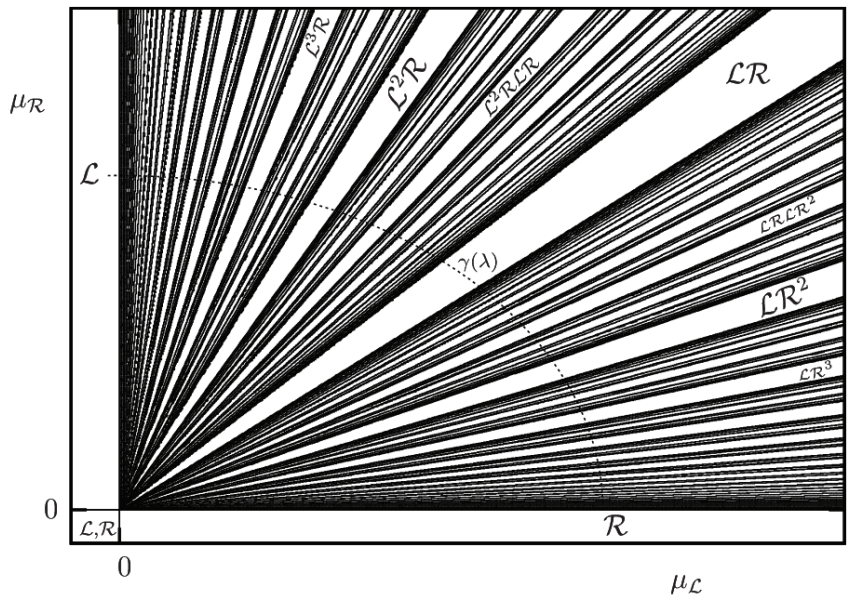

Fig. 2.1 *Bifurcation curves on the two-dimensional parameter space $\mu_{\mathcal{L}} \times \mu_{\mathcal{R}}$ for a linear increasing-increasing piecewise-smooth map. The periods of the periodic orbits found along the curve $\gamma(\lambda)$ are shown in Figure* 2.2(a).

As will be argued in section 2.4, the decreasing-decreasing case is straightforward under the assumption of contractiveness.

2.2. Overview of the Orientation Preserving Case: Period Adding. The bifurcation scenario when both $f_{\mathcal{L}}$ and $f_{\mathcal{R}}$ are increasing is shown in Figures 2.1 and 2.2. As shown in Figure 2.1, there exist an infinite number of bifurcation curves emerging from the origin of the parameter space $\mu_{\mathcal{L}} \times \mu_{\mathcal{R}}$. Note that these curves are straight lines due to the fact that the map chosen for the simulations was linear. As will be shown in Theorem 13, this is not a particularity of the chosen system, and similar nonlinear curves can be obtained otherwise. Moreover, due to this linearity, these curves extend to infinity due to the fact that the maps chosen are globally contracting. If contractiveness was lost, other bifurcations would appear.

The bifurcation curves shown in Figure 2.1 separate regions of existence of periodic orbits. The periods of these periodic orbits are given by "successive addition" of those of "neighboring regions."[1] We will make this more precise in section 3, but it can be seen in Figure 2.2(a), where we show the periods of the periodic orbits found along the curve shown in Figure 2.1 parametrized counterclockwise by a parameter λ which will be clarified in section 2.4. It can also be seen there that the symbolic sequences (some of them labeled) of obtained periodic orbits are given by successive concatenation of the "neighboring" ones.

Of relevant interest is the evolution of the η-number (see Definition 11) along the aforementioned curve in Figure 2.1. This is shown in Figure 2.2(b), and follows a *devil's staircase* (a continuous and monotonically increasing function which is constant locally almost everywhere).

[1]The term "neighbor" refers to the concept of Farey neighbors; see section 3.1.

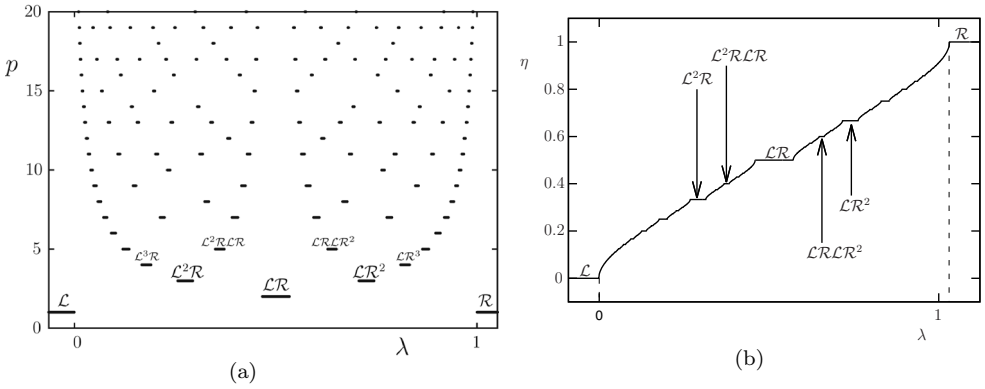

Fig. 2.2 *Bifurcation scenario along the curve, $\gamma(\lambda)$, shown in Figure* 2.1 *and defined in* (2.7). (a) *Periods of the existent periodic orbits.* (b) *η-number: ratio between number of $\mathcal{R}$'s and the period.*

As explained in section 1, to our knowledge, this bifurcation scenario was first described by Leonov in the late 1950s [95, 96, 97, 98] when studying a piecewise-linear map similar to (2.1) by means of direct computations. Later on, this phenomenon was studied in more detail from different perspectives. It was observed when studying homoclinic bifurcations for flows [122, 40, 62, 130, 113, 60, 63, 100, 66, 80] (see section 7.1.1 for more details), but also in electronic circuits given by the Van der Pol oscillator [90, 99] or circle maps [88, 104]. Later on, it was rediscovered by the nonsmooth community and called *period adding* in [22]. This is precisely defined in Definition 19. However, this terminology is also used in some areas when referring to other types of bifurcation scenarios, and especially frequently to what we call here *period incrementing* bifurcation (see section 2.3). This is, for example, the case for the area of *grazing* bifurcations (see [110]).

2.3. Overview of the Nonorientable Case: Period Incrementing. For the increasing-decreasing case, one finds the bifurcation scenario shown in Figures 2.3 and 2.4. In Figure 2.3, as in the previous case, one can see that there exist an infinite number of bifurcation curves emerging from the origin of the parameter space $\mu_{\mathcal{L}} \times \mu_{\mathcal{R}}$. Also as before the map chosen for the simulations was linear and globally contracting, so the observed bifurcation curves are straight lines extending to infinity. For a nonlinear case these lines would become nonlinear curves and, if contractiveness was lost for larger values of the parameters, new bifurcations would be observed.

Unlike in the orientable case, only families of periodic orbits of the form $\mathcal{L}^n\mathcal{R}$ exist for the nonorientable case. Moreover, there exist regions in the parameter space (marked in gray in Figures 2.3 and 2.4) where periodic orbits with symbolic sequences $\mathcal{L}^n\mathcal{R}$ and $\mathcal{L}^{n+1}\mathcal{R}$ coexist.

As mentioned in section 1, this bifurcation scenario was first described by Leonov [95, 96, 97, 98]. Later on, it was studied for its relevance in homoclinic bifurcations involving nonorientable homoclinic manifolds [80, 66]. It was rediscovered in [22] when studying a linear piecewise-smooth map and named *period incrementing*. Full details proving that the increasing-decreasing case leads to the occurrence of the period-incrementing bifurcation scenario were given in [18].

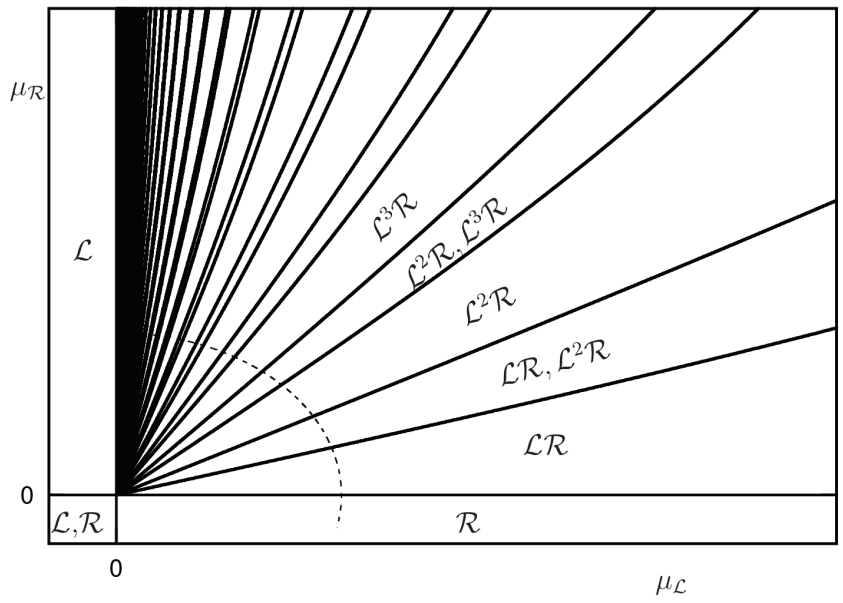

Fig. 2.3 *Bifurcation curves on the two-dimensional parameter space $\mu_{\mathcal{L}} \times \mu_{\mathcal{R}}$ for a linear increasing-decreasing piecewise-smooth map. Regions of coexistence are filled in gray. The periods of the periodic orbits found along the curve $\gamma(\lambda)$ are shown in Figure* 2.4(a).

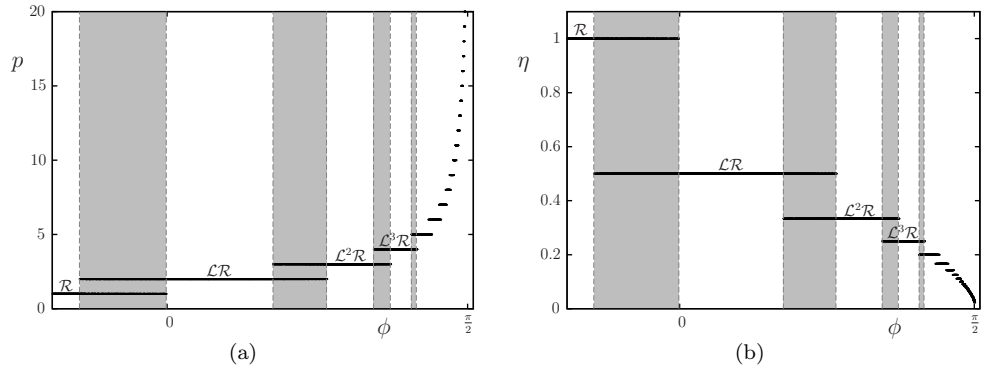

Fig. 2.4 *Bifurcation scenario along the curve, $\gamma(\lambda)$, shown in Figure* 2.3. (a) *Periods of the existent periodic orbits. Regions where periodic orbits coexist are filled in gray.* (b) *η-number: ratio between number of $\mathcal{R}$'s and the period.*

2.4. Summarizing Theorem. The results presented in the previous sections are summarized in the following theorem.

THEOREM 13. *Let f be a map as in* (2.1) *satisfying conditions* h.1–h.3. *Let γ be a C^1 curve in the parameter space $\mu_{\mathcal{L}} \times \mu_{\mathcal{R}}$ (see Figures* 2.1 *and* 2.3*),*

$$\gamma : \begin{array}{ccc} [0,1] & \longrightarrow & \mathbb{R}^2, \\ \lambda & \longmapsto & (\mu_{\mathcal{L}}(\lambda), \mu_{\mathcal{R}}(\lambda)), \end{array} \tag{2.7}$$

satisfying

H.1. $\mu_{\mathcal{L}}(\lambda) > 0$ *and* $\mu_{\mathcal{R}}(\lambda) > 0$ *for* $\lambda \in (0,1)$,

H.2. $(\mu_{\mathcal{L}}(\lambda))' > 0$ *and* $(\mu_{\mathcal{R}}(\lambda))' < 0$ *for* $\lambda \in [0,1]$,

H.3. $\mu_{\mathcal{L}}(0) = 0$, $\mu_{\mathcal{R}}(1) = 0$.

Then the bifurcation diagram exhibited by the map f_λ *obtained from* (2.1) *after performing the reparametrization given by* γ *follows*

(i) *a period adding structure if* $0 < f'_{\mathcal{R}}(x) < 1$, $x \in (0,\infty)$;

(ii) *a period incrementing structure if* $-1 < f'_{\mathcal{R}}(x) < 0$, $x \in (0,\infty)$, *for* $\lambda \in [0,1]$.

For a description of the bifurcation scenarios given in (i) and (ii) above, the period adding and period incrementing cases, see, respectively, sections 2.2 and 2.3 for an overview, and sections 3 and 4 for more details and proofs.

We now explain briefly the case when condition h.2 is not satisfied ($f_{\mathcal{L}}$ is decreasing).

REMARK 14. *If condition* h.2 *is not satisfied and* $f'_{\mathcal{L}}(x) < 0$ *in* $(-\infty, 0)$, *then*

(iii) *if* $f'_{\mathcal{R}}(x) < 0$ *for* $(0,\infty)$, *only an* $\mathcal{LR}$*-periodic orbit can exist for all* $\lambda \in (0,1)$;

(iv) *if* $f'_{\mathcal{R}}(x) > 0$, *for* $x \in (-\infty, 0)$ *the bifurcation scenario is equivalent to* (ii) *after interchanging* $\mathcal{L}$ *and* $\mathcal{R}$ *in the symbolic dynamics.*

Clearly, (iii) comes from the fact that, under these conditions, $f_{\mathcal{L}}((-\infty,0)) \subset (\mu_{\mathcal{L}}, \infty)$ and $f_{\mathcal{R}}((0,\infty)) \subset (-\infty, -\mu_{\mathcal{R}})$, and hence, due to the contractiveness of these maps, f must possess an $\mathcal{LR}$-periodic orbit.

The fact that the cases (iv) and (ii) are conjugate comes from applying the symmetries given by the change of variables $x \longleftrightarrow -x$.

3. Orientation Preserving Case.

3.1. Detailed Description. We first provide a detailed description of the period adding bifurcation structure by stating some results which will be proved in the rest of this section.

The bifurcation structure given by so-called *period adding* is strongly linked with the ordering of the rational numbers given by the Farey tree. In order to explain how this tree is generated, we first define the Farey neighbors. Recall that a rational number p/q is irreducible if $(p,q) = 1$.

DEFINITION 15. *We define the Farey sequence of order* n ($n \geq 1$), $\mathcal{F}_n$, *as the succession of rational numbers* $p/q \in [0,1]$ *in ascending order, starting with* $0/1$ *and ending with* $1/1$, *such that* $(p,q) = 1$ *and* $q \leq n$.

For example, the Farey sequence of order 6 becomes

$$\frac{0}{1}, \frac{1}{6}, \frac{1}{5}, \frac{1}{4}, \frac{1}{3}, \frac{2}{5}, \frac{1}{2}, \frac{3}{5}, \frac{2}{3}, \frac{3}{4}, \frac{4}{5}, \frac{5}{6}, \frac{1}{1}.$$

Note that all rational numbers are contained in $\mathcal{F}_n$ for some $n > 0$. We then have the following well-known result (see [77]).

THEOREM 16. *The following hold:*

(i) $p/q < r/s$ *are Farey neighbors in* $\mathcal{F}_n$ *if and only if* $rq - ps = 1$;

(ii) *if* $p/q < r/s$, *then*

$$\frac{p}{q} < \frac{p+r}{q+s} < \frac{r}{s}.$$

Moreover, if p/q *and* r/s *are Farey neighbors in* $\mathcal{F}_n$, *then* $p/q < (p+r)/(q+s)$ *and* $(p+r)/(q+s) < \frac{r}{s}$ *are Farey neighbors in* $\mathcal{F}_{q+s}$.

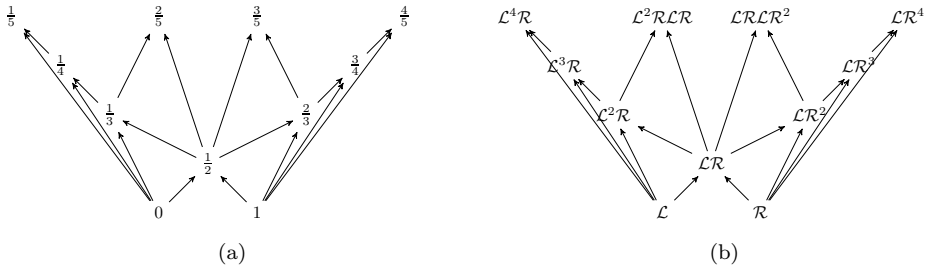

Fig. 3.1 (a) *Farey tree of rational numbers.* (b) *Farey tree of symbolic sequences. Both trees are isomorphic by construction but also through dynamical properties of periodic orbits of orientation preserving circle maps (see section* 3.4*).*

DEFINITION 17. *The fraction* $\frac{p+r}{q+s}$ *given in Theorem* 16 *is called the Farey sum or mediant of the numbers* $\frac{p}{q}$ *and* $\frac{r}{s}$.

We now construct the Farey tree of rational numbers (see Figure 3.1(a)). Starting with the Farey neighbors $0/1$ and $1/1$, the Farey tree is generated by obtaining rational numbers by adding their numerators and denominators. That is, given two Farey neighbors p/q and p'/q', they generate the child given by their mediant, $(p+p')/(q+q')$, and p/q and p'/q' become the Farey parents of the rational number $(p+p')/(q'+q')$. Note that this provides all the Farey sequences $\mathcal{F}_n$ and, hence, all rational numbers are found in the Farey tree and are uniquely identified with their Farey parents.

Consider a piecewise-smooth map as defined in (2.1), and recall that we are interested in the simultaneous variation of the parameters $\mu_{\mathcal{L}}$ and $\mu_{\mathcal{R}}$ parametrized by $\lambda \in [0,1]$ through the reparametrization shown in (2.7). Then, under condition (i) of Theorem 13, when this parameter is varied from 0 to 1, the periods of these periodic orbits are given by the denominators of the rational numbers given in the Farey tree (see Figure 3.1(a)).

As noted by some authors [57], other trees, such as the Stern–Brocot tree, can also generate this sequence of periods. However, the most interesting relationship between the Farey tree and the sequence of periodic orbits given by the period adding concerns their associated symbolic sequences, not only their periods. To explain this, we recall that the η-number (Definition 11) is given by the ratio between the number of $\mathcal{R}'s$ contained in a symbolic sequence and its length.

REMARK 18. *As we will show in section* 3.4 *(Corollary* 46*), under condition* (i) *of Theorem* 13*, the map* f *given in* (2.1) *can be reduced to a circle map, and the number* η *of a symbolic sequence of a periodic orbit becomes the rotation number of the circle map (see Remark* 41*).*

Under condition (i) of Theorem 13, when λ in (2.7) is varied from 0 to 1, one obtains periodic orbits with symbolic sequences $\mathbf{x}^\infty \in W$, with $\mathbf{x} = \mathbf{x}(\lambda) \in W_{p,q}$. If one then considers the η-number associated with these symbolic sequences, $\eta(\lambda)$, it turns out that it is a continuous and monotonically increasing function of λ whose images are all rational values between 0 and 1. However, the set of values of λ for which $\eta(\lambda)$ is not defined (it "becomes irrational") forms a Cantor set of zero measure. Hence, $\eta(\lambda)$ is a *devil's staircase*, as it is continuous, monotonically increasing, and locally constant almost everywhere. This function is shown in Figure 2.2(b) and is the well-known function formed by the rotation numbers of the periodic orbits of the

so-called Arnold circle map

$$\theta_{n+1} = \theta_n + \Omega - \frac{1}{2\pi}\sin(2\pi\theta_n),$$

when Ω is varied from 0 to 1.

Note that, for $\eta = 0$ and $\eta = 1$, the map possesses fixed points with symbolic sequences $\mathcal{L}$ and $\mathcal{R}$, respectively. These undergo border collision bifurcations for $\lambda = 0$ and $\lambda = 1$, respectively.

Although each periodic orbit for $\lambda \in (0, 1)$ is in one-to-one correspondence with a rational number in the Farey tree through the η-number, their symbolic sequences are not, in principle, uniquely identified. For example, assume that for a certain value $\lambda = \lambda_{2/5}$ there exists a periodic orbit with $\eta = 2/5$. Its symbolic sequence could be given by any of the generating minimal blocks $\mathcal{L}^2\mathcal{R}\mathcal{L}\mathcal{R}$ or $\mathcal{L}^3\mathcal{R}^2$, as they have length 5 and contain two $\mathcal{R}$ symbols. It turns out that the symbolic sequence of a periodic orbit with η-number p/q is uniquely determined. To explain this correspondence between periodic orbits and symbolic sequences we construct the Farey tree of symbolic sequences as follows. Starting with the sequences $\mathcal{L}$ and $\mathcal{R}$, one concatenates those sequences whose η-numbers are Farey numbers. By construction, this provides a unique correspondence between rational numbers and symbolic sequences through their η-number and the Farey tree. That is, to each rational number P/Q in the Farey tree one associates a symbolic sequence Δ given by the concatenation

$$\Delta = \alpha\beta,$$

where α and β are the (minimal) symbolic sequences of the Farey neighbors rational numbers p/q and p'/q', respectively:

- $p/q < p'/q'$,
- $p'q - pq' = 1$,
- $P/Q = (p + p')/(q + q')$.

As will be discussed in section 6, this concatenation provides the so-called *maximin* sequences (see Definition 56).

We will prove in section 3.4 (Propositions 45 and 47) that the following correspondence holds. The symbolic sequence of the periodic orbit with η-number p/q is the one which corresponds to rational number p/q in the Farey tree of symbolic sequences.

We are now ready to provide a formal description of the period adding bifurcation structure.

DEFINITION 19. *We say that f_λ, as in Theorem* 13(i)*, undergoes a period adding bifurcation structure if the following hold:*

(i) *for all values of λ, except for a Cantor set with zero measure, the map f_λ possesses a unique attracting periodic orbit;*

(ii) *the η-number, $\eta \in \mathbb{Q}$, as a function of λ follows a devil's staircase: it is a monotonically increasing continuous function not defined in a Cantor set of zero measure (it is hence locally constant for almost all values of λ);*

(iii) *f_{λ_Δ} possesses a Δ-periodic orbit with $\eta = P/Q$, $(P, Q) = 1$ and there exist values $\lambda_\alpha < \lambda_\Delta < \lambda_\beta$ for which f_{λ_α} and f_{λ_β} possesses α- and β-periodic orbits, respectively, whose η-numbers are Farey neighbors with mediant P/Q, and Δ is the concatenation of α and β: $\Delta = \alpha\beta$.*

3.2. Summary of the Proof. In order to facilitate the proof of the result described in detail in section 3.1, we provide a schematic summary of the necessary steps.

(1) By performing the change of variables given in (3.1), we first show that a piecewise-defined map f as in (2.1) satisfying (i) in Theorem 13 is an orientation preserving circle map (see Definition 20). Although this circle map will be discontinuous, in section 3.3 we will show how classical results for continuous circle maps also hold. In particular, we will show the following:
   (a) Given a map as above, its rotation number exists and is unique (Proposition 25).
   (b) If a map as above has a rational rotation number, then it possesses a unique and stable periodic orbit (Proposition 28 + contractiveness).
   (c) When a map as above has a rational rotation number, the unique periodic orbit must be p, q-ordered (it is a twist orbit; see Definition 37) (Proposition 38).

(2) In section 3.4 we provide symbolic properties of the itineraries of periodic orbits of orientation preserving circle maps. More precisely:
   (a) In Proposition 45 we show that the symbolic itinerary of a twist periodic orbit is a p, q-ordered symbolic sequence. This identifies each periodic orbit of an orientation preserving map with a unique symbolic itinerary through its rotation number.
   (b) In Proposition 47 we show that the itineraries of p, q-ordered periodic orbits are given by concatenation of the itineraries of the periodic orbits with rotation numbers the Farey parents of p/q. Hence, they are in the Farey tree of symbolic sequences shown in Figure 3.1(b).

(3) In section 3.4 we also study one-parameter families of orientation preserving (discontinuous) circle maps. This is equivalent to varying the parameter λ under the conditions of Theorem 13 (i). Using the continuity of the rotation number (Proposition 35) and a result of Boyd (Theorem 49), we show that the rotation number (and hence the η-number) follows a devil's staircase leading to the adding scenario when λ is varied from 0 to 1.

We emphasize that the previous steps provide (to our knowledge) the shortest path to proving (i) of Theorem 13. However, it is not the only one. In section 6.4 we provide an alternative to cover some of the steps mentioned above. These involve the concepts of *maximin* sequences and *quasi-contractions*.

3.3. Reduction to an Orientation Preserving Circle Map and Some Properties. In this section we first show that, under condition (i) of Theorem 13, the piecewise-smooth map (2.1) can be reduced to a class of orientation preserving (increasing) discontinuous circle maps.

Then we present results on circle maps which are well known in the continuous case. However, by making small modifications to the classical proofs we adapt them to the discontinuous case. We will make this clear in each particular situation.

Let us observe that, under condition (i) of Theorem 13, the piecewise-smooth map (2.1) is increasing on both sides of the discontinuity $x = 0$. Hence, all the dynamics are attracted into the interval $[f_{\mathcal{L}}(0), f_{\mathcal{R}}(0)] = [-\mu_{\mathcal{R}}, \mu_{\mathcal{L}}]$ (see Figure 3.2). By identifying these two values and considering the circle as $\mathbb{R}/[-\mu_{\mathcal{R}}, \mu_{\mathcal{L}}]$, the map becomes a circle map which is continuous at $x = 0$, but not necessarily at $x = -\mu_{\mathcal{R}} \sim \mu_{\mathcal{L}}$ (see Figure 3.2(a)). As we are interested in varying the parameters $\mu_{\mathcal{R}}$ and $\mu_{\mathcal{L}}$,

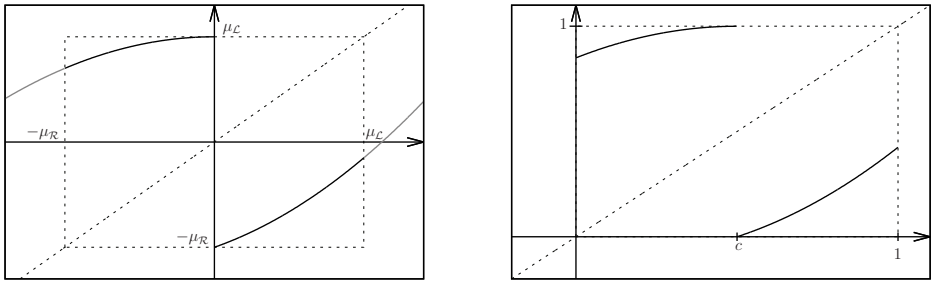

(a) (b)

Fig. 3.2 (a) *Reduction of an increasing-increasing piecewise-smooth map to an orientation preserving circle map.* (b) *Circle map after the change of variables given in* (3.1).

we perform the change of variables

$$\begin{array}{rccc} \phi: & [-\mu_R, \mu_{\mathcal{L}}] & \longrightarrow & [0,1], \\ & x & \longmapsto & \frac{x+\mu_{\mathcal{R}}}{\mu_{\mathcal{L}}+\mu_R}, \end{array} \tag{3.1}$$

which is a strictly increasing homeomorphism mapping $-\mu_{\mathcal{R}}$ to 0 and $\mu_{\mathcal{L}}$ to 1. Of special interest will be the value

$$c = \phi(0) = \frac{\mu_{\mathcal{R}}}{\mu_{\mathcal{R}} + \mu_{\mathcal{L}}},$$

which separates the behaviors given by $\phi \circ f_{\mathcal{L}} \circ \phi^{-1}$ and $\phi \circ f_{\mathcal{R}} \circ \phi^{-1}$. Hence, by identifying the circle with the interval $[0,1]$, $S^1 = \mathbb{R}/\mathbb{Z}$, we have reduced the piecewise-smooth map to a class of circle maps which consists of increasing (orientation preserving) circle maps reaching exactly once the value 1 (degree one) and not necessarily continuous at $x = 0 \sim 1$. In the following definition we make precise such a class of maps.

DEFINITION 20. *We say that*

$$f : S^1 \longrightarrow S^1, \tag{3.2}$$

$S^1 = \mathbb{R}/\mathbb{Z}$, *is an orientation preserving circle map (of degree one) if there exists a unique* $c \in [0,1]$ *(where* $[0,1]$ *is identified with the circle* S^1*) such that the following hold:*

C.1. f *is* C^0 *in* $(0,c)$ *and* $(c,1)$.
C.2. *There exists* $c \in [0,1]$ *such that* f *is increasing in* $[0,c)$ *and* $(c,1]$.
C.3. $f(c^-) = 1$ *and* $f(c^+) = 0$.
C.4. $f(0^+) \geq f(1^-)$.

Due to the existence of c fulfilling C.3, such a circle map is of degree one, as the image of S^1 by f twists at most once around S^1. When also considering condition C.4 we ensure that such an orientation preserving map is invertible. However, condition C.4 allows this class of maps to be not necessarily continuous at $x = 0$. Hence, at $x = 0$ and $x = 1$ one can choose between the images from the left or right of $x = 0$ (or indeed any other value). When convenient, we will choose both values at $x = 0$ and $x = 1$ and deal with a two-valued function.

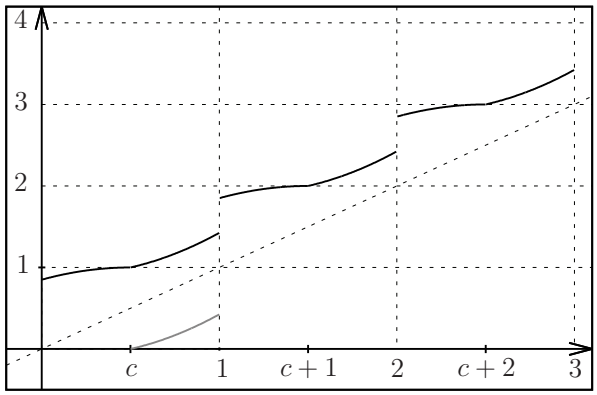

Fig. 3.3 *Lift of the of the circle map shown in Figure* 3.2(b). *In gray we show the circle map for* $x \in (c, 1)$.

Notice that, at this point, we are not requiring contractiveness, and all results in this section hold also for expansive maps as long as conditions C.1–C.4 are satisfied.

DEFINITION 21. *Let* f *be a map satisfying conditions* C.1–C.4. *We will say that* F *is a lift of* f *of degree* $N \geq 0$ *if*

$$\begin{aligned} F(x+n) &= f(x) + nN \qquad \text{if } 0 \leq x < c, \\ F(x+n) &= f(x) + nN + 1 \quad \text{if } c \leq x < 1. \end{aligned} \tag{3.3}$$

If $N = 1$, *we will refer to* F *simply as the lift of* f.

REMARK 22. *The previous definition of the degree of a circle map differs from the standard one. When* f *is a continuous circle map, the degree of its lift* F *is the integer number* N *such that*

$$F(x+1) = F(x) + N,$$

and F *is also continuous. In our case, as* f *is discontinuous at* $x = 1$, *the lift* F *cannot be continuous and, hence, there is some freedom when choosing its degree.*

Note that if f *is a circle map satisfying* C.1–C.4, *then, if it is continuous at* $x = 0 \sim 1$ *and* F *is its continuous lift, then necessarily* $N = 1$ *and* F *is of degree one in the classical sense.*

From now on, we will restrict our consideration to lifts of degree one.

REMARK 23. *Due to condition* C.4, *the lift of an orientation preserving map is an increasing map, possibly discontinuous at integer numbers, where it undergoes a positive gap (see Figure* 3.3*).*

REMARK 24. *In Definition* 21 *the value of the lift* F *at integer numbers* n *is not uniquely defined. When convenient, we will use the lift given by* $f(1^-)+n$, $f(0^+)+n$, *or both. The latter will lead to a two-valued lift.*

The following result is well known and provides the definition of the rotation number of an orientation preserving circle map satisfying C.1–C.4. This was introduced

by Poincaré [111] for homeomorphisms of the circle of degree one and later studied and extended to rotation intervals by many authors (see [3] and references therein). For discontinuous orientation preserving circle maps, this was proven in [115, 59]. However, if one considers a two-valued lift at integer numbers (see Remark 24), then the standard proof holds.

PROPOSITION 25 (see [59, III.1.1-1], [115, Theorem 1]). *Let f be a discontinuous orientation preserving map satisfying* C.1–C.4*, and let F be its lift. Then, for all $x \in \mathbb{R}$, the limit*

$$\lim_{x\to\infty} \frac{F^n(x) - x}{n} \tag{3.4}$$

exists and is independent of x.

Proof. We give the standard proof a slight modification to overcome the discontinuities at integer numbers.

As F is increasing, we find that, for $0 \le x \le 1$,

$$\frac{F^n(0^-)}{n} \le \frac{F^n(0^+)}{n} \le \frac{F^n(x)}{n} \le \frac{F^n(1^-)}{n} \le \frac{F^n(1^+)}{n}.$$

Noting that we take F two-valued at integer values, we can write this as

$$\frac{F^n(0)}{n} \le \frac{F^n(x)}{n} \le \frac{F^n(1)}{n},$$

where $F(0)$ and $F(1)$ can be each of the lateral values.

Using that $F(x+1) = F(x)+1$ and applying it recursively to $F^n(1)$ we have that

$$\frac{F^n(0^+)}{n} \le \frac{F^n(x)}{n} \le \frac{F^n(1^+)}{n} = \frac{F^n(0^+)+1}{n},$$

which we can write as

$$\frac{F^n(0)}{n} \le \frac{F^n(x)}{n} \le \frac{F^n(0)+1}{n},$$

where $F(1) = F(0)+1$ means $F(1^\pm) = F(0^\pm)+1$.

Hence, taking limits we get

$$\lim_{n\to\infty} \frac{F^n(x) - x}{n} = \lim_{n\to\infty} \frac{F^n(x)}{n} = \lim_{n\to\infty} \frac{F^n(0)}{n},$$

and the limit does not depend on x. We next show that this limit indeed exists. We apply Proposition 1 of [115], which states that, if a sequence a_n satisfies

$$|a_{m+n} - a_m - a_n| \le A \tag{3.5}$$

for all $n, m \ge 1$ and some constant A, then there exists some ρ such that

$$|a_n - n\rho| \le A.$$

The sequence $F^n(0)$ satisfies (3.5) with $A = 1$. To see this, we use that $F(x+n) = F(x)+n$ to obtain, for any $x \ge 0$,

$$F^n(x) = F^n(x \pmod 1) + [x] < F^n(1) + x = F^n(0) + x + 1,$$

where $[\cdot]$ denotes the integer part. Then, taking $x = F^m(0)$, we get

$$F^{n+m}(0) < F^n(0) + F^m(0) + 1,$$

and (3.5) is satisfied with $A = 1$. Then, there exists some ρ such that

$$\lim_{n\to\infty} \frac{F^n(0)}{n} \leq \lim_{n\to\infty} \frac{1 + n\rho}{n} = \rho,$$

and the limit exists. ∎

Note that this proof differs from the one given in [3]. There, it is first proved that if f possesses a periodic orbit, then this limit exists and is rational; then it is shown that, as above, it does not depend on x. Subsequently, the definition is extended to all real numbers using monotonicity and the Dedekind cut construction. In this approach we show the existence of this limit and then we discuss the dynamics of the map depending on its value.

The previous result permits one to define the rotation number of a circle map f fulfilling C.1–C.4. Note that, in general, this depends on the lift of F. However, recall that we have restricted consideration to lifts of degree one.

DEFINITION 26 (rotation number). *Given a map f satisfying* C.1–C.4 *and F its lift, we define the rotation number of f as*

$$\rho(f) = \lim_{n\to\infty} \frac{F^n(x) - x}{n}$$

for any $x \in \mathbb{R}$.

REMARK 27. *The fact that the limit given in* (3.4) *exists implies that $F^n(x)$ grows linearly with n:*

$$F^n(x) - x \sim n\rho(f),\ n >> 1.$$

Recalling the properties shown in (3.3)*, the rotation number $\rho(f)$ can be seen as the average number of times that the lift F crosses an integer number per iteration.*

The next result is also standard for continuous circle maps (see Proposition 3.7.11 of [3]) and provides the existence of a periodic orbit if the rotation number is rational. Below we prove that it also holds for discontinuous circle maps.

PROPOSITION 28. *Let F be the lift (of degree one following Definition* 21*) of a circle map satisfying* C.1–C.4*. Then $\rho(F) = p/q$, $(p, q) = 1$, if and only if there exists x_0 s.t. $F^q(x_0) = x_0 + p$.*

Proposition 28, whose proof is given below, is stated assuming that the map F is two-valued at integer values (see Remark 24). This ensures that one always finds a periodic orbit if the rotation number is rational. However, if one considers only one image at integer numbers, given by $f(0^+)$ or $f(1^-)$, one can lose the existence of a periodic orbit and and end up with an ω-limit consisting of q points mimicking a periodic orbit. That is, one recovers a result given in [115], which we repeat next for completeness.

PROPOSITION 29 (see [115, Theorem 2]). *Let F be the lift (of degree one following Definition* 21*) of a circle map satisfying* C.1–C.4 *and $p, q \in \mathbb{Z}$ with $q > 0$. If $\rho(F) = p/q$, then exactly one of the following holds:*

(i) *There exists* $x_0 \in \mathbb{R}$ *such that* $F^q(x_0) = x_0 + p$.
(ii) *For all* $x \in \mathbb{R}$, $F^q(x) > x + p$, *and there exists* $x_0 \in \mathbb{R}$ *such that*

$$\lim_{x \to x_0^-} F^q(x) = x_0 + p.$$

(iii) *For all* $x \in \mathbb{R}$, $F^q(x) < x + p$, *and there exists* $x_0 \in \mathbb{R}$ *such that*

$$\lim_{x \to x_0^+} F^q(x) = x_0 + p.$$

Conversely, if either (i), (ii), *or* (iii) *holds, then* $\rho(F) = p/q$.

REMARK 30. *The situations* (ii) *or* (iii) *occur when* $x_0 = c$, *that is, when a periodic orbit bifurcates and the image of* $x = 0$ *by the circle map takes the value on the "wrong" side. More precisely, if* $f(0) = f(0^+)$, *then* (ii) *occurs when a periodic orbits bifurcates when approaching* $x = c$ *from the left. Similarly, if* $f(0) = f(1^-)$, (iii) *occurs when a periodic orbit bifurcates by colliding with* $x = c$ *from the right.*

For completeness, we will provide a proof of Proposition 28 based on [3] but adapting it to the discontinuous case, as in the proof of Proposition 28. It relies on the following two lemmas.

The first lemma is equivalent to Lemma 2 of [115]. We state it as in Lemma 3.7.10 of [3], but we adapt its proof to also hold for discontinuous circle maps.

LEMMA 31. *Let* F *be the lift of a circle map satisfying* C.1–C.4, *and let* $p \in \mathbb{Z}$. *Then the following hold:*
(i) *If* $F^q(x) - p > x$ *for all* $x \in \mathbb{R}$, *then there exists* $\varepsilon > 0$ *such that* $\rho(F) \geq p/q + \varepsilon$.
(ii) *If* $F^q(x) - p < x$ *for all* $x \in \mathbb{R}$, *then there exists* $\varepsilon > 0$ *such that* $\rho(F) \leq p/q - \varepsilon$.

Obviously, the proof provided in [115] also holds. However, by considering that F is two-valued at integer numbers, we can proceed as in the proof for the continuous case [3], which we repeat for completeness.

Proof. We show (i); (ii) can be proven analogously. Note that $G(x) = F^q(x) - p - x$ is of degree of zero, i.e., $G(x + 1) = G(x)$. Hence, recalling that F is two-valued at its discontinuities and hence $F^q(x) - p - x > 0$ holds for each lateral value, it follows that there exists some $\delta > 0$ such that, for every x, $F^q(x) - p - x \geq \delta$. Then, for all k we find

$$F^{qk}(x) - x = \sum_{i=0}^{k-1} \left(F^q \left(F^{qi}(x) \right) - F^{qi}(x) \right) \geq k(p + \delta).$$

Hence, as from Proposition 25 the rotation number exists and is unique, we have that

$$\rho(F) = \lim_{k \to \infty} \frac{F^{qk}(x) - x}{qk} \geq \frac{k(p + \delta)}{kq} = \frac{p}{q} + \frac{\delta}{q},$$

which proves (i) with $\varepsilon = \delta/q$. ∎

Note that the proof given in [3] is slightly different, as it does not use the uniqueness of the rotation number.

The following lemma is trivial for the continuous case.

LEMMA 32 (see [115, Lemma 3]). *Let*

$$F : \mathbb{R} \longrightarrow \mathbb{R}$$

be a (not necessarily continuous) nondecreasing map fulfilling $F(x+1) = x+1$ *for all* $x \in \mathbb{R}$. *Assume that* $F(x_1) > x_1$ *and* $F(x_2) < x_2$ *for some* $x_1, x_2 \in \mathbb{R}$. *Then there exists some* x_0 *such that* $F(x_0) = x_0$, *and* F *is continuous at the left at* x_0.

We provide a more intuitive proof of this lemma.

Proof. Assume $F(x) \neq x$ for all x and recall that if F undergoes a discontinuity, the jump must be positive. Suppose $F(0) > 0$. Then the existence of x_2 implies that F either crosses the diagonal or undergoes a negative jump, both of which give a contradiction. If $F(0) < 0$, then the existence of x_1 implies that F cannot stay below the diagonal, unless it skips over it by a positive jump. In this case, as $F(1) = F(0) + 1 < 1$, arguing as before we conclude that F has to cross the diagonal. ∎

REMARK 33. *The class of maps considered in Lemma* 32 *is not necessarily restricted to lifts of circle maps satisfying* C.1–C.4. *Note that they may undergo discontinuities with positive jumps between* 0 *and* 1, *whereas the lifts of circle maps satisfying* C.1–C.4 *are continuous in* $(0, 1)$.

We now prove Proposition 28 by adapting as before the proof given in [3] to the discontinuous case.

Proof of Proposition 28. Assume that $F^q - p$ has a fixed point. Then we find that $F^{nq}(x_0) - np = x_0$ for all $n > 0$, which implies that $\rho(F) = p/q$.

Assume that $\rho(F) = p/q$ and that $F^q(x) - p$ does not have a fixed point. Then, by Lemma 32, we get that either $F^q(x) - p < x$ or $F^q(x) - p > x$. However, then, by Lemma 31, there exists $\varepsilon > 0$ such that either $\rho(F) > p/q + \varepsilon$ or $\rho(F) < p/q - \varepsilon$, which is a contradiction. ∎

Note that, besides the fact that we deal with a discontinuous lift, the proof above differs from the one given in [3] in the fact that we can use the existence and uniqueness of the rotation number provided by Proposition 25.

REMARK 34. *Proposition* 28 *provides neither the uniqueness nor the stability of periodic orbits. However, if, in addition to* C.1–C.4, *one adds contractiveness, i.e.,* $f'(x) < 1$ *for* $x \in (0, c) \cup (c, 1)$, *then one gets that such a periodic orbit is unique and attracting. Note that* f *might not be differentiable at* $x = 0 \sim 1$ *and* $x = c$.

The next result provides the continuity of the rotation number; i.e., if two lifts of orientation preserving maps are "close" (using the uniform norm), then so are their rotation numbers. Note that, assuming that these maps are two-valued at integer values, one can always choose the proper images to properly compare them. Hence, its proof for the discontinuous case becomes the standard one though taking into account this fact and Lemmas 31 and 32.

PROPOSITION 35 (see [3, Lemma 3.7.12]). *The function*

$$F \longmapsto \rho(F)$$

considered in the space of lifts of circle maps satisfying C.1–C.4 *is continuous with the norm of uniform convergence.*

Proof. We proceed as in [3] by adapting the proof to the fact that F is two-valued in order to overcome the discontinuities at integer numbers.

Assume $\rho(F) \neq p/q$. Then the function $G(x) = F^q(x) - p - x$ is away from zero. By Lemma 32 (applied to $G(x) + x$), we get that either $G(x) < 0$ or $G(x) > 0$ for all $x \in \mathbb{R}$. Then, by Lemma 31, we have that either $\rho(F) < p/q$ or $\rho(F) > p/q$, respectively.

We now note that $G(x)$ has degree 0; that is, $G(x+1) = F^q(x+1) - p - (x+1) = F^q(x) - p - x = G(x)$. Hence, we can ensure that if $\tilde{G}$ is in a small enough neighborhood of G, then either $\tilde{G} < 0$ or $\tilde{G} > 0$, respectively. This implies that if $\tilde{F}$ is in a small enough neighborhood of F, then either $\rho(\tilde{F}) < p/q$ or $\rho(\tilde{F}) > p/q$, respectively.

Hence, we have shown that if there exist p_1/q_1 and p_2/q_2 such that

$$\frac{p_1}{q_1} < \rho(F) < \frac{p_2}{q_2},$$

and $\tilde{F}$ is sufficiently close to F, then

$$\frac{p_1}{q_1} < \rho(\tilde{F}) < \frac{p_2}{q_2},$$

and hence $F \longmapsto \rho(F)$ is continuous. □

The next lemma shows that the rotation number is increasing as a function of F.

LEMMA 36. *Let f and g be two circle maps satisfying* C.1–C.4 *and let F and G be their lifts, respectively. If $F \geq G$, then $\rho(f) \geq \rho(g)$.*

Proof. Let $x < c$ and F and G be two lifts of f and g such that $F(x+1) = F(x)+1$ and $G(x+1) = G(x)+1$. As F and G are increasing functions undergoing a positive gap at $x = k$, $F^n(x) > G^n(x)$, even if, for some n, $F^n(x)$ or $G^n(x)$ reach any of the discontinuities at $x = k$. Hence,

$$\frac{F^n(x) - x}{n} \geq \frac{G^n(x) - x}{n}.$$

As the rotation number does not depend on x, we obtain $\rho(f) \geq \rho(g)$. □

We next study properties of the periodic orbits of orientation preserving circle maps satisfying C.1–C.4. These will be crucial to show symbolic properties of periodic orbits in section 3.4. To this end, we provide the following definitions.

DEFINITION 37 (twist and p,q-ordered lifted cycle). *Let f be a circle map and $x_i \in S^1 = \mathbb{R}/\mathbb{Z}$ such that*

$$0 < x_0 < x_1 < \cdots < x_{q-1} < 1 \tag{3.6}$$

and $f^q(x_i) = x_i$, $0 \leq i \leq q-1$. Consider the projection

$$\begin{array}{rccc} \Pi: & \mathbb{R} & \longrightarrow & S^1 = \mathbb{R}/\mathbb{Z}, \\ & x & \longmapsto & x \pmod 1, \end{array} \tag{3.7}$$

and the lifted orbit or lifted cycle

$$S = \left\{\Pi^{-1}(x_i)\right\},$$

which consists of adding $\mathbb{Z}$ to the orbit (3.6). *Let F be the lift of f. We say that S is a twist lifted cycle or orbit of F if F restricted to S is increasing.*

If S is a twist lifted cycle of f and

$$\lim_{n\to\infty} \frac{F^n(x) - x}{n} = \frac{p}{q}$$

for all $x \in S$, we say that S is a p,q-ordered lifted cycle of F and $x_0 < \cdots < x_{q-1}$ is a p,q-ordered cycle or periodic orbit of f.

The following result shows us the relationship between the spatial and dynamical orderings of a p, q-ordered lifted cycle.

PROPOSITION 38. *Let $0 < x_0 < \cdots < x_{q-1}$ be a p, q-ordered cycle of the circle map f, and let F be its lift and S the corresponding lifted cycle. Assume that S is given by*

$$S = \{x_0 < \cdots < x_{q-1} < x_q < \cdots < x_{2q-1} < \cdots\}$$

with $x_j = x_i + n$ if $j = i + nq$, $0 \le i \le q-1$. Then

$$F(x_i) = x_{i+p}, \tag{3.8}$$

$$F^q(x_i) = x_i + p. \tag{3.9}$$

The proof of this result is as in the continuous case (see [3, Lemma 3.7.4]) but taking into account that the lift F is two-valued at integer numbers. We include it here for completeness.

Proof. By properly choosing the image of F at integer values, the lift F restricted to the lifted cycle of the periodic orbit is an order preserving bijection. That is, by iterating the points $x_0 < \cdots < x_{q-1}$ one visits all the points of the lifted cycle exactly once, and the order is preserved ($F(x_j) < F(x_i)$ if and only if $x_j < x_i$). Hence, $F(x_i) = x_{i+r}$ for all i and some integer r. If not, then one finds that $F(x_j) = x_{j+r_1}$ and $F(x_i) = x_{i+r_2}$. If $r_1 \neq r_2$, then the numbers of points of the lifted orbit in $[x_{j+r_1}, x_{i+r_2}]$ and in $[x_j, x_i]$ do not coincide, and hence the order cannot be preserved.

As the rotation number is $\rho(F) = p/q$, we have that necessarily $x_i + p = F^q(x_i) = x_{i+qr}$. As x_i belongs to a q-periodic cycle, we get $x_{i+qr} = x_i + r$, which is what we wanted to show. ∎

The next result is also very well known for continuous circle maps. As in previous results, we provide a standard proof adapted for the discontinuous case.

PROPOSITION 39. *Let f be a circle map satisfying* C.1–C.4 *and assume that $\rho(f) \in \mathbb{R}\backslash\mathbb{Q}$. Then if f is contracting ($f'(x) < 1$, $x \in (0, c) \cup (c, 1)$) and condition* C.4 *is a strict inequality, the ω-limit set of the circle is a Cantor set.*

Proof. Recall that if $f(0^+) > f(1^-)$, then f is invertible but not injective. Let $U = (x_-, x_+)$ with $x_- = f(1^-)$ and $x_+ = f(0^+)$. We first show that, if $\rho(f)$ is irrational, then $c \notin f^n(U)$ for all $n \ge 1$. As f is invertible in $S^1\backslash U$, we consider f^{-1}, which is a function with a "hole," as it is not defined in U. After filling this hole with the value 1, we obtain the continuous function

$$g(y) = \begin{cases} f^{-1}(y) & \text{if } y \in [0, x_-], \\ 1 & \text{if } y \in [x_-, x_+], \\ f^{-1}(y) & \text{if } y \in [x_+, 1] \end{cases} \tag{3.10}$$

(see Figure 3.4), which has the same rotation number as f with different sign. Note that

$$g(U) = 1,$$
$$g(1) = c.$$

Hence, if, for some n, $c \in f^n(U)$, then $g^n(c) \in U$, $g^{n+1}(c) = 1$, $g^{n+2}(c) = c$, and hence g has a periodic orbit of period $n + 2$, which is not compatible with having an irrational rotation number (see Proposition 28).

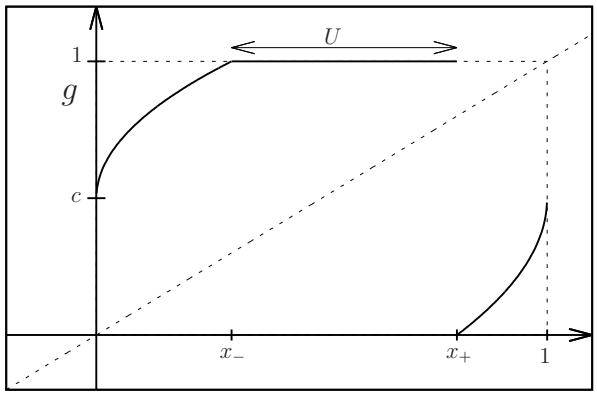

Fig. 3.4 *Inverse of an orientation preserving circle map satisfying* C.1–C.4 *with a flat part. See* (3.10).

Next we show that

$$\bigcap_{n\geq 0} f^n(S^1) = S^1 \setminus \bigcup_{i\geq 0} f^i(U)$$

is a Cantor set. As long as $c \notin f^n(U)$, at each iteration, $f^n(S^1) = S^1 \setminus f^{n-1}(U)$ consists of subtracting a nonempty interval from the interior of $S^1 \setminus f^{n-1}(U)$ (see Figure 3.5). Due to the contraction of f, the length of the subtracted interval tends to 0. Moreover, by Corollary 3.3 of [133], the total removed amount, $\cup_{i\geq 0} f^i(U)$, is dense. This comes from the fact that, although the map g is not differentiable, the Denjoy theorem holds and, if the rotation number is irrational, g has no "homtervals"; in particular, U is not a homterval and the sequence $g^n(U)$ is pairwise disjoint. Therefore, by construction, $S^1 \setminus \cup_{i\geq 0} f^i(U)$ is a Cantor set. Moreover, also by construction, the images of x_- and x_+ are dense in this set. Thus, every point in $S^1 \setminus \cup_{i\geq 0} f^i(U)$ has a dense orbit, and hence this set becomes the ω-limit of f. □

REMARK 40. *If condition* C.4 *is satisfied by an equality (the map becomes continuous) and the rotation number is irrational, then the ω-limit of f might also be a Cantor set or might be the whole circle. If f is C^2, then the Denjoy theorem holds and the latter occurs. However, if it is C^1 or C^0, f might become a Denjoy counterexample (see* [107]*), and its ω-limit might be a Cantor set.*

To conclude this section, we recover a piecewise-smooth map as defined in (2.1). As mentioned above, after applying the change of variables given in (3.1), the map $\bar{f}(x) = \phi \circ f \circ \phi^{-1}(x)$ becomes an orientation preserving map satisfying C.1–C.4 with

$$c = \phi(0) = \frac{\mu_{\mathcal{R}}}{\mu_{\mathcal{R}} + \mu_{\mathcal{L}}}.$$

After applying the reparametrization γ given in (2.7), the value

$$c_\lambda = \frac{\mu_{\mathcal{R}}(\lambda)}{\mu_{\mathcal{R}}(\lambda) + \mu_{\mathcal{L}}(\lambda)}$$

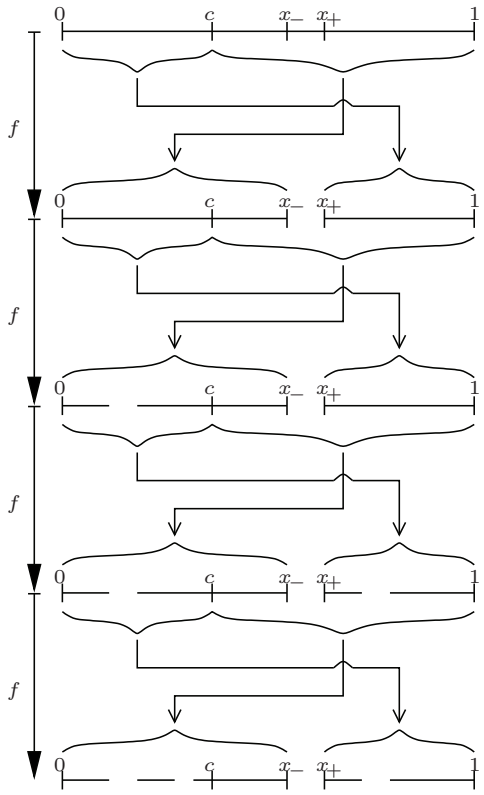

Fig. 3.5 *Cantor set generated by iterating U: new "holes" are created as long as $c \notin f^n(U)$.*

becomes a strictly decreasing function of λ such that

$$\lim_{\lambda \to 0^+} c_\lambda = 1,$$
$$\lim_{\lambda \to 1^-} c_\lambda = 0.$$

Moreover, for $\lambda = 0$ and $\lambda = 1$, the map $\bar{f}$ possesses fixed points at $x = 1$ and $x = 0$, respectively.

Given a piecewise-smooth map f satisfying h.1–h.3, we will define its rotation number as the rotation number of the map $\bar{f} = \phi \circ f \circ \phi^{-1}$ obtained after a reduction to a circle map:

$$\rho(f) = \rho(\bar{f}).$$

By abusing notation, we will also refer to the lift of f as the lift of $\bar{f}$.

REMARK 41. *Let $(x_0, \ldots, x_{q-1})$ be a periodic orbit of a piecewise-smooth map whose associated circle map satisfies conditions* C.1–C.4*, and let $\mathbf{x} = (\mathbf{x}_0 \cdots \mathbf{x}_{q-1}) \in \{\mathcal{L}, \mathcal{R}\}^q$ be its associated symbolic sequence following the symbolic encoding given in* (2.3)*:*

$$\mathbf{x}_i = a(f^i(x_i)), \quad 0 \le i \le q-1.$$

Then, recalling Remark 27 *and the fact that the image of x by the lift of f, $F(x)$,*

crosses an integer number m when $x < c+m < F(x)$, the rotation number of f, $\rho(f)$, becomes the η-number defined in (2.6)*. That is, it becomes the ratio of the number of symbols $\mathcal{R}$ contained in $\mathbf{x}$ to the length of the sequence $\mathbf{x}$, q.*

3.4. Symbolic Dynamics and Families of Orientation Preserving Maps. In this section we describe some dynamical properties of maps satisfying conditions C.1–C.4, focusing specifically on periodic orbits, their symbolic itineraries, and their relationship with the rotation number. In some of the results, we will additionally require the map to be contractive; however, we emphasize that, when not specified, the results that we present here do not require contractiveness.

The main result in this section is the following theorem, which is, recalling that periodic orbits of orientation preserving circle maps satisfying C.1–C.4 are well ordered, a straightforward consequence of Proposition 47.

THEOREM 42. *The symbolic sequence of the itinerary of a periodic orbit of a circle map satisfying* C.1–C.4 *with rotation number P/Q is the sequence in the Farey tree of symbolic sequences associated with the rational number P/Q.*

At the end of this section (Lemma 50) we show that, for a piecewise-smooth map (2.1) satisfying (i) of Theorem 13, the η-number defined in Definition 11 follows a devil's staircase. This is a consequence of Theorem 49 proved in [34].

To show this, we recall that the set $W_{p,q}$ consists of the q-periodic symbolic sequences with p symbols $\mathcal{R}$ (see Definition 9). Of special interest will be the *well-ordered* symbolic sequences contained in these sets.

DEFINITION 43. *Let $\mathbf{x} \in W_{p,q}$ be a periodic symbolic sequence. Consider the (lexicographically) ordered sequence given by the iterates of $\mathbf{x}$ by σ,*

$$\sigma^{i_0}(\mathbf{x}) < \sigma^{i_1}(\mathbf{x}) < \sigma^{i_2}(\mathbf{x}) < \cdots < \sigma^{i_{q-1}}(\mathbf{x}). \tag{3.11}$$

We say that the sequence $\mathbf{x}$ is a p,q-ordered (symbolic) sequence if

$$i_j - i_{j-1} = \text{constant}.$$

In other words, σ acts on the sequence (3.11) *as a cyclic permutation: there exists some $k \in \mathbb{N}$, $0 < k < q$, such that*

$$i_j = i_{j-1} + k \pmod{q}.$$

The next example illustrates the previous definition.

EXAMPLE 44. *The sequence $\mathbf{x} = (\mathcal{L}^2\mathcal{R}\mathcal{L}\mathcal{R})^\infty \in W_{2,5}$ is $2,5$-ordered, and the sequence $\mathbf{y} = (\mathcal{L}^3\mathcal{R}^2)^\infty \in W_{2,5}$ is not. If we consider the four iterates of $\mathbf{x}$ and $\mathbf{y}$ by σ, we obtain*

$$\begin{aligned}
\sigma(\mathbf{x}) &= (\mathcal{L}\mathcal{R}\mathcal{L}\mathcal{R}\mathcal{L})^\infty, & \sigma(\mathbf{y}) &= (\mathcal{L}^2\mathcal{R}^2\mathcal{L})^\infty,\\
\sigma^2(\mathbf{x}) &= (\mathcal{R}\mathcal{L}\mathcal{R}\mathcal{L}^2)^\infty, & \sigma^2(\mathbf{y}) &= (\mathcal{L}\mathcal{R}^2\mathcal{L}^2)^\infty,\\
\sigma^3(\mathbf{x}) &= (\mathcal{L}\mathcal{R}\mathcal{L}^2\mathcal{R})^\infty, & \sigma^3(\mathbf{y}) &= (\mathcal{R}^2\mathcal{L}^3)^\infty,\\
\sigma^4(\mathbf{x}) &= (\mathcal{R}\mathcal{L}^2\mathcal{R}\mathcal{L})^\infty, & \sigma^4(\mathbf{y}) &= (\mathcal{R}\mathcal{L}^3\mathcal{R})^\infty.
\end{aligned}$$

Note that $\sigma^5(\mathbf{x}_i) = \mathbf{x}_i$. When we order the iterates by σ, we obtain

$$\begin{aligned}
\mathbf{x} < \sigma^3(\mathbf{x}) < \sigma(\mathbf{x}) < \sigma^4(\mathbf{x}) < \sigma^2(\mathbf{x}),\\
\mathbf{y} < \sigma(\mathbf{y}) < \sigma^2(\mathbf{y}) < \sigma^4(\mathbf{y}) < \sigma^3(\mathbf{y}),
\end{aligned}$$

and $\mathbf{x}$ is $2,5$-ordered with $k = 3$ while $\mathbf{y}$ is not well ordered.

The following result identifies the symbolic sequences of periodic orbits whose lifted cycles are twist cycles (see Definition 37).

PROPOSITION 45 (see [59, Proposition III.1.1-2]). *Under the conditions of Proposition* 38*, if the lifted cycle S is p,q-ordered by F (see Definition* 37*), then the itinerary $I_f(x_i) \in W_{p,q}$ is a p,q-ordered symbolic sequence (see Definition* 43*).*

Proof. Let k be such that

$$(k-1)p < q \leq kp. \tag{3.12}$$

We first note that, for $0 \leq i, j \leq q-1$, we have

$$I_f(x_i) \leq I_f(x_j) \Longleftrightarrow i \leq j.$$

We then write

$$kp = q + r,\ r \geq 0.$$

Then the result comes from the fact that

$$x_0 < x_r \leq x_p,$$

which occurs if and only if $0 < r \leq p$. Assume that $r > p$. Then $q + r - p > q$ and hence $(k-1)p > q$, which contradicts (3.12). Letting $\mathbf{x} = I_f(x_0)$, this implies

$$\mathbf{x} < \sigma^{k \,(\mathrm{mod}\ q)}(\mathbf{x}) < \sigma^{2k \,(\mathrm{mod}\ q)}(\mathbf{x}) < \cdots < \sigma^{(N-1)k \,(\mathrm{mod}\ q)}(\mathbf{x}) = \sigma^{Nk \,(\mathrm{mod}\ q)}(\mathbf{x}),$$

where N is the smallest such that $Nk = 0 \pmod{q}$. ∎

The next result formalizes what was stated in Remark 41: the η-number associated with the symbolic sequence of a periodic orbit (Definition 11) of a piecewise-smooth map satisfying (i) of Theorem 13 becomes the rotation number (Definition 26) of the orientation preserving circle map obtained after the change (3.1).

COROLLARY 46. *Let f be an orientation preserving map, and let x belong to a q-periodic orbit with symbolic sequence $I_f(x) = \mathbf{x}^\infty \in W_{p,q}$. Then the rotation number becomes*

$$\rho(f) = \frac{p}{q} = \eta(\mathbf{x}).$$

That is, it is given by the ratio between the number of $\mathcal{R}$ symbols contained in $\mathbf{x}$ and the period, q, of the sequence.

Our next step consists of showing that the symbolic sequence associated with a periodic orbit of an orientation preserving circle map belongs to the Farey tree of symbolic sequences shown in Figure 3.1(b). More precisely, we show that such a symbolic sequence is obtained by the concatenation of the symbolic sequences associated with the periodic orbits of the Farey parents of its rotation number. As a consequence, one obtains Theorem 42, given above.

Note that this result provides an alternative isomorphism between the Farey tree of rational numbers and the Farey tree of symbolic sequences (see Figures 3.1(a) and 3.1(b), respectively) by means of the dynamical properties of circle maps.

In section 6.4 we will present an alternative approach using the *maximin* properties of these sequences.

PROPOSITION 47. *Let f be a circle map satisfying* C.1–C.4 *and assume it has a periodic orbit with rotation number P/Q, $(P,Q)=1$. Let $\Delta^\infty \in W_{P,Q}$ be its symbolic sequence, and assume that Δ is minimal:*

$$\Delta = \min_{k\geq 0} \sigma^k(\Delta).$$

Let p, q, p', and q' be natural numbers such that

- $P/Q = (p+p')/(q+q')$,
- $(p,q) = (p',q') = 1$,
- $p'q - pq' = 1$,

that is, $p/q < p'/q'$ are the Farey parents of P/Q.

Let $\alpha^\infty \in W_{p,q}$ and $\beta^\infty \in W_{p',q'}$ be the symbolic sequences of the periodic orbits with rotation numbers p/q and p'/q', respectively. Assume that α and β are minimal. Then Δ is the concatenation of α and β:

$$\Delta = \alpha\beta.$$

Proof. Let

$$0 < z_0 < z_1 < \cdots < z_{Q-1} < 1$$

be a periodic orbit with rotation number P/Q. Let us consider the lifted cycle given by $\Pi^{-1}(z_i)$ given in (3.7),

$$\begin{gathered} 0 < z_0 < z_1 < \cdots < z_{Q-1} < 1 < z_Q < z_{Q+1} < \cdots < z_{2Q-1} < 2 < z_{2Q} < \cdots \\ \cdots < z_{PQ-1} < P < z_{PQ} < \cdots . \end{gathered}$$

Consequently, the following identity holds:

$$z_{j+mQ} = z_j + m, \quad \text{where } j,\ m \in \mathbb{Z}. \tag{3.13}$$

Let F be the lift of f as in Definition 21. Due to Proposition 38, the points z_i are P,Q-ordered by F:

$$\begin{aligned} F(z_i) &= z_{i+P}, \\ F^Q(z_i) &= z_i + P. \end{aligned}$$

We now construct two subsequences, (x_i) and (y_i), as follows (see Example 48).

The first consists of the lifting of the set $\{z_0, f(z_0), \ldots, f^{q-1}(z_0)\}$ (the first q iterates of z_0), given by

$$\{z_{nP+iQ} \,|\, 0 \leq n \leq q-1,\ i \in \mathbb{Z}\}.$$

Since p and q are relatively prime, every integer j is uniquely represented as $j = np+iq$. Let $(x_j)_{j\in\mathbb{Z}}$ be the sequence defined by

$$x_{np+iq} = z_{nP+iQ}, \quad 0 \leq n \leq q-1, \quad i \in \mathbb{Z}. \tag{3.14}$$

We first prove that $(x_j)_{j\in\mathbb{Z}}$ satisfies

$$\begin{gathered} 0 < x_0 < x_1 < \cdots < x_{q-1} < 1 < x_q < x_{q+1} < \cdots < x_{2q-1} < 2 < x_{2q} < \cdots \\ \cdots < x_{pq-1} < p < x_{pq} < \cdots . \end{gathered} \tag{3.15}$$

To see this, we show that the sequences $(z_{kP})_{k\in\mathbb{Z}}$ and $(x_{kp})_{k\in\mathbb{Z}}$ skip integer numbers at the same iterates; that is, if

$$z_{(k-1)P} < i < z_{kP} \Big(\Longleftrightarrow (k-1)P < iQ < kP \Big),$$

then

$$x_{(k-1)p} < i < x_{kp} \Big(\Longleftrightarrow (k-1)p < iq < kp \Big).$$

This comes from the fact that, recalling (ii) of Theorem 16, p/q and P/Q are Farey neighbors, and hence they are in the path of the Farey neighbors i/k and $i/(k-1)$. Therefore, we have

$$\frac{i}{k} < \frac{p}{q} < \frac{P}{Q} < \frac{p'}{q'} < \frac{i}{k-1},$$

because P/Q is the Farey median of p/q and p'/q'.

Now let $l = kP \pmod{Q}$ and let t be such that

$$z_{(t-1)P} \le z_l < z_{tP}.$$

Then we must have

$$x_{(t-1)p} \le x_{\tilde{l}} < x_{tp},$$

where $\tilde{l} = kp \pmod{q}$. Otherwise, the sequences z_{iP} and x_{ip} could not skip integer numbers at the same time. This shows that necessarily the sequence $(x_j)_{j\in\mathbb{Z}}$ must satisfy (3.15). Further, it follows from (3.13) and (3.14) that

$$x_{j+qp} = x_j + p,\ j \in (0, \dots, q-1\}. \tag{3.16}$$

Moreover, for $j = np + iq$, $n \neq q-1$, we have

$$F(x_j) = F(z_{nP+iQ}) = z_{nP+iQ+P} = x_{(n+1)p+iq} = x_{j+p}. \tag{3.17}$$

Note that, for $n = q-1$, (3.17) does not hold, as $F(z_{(q-1)P+iQ}) = z_{qP+iQ}$ does not belong to the sequence $(x_i)_{i\in\mathbb{Z}}$.

Hence, we have that

$$F(x_j) = x_{j+p},\ j = np + iq,\ n \neq q-1 \pmod{q}. \tag{3.18}$$

As the lifted sequence $(x_j)_{j\in\mathbb{Z}}$ satisfies (3.16) and (3.18), its symbolic sequence, $\alpha \in W_{p,q}$, is the one associated with a p,q-ordered lifted cycle.

We now obtain another subsequence derived from the last q' points of the first Q iterates of the point z_0. The first of these q' points is

$$F^q(z_0) = z_{qP}.$$

Note that, as $p/q < p'/q'$ are Farey neighbors, we obtain

$$1 = p'q - pq' = p'q + pq - pq - pq' = (p'+p)q - p(q+q') = qP - pQ.$$

Therefore,

$$qP = 1 + pQ = 1 \pmod{Q}.$$

This implies that, when projecting the point z_{qP} at the circle $\mathbb{R}/\mathbb{Z}$ (identified with $[0,1]$), we obtain $\Pi(z_{qP}) = z_1$. Therefore, when lifting the projection of the last q' points of the first Q iterates of z_0, we obtain the sequence given by

$$y_{np'+iq'} = z_{1+nP+iQ}, \quad 0 \le n \le q'-1, \quad i \in \mathbb{Z}. \tag{3.19}$$

Arguing as before, this sequence has the form

$$\begin{aligned} 0 < y_0 < y_1 < \cdots < y_{q'-1} < 1 < y_{q'} < y_{q'+1} < \cdots < y_{2q'-1} < 2 < y_{2q'} < \cdots \\ \cdots < y_{p'q'-1} < p' < y_{p'q'} < \cdots \end{aligned}$$

and satisfies

$$\begin{aligned} &F^i(y_0) = y_{ip'},\ q \le i \le q+q'-1, \\ &y_{i+q'p'} = y_i + p'. \end{aligned}$$

Hence, its symbolic sequence $\beta \in W_{p',q'}$ is the one associated with a p',q'-ordered lifted cycle.

Note that α and β are minimal, as they are associated with the iterates of the lowest positive point of the sequences (x_i) and (y_i), $x_0 = z_0$ and $y_0 = z_1$, respectively.

By construction, the symbolic sequence $\Delta \in W_{P,Q}$ is the concatenation of α and β, as we wanted to show. ∎

EXAMPLE 48. *Let $P/Q = 8/11$, and assume that a circle map f satisfying* C.1–C.4 *has rotation number P/Q. From Propositions* 28 *and* 45 *we know that f has an* 11*-periodic orbit whose lifted cycle is* $8,11$*-ordered. We wish to show that, as is given by Proposition* 47*, its symbolic sequence is given by the concatenation of the symbolic sequences associated with p,q- and p',q'-ordered lifted cycles of periodic orbits with rotation numbers p/q and p'/q', respectively, where $p/q < p'/q'$ are the Farey parents of* $8/11$.

In order to find the Farey parents of $8/11$ *one can construct the Farey tree and locate them as the unique Farey neighbors of* $8/11$ *in the Farey sequence $\mathcal{F}_{11}$. However, the proof of Proposition* 47 *gives us a method of finding q and q': q is the smallest number such that $\Pi\left(F^q(z_0)\right) = z_1$.*

In Figure 3.6 *we show the* $8,11$*-ordered lifted cycle (z_i) of the periodic orbit with rotation number* $8/11$. *Starting at z_0, the arrows provide the sequence obtained when iterating z_0 by F. Note that, at each iterate, one adds* 8 *to the subindex. We obtain that $F^7(z_0) = z_{56}$ and $56 = 1 \pmod{11}$. Hence, $q = 7$ and $q' = 11 - 7 = 4$. Using that $8 = p + p'$ and $p'q - pq' = 1$, we obtain $p = 5$ and $p' = 3$:*

$$\frac{8}{11} = \frac{5+3}{7+4}.$$

We can now construct the sequence x_i. We start with $x_0 = z_0$ and add 5 *to the subindex of x at each iteration: $x_{5i} = z_{8i}$ for $0 \le i < 7$. This provides the points $x_0 < x_5 < x_{10} < \cdots < x_{30}$. By lifting these points (adding multiples of* 7 *to their subindices), we obtain a lifted cycle defined in* (3.14)*, which is* $5,3$*-ordered.*

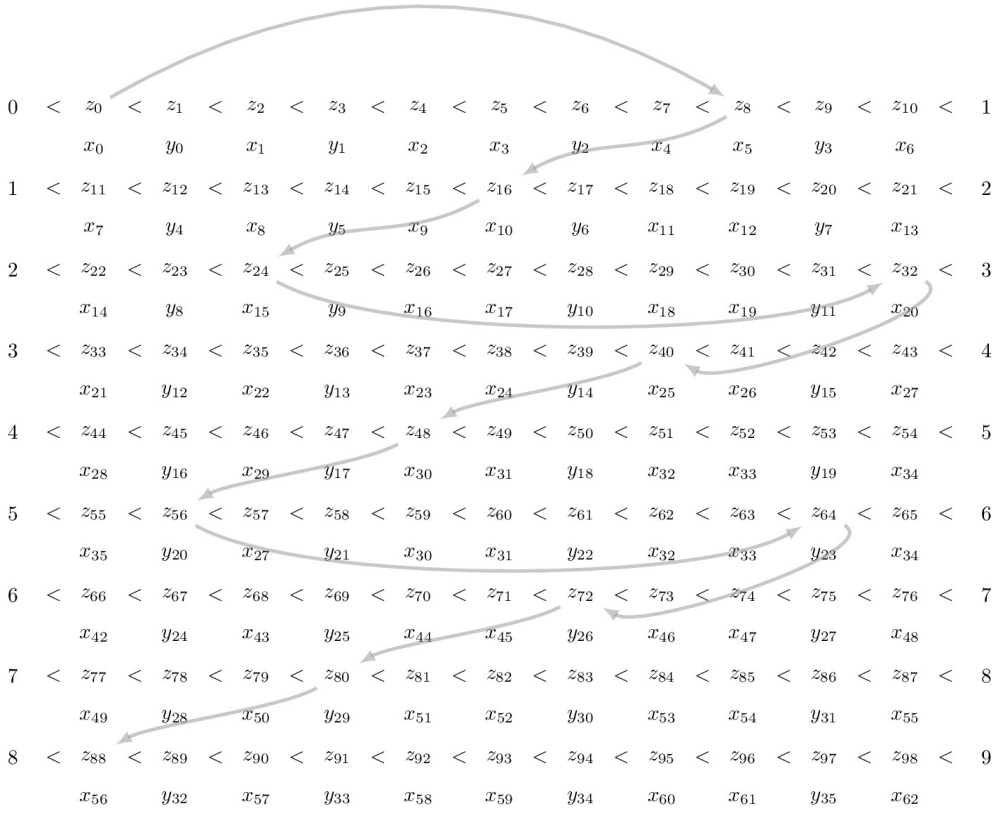

Fig. 3.6 *Lifted cycle of a* $8, 11$*-periodic orbit* (z_i) *split into two subsequences,* x_i *and* y_i*, as in the proof of Proposition* 47 *(see Example* 48 *for text).*

Next we construct the subsequence y_i*. Following* (3.19)*, we start with* $y_{pq'} = y_{20} = z_{1+pQ} = z_{56}$*. By further iterating, we add* p' *at the subindices of* y_i*:* $y_{20+ip'} = z_{56+iP}$ *for* $0 \le i < 4$*. This leads to the sequence* $y_{20} < y_{23} < \cdots < y_{29}$*. Finally, by lifting these points, that is, adding multiples of* 4 *to their subindices, we obtain the* $3, 4$*-ordered lifted cycle of a periodic orbit with rotation number* $3/4$*.*

Note that the next iterate of $y_{29} = z_{80}$ *becomes* z_{88}*, which satisfies* $\Pi(z_{80}) = z_0$*. Hence, after following the sequence* (y_i)*, the lifted cycle* (z_i) *switches back to the sequence* (x_i)*, and the symbolic sequence is repeated.*

In the rest of this section we study the rotation number for families of orientation preserving circle maps; that is, under the variation of the parameter c in condition C.3, which, by means of the change of variables given in (3.1), is equivalent to the parameter λ that parametrizes the curve in parameter space mentioned in Theorem 13.

Recalling Proposition 35 and Lemma 36, we already have that, when varying λ from 0 to 1, the rotation number (and hence the η-number) is continuous and monotonically increases from 0 to 1. In order to show that, moreover, it is a devil's staircase, we need to show that, in addition, it is constant for all values of λ except for a Cantor set of zero measure. This will come from the following theorem.

THEOREM 49 (see [34, Theorem 1′]). *Let* f *be a continuous monotonic non-decreasing map of the circle of degree one satisfying*

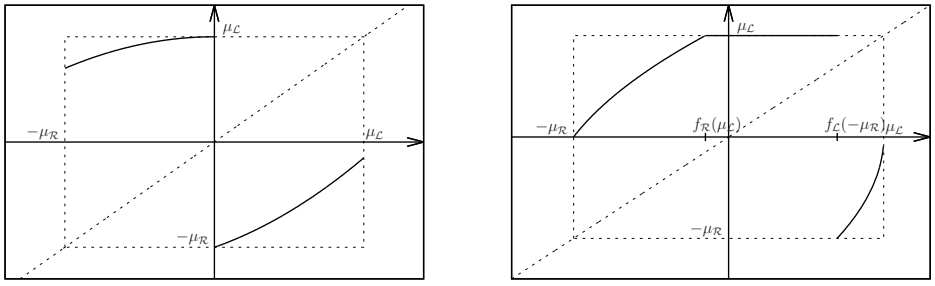

(a) (b)

Fig. 3.7 (a) *Piecewise-smooth map satisfying* C.1–C.4. (b) *Its inverse.*

(i) *f is constant on an interval $[a,b]$ and is of class C^1 outside $[a,b]$;*
(ii) $\inf_{y\notin[a,b]}(f'(y)) > 1$.

Let f_t be the map defined by $f_t(y) = f(y) + t$, $t \in [0,1]$. Let

$$E = \{t \mid f_t \text{ has irrational rotation number}\}.$$

Then $m(E) = 0$, where m denotes Lebesgue measure, and furthermore E has zero Hausdorff dimension.

Generalizations of the previous theorem can be found in [133, 123].

Finally, we show that Theorem 49 extends to a piecewise-smooth system of the form (2.1) satisfying h.1–h.3 and (i) of Theorem 13 (or an orientation preserving circle map satisfying C.1–C.4). This will prove that the η-number follows a devil's staircase.

LEMMA 50. *Let f be piecewise-smooth map as in* (2.1) *satisfying conditions* h.1–h.3 *and* (i) *of Theorem* 13*, and let $\bar{f}_\lambda$ be the orientation preserving circle map obtained after applying the change of variables* (3.1)*. Then, the set of values of λ for which the map $\bar{f}_\lambda$ has irrational rotation number consists of a Cantor set with zero measure.*

Proof. We note that the map $\bar{f}_\lambda$ is invertible. Let ϕ be as in (3.1) and define

$$\begin{aligned} a &:= \bar{f}(1^-) = \phi(f_{\mathcal{R}}(\mu_{\mathcal{L}})), \\ b &:= \bar{f}(0^+) = \phi(f_{\mathcal{L}}(-\mu_{\mathcal{R}})). \end{aligned}$$

Then the inverse $\bar{f}_\lambda^{-1}(y)$ is an increasing expanding map with a "hole" for $y \in [a,b]$ (see Figure 3.7(b)). As the trajectories of any point $x \in [0,1]$ by $\bar{f}$ do not reach the interval $[a,b]$, we can proceed as in the proof of Proposition 39 and complete the map $\bar{f}_\lambda^{-1}$ with a horizontal part equal to 1 for $y \in [a,b]$. This allows us to consider a map

$$g(y) = \begin{cases} \phi^{-1} \circ f_{\mathcal{R}}^{-1} \circ \phi(y) & \text{if } y \in [0,a], \\ 1 & \text{if } y \in [a,b], \\ \phi^{-1} \circ f_{\mathcal{L}}^{-1} \circ \phi(y) & \text{if } y \in [b,1], \end{cases}$$

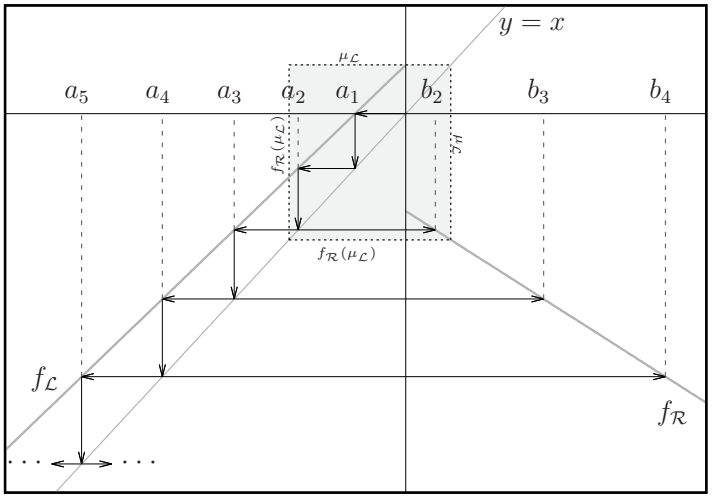

Fig. 4.1 *Piecewise-smooth map as in* (2.1) *satisfying* (ii) *of Theorem* 13 *and the sequences defined in* (4.2)–(4.3) *The gray box represents the absorbing interval* (4.1).

which coincides with $\bar{f}_\lambda^{-1}(y)$ for $y \notin (a, b)$. Let

$$\begin{array}{rccc} \gamma: & [0,1] & \longrightarrow & \mathbb{R}^2, \\ & \lambda & \longmapsto & (\mu_{\mathcal{L}}(\lambda), \mu_{\mathcal{R}}(\lambda)), \end{array}$$

be a parametrization satisfying H.1–H.3 of Theorem 13. Then, the interval $[a, b]$ smoothly varies from $[0, \phi(f_{\mathcal{L}}(-\mu_R(0)))]$ to $[\phi(f_{\mathcal{R}}(\mu_{\mathcal{L}}(1))), 1]$ when λ is varied from $\lambda = 0$ to $\lambda = 1$. Let $g_\lambda(y)$ be $g(y)$ after applying the reparametrization γ. Then we have

$$g_\lambda(y) = g_0(y) + \lambda,$$

and hence we can apply Theorem 49 and get the result. □

4. Nonorientable Case. The nonorientable (increasing-decreasing) case occurs under condition (ii) of Theorem 13. In this case, the map (2.1) becomes increasing for $x < 0$ and decreasing for $x > 0$.

As mentioned in sections 1 and 2.3, this situation was discussed in [80, section 3.3] and proven in full detail in [18]. For completeness, we provide in this section an overview of this proof.

We first observe (see Figure 4.1) that a map f as in (2.1) satisfying conditions h.1–h.3 and (ii) of Theorem 13 is a map on the interval

$$f : [f_{\mathcal{R}}(\mu_{\mathcal{L}}), \mu_{\mathcal{L}}] \longrightarrow [f_{\mathcal{R}}(\mu_{\mathcal{L}}), \mu_{\mathcal{L}}]. \tag{4.1}$$

We now consider the symbolic itineraries of periodic orbits for a map (4.1) under the aforementioned conditions. Clearly, when the parameters $\mu_{\mathcal{L}}$ and $\mu_{\mathcal{R}}$ are varied along the parametrization (2.7) satisfying H.1–H.3, the map (4.1) becomes negative for

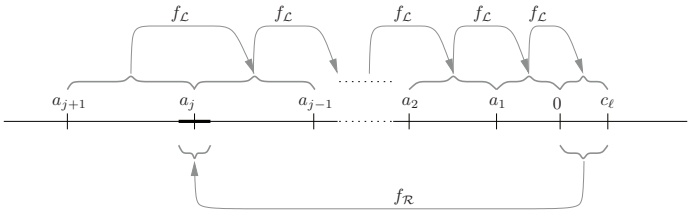

Fig. 4.2 *Backward and forward iterates of* $(0, \mu_{\mathcal{L}}]$. $f_{\mathcal{R}}((0, \mu_{\mathcal{L}}])$ *(dark segment) is smaller than* $f_{\mathcal{L}}^{-n}((0, \mu_{\mathcal{L}}])$ $\forall n$. *Therefore, at most one* a_j *can be reached by* $f_{\mathcal{R}}((0, \mu_{\mathcal{L}}])$.

$x \in [0, \mu_{\mathcal{L}}]$. Hence, periodic orbits cannot have symbolic itineraries with consecutive $\mathcal{R}$ symbols.

In order to show that the only possible itineraries for periodic orbits are of the form $\mathcal{L}^n\mathcal{R}$, we define the sequences of preimages of $x = 0$ by $f_{\mathcal{L}}$ and $f_{\mathcal{R}}$:

$$a_0 = 0, \quad a_n = f_{\mathcal{L}}^{-1}(a_{n-1}) \qquad \text{if } n > 0, \tag{4.2}$$

$$b_n = f_{\mathcal{R}}^{-1}(a_n) \qquad \text{if } n \geq n_0. \tag{4.3}$$

Due to the contractiveness of $f_{\mathcal{R}}$ and $f_{\mathcal{L}}$, we have that

$$\begin{aligned} \frac{m([a_{n+1}, a_n])}{m([a_n, a_{n-1}])} &> 1, \ n > 0, \\ \frac{m([b_n, b_{n+1}])}{m([b_{n-1}, b_n])} &> 1, \ n > n_0, \end{aligned} \tag{4.4}$$

where m indicates the length of the interval.

Then we have the following lemma.

LEMMA 51. *Suppose* f *is a map of type* (2.1) *fulfilling conditions* h.1–h.3 *and* (ii) *of Theorem* 13. *Then there exists at most one* a_j *(equiv.,* b_j*) such that* $a_j \in f_r((0, \mu_{\mathcal{L}}])$ *(equiv.,* $b_j \in (0, \mu_{\mathcal{L}}]$*).*

Proof. Recalling that $\mu_{\mathcal{L}} = f_{\mathcal{L}}(0)$, one has (see Figure 4.2)

$$\begin{aligned} [a_{n+1}, a_n] &= f_{\mathcal{L}}^{-1}([a_n, a_{n-1}]), \\ [a_1, 0] &= f_{\mathcal{L}}^{-1}([0, \mu_{\mathcal{L}}]). \end{aligned}$$

Using the property shown in (4.4), one has

$$m([0, c_m]) < m([a_{n+1}, a_n]) \quad \forall n,$$

and, since $f_{\mathcal{R}}$ is contracting one obtains

$$m(f_r((0, \mu_{\mathcal{L}}]) < m([a_{n+1}, a_n]) \quad \forall n.$$

Therefore, at most one a_n can be located in $f((0, \mu_{\mathcal{L}}])$. ∎

The next lemma tells us what symbolic itineraries are possible.

LEMMA 52 (see [18, Lemma 7]). *Let* f *be a piecewise-smooth map as considered above, and let* $x_0 < \cdots < x_n$, $x_i \in [f_{\mathcal{R}}(\mu_{\mathcal{L}}), \mu_{\mathcal{L}}]$, *be a periodic orbit. Then* $I_f(x_0) = (\mathcal{L}^n\mathcal{R})^\infty$.

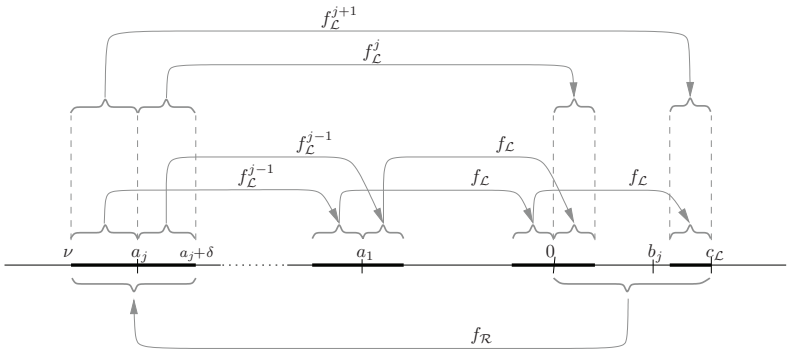

Fig. 4.3 *The interval $f_{\mathcal{R}}((0,\mu_{\mathcal{L}}])$ is split when it returns to the right domain.*

The proof of this lemma is in fact an extension of the arguments presented in [80, section 3.3] and it was provided in full detail in [18]. We repeat it here for completeness.

Proof. If f has periodic orbit of period $n \geq 2$, we necessarily have

$$f_{\mathcal{R}}((0,\mu_{\mathcal{L}}]) \cap [a_n, a_{n-1}] \neq \emptyset,$$

which can arise as a result of one of the following three situations (see Figures 4.2 and 4.3):

S.1. $a_{n-1} \in f_{\mathcal{R}}((0,\mu_{\mathcal{L}}])$.
S.2. $f_{\mathcal{R}}((0,\mu_{\mathcal{L}}]) \subset (a_n, a_{n-1})$.
S.3. $a_n \in f_{\mathcal{R}}((0,\mu_{\mathcal{L}}])$.

If S.1 holds, $b_{n-1} \in (0,\mu_{\mathcal{L}}]$ and

$$f_{\mathcal{L}}^{n} f_{\mathcal{R}} : [b_{n-1},\mu_{\mathcal{L}}] \longrightarrow [b_{n-1},\mu_{\mathcal{L}}],$$
$$f_{\mathcal{L}}^{n-1} f_{\mathcal{R}} : (0, b_{n-1}) \longrightarrow (0, b_{n-1}),$$

are continuous contracting functions which must have a unique (stable) fixed point. Therefore, two stable periodic orbits of types $\mathcal{L}^n\mathcal{R}$ and $\mathcal{L}^{n-1}\mathcal{R}$ coexist. Note that for $n = 2$ this proves also the existence of an $\mathcal{LR}$-periodic orbit.

In the second case (S.2), $b_{n-1} \notin (0,\mu_{\mathcal{L}}]$ ($[0,\mu_{\mathcal{L}}] \subset (b_{n-1}, b_n)$) and

$$f_{\mathcal{L}}^{n} f_{\mathcal{R}} : (0,\mu_{\mathcal{L}}] \longrightarrow (0,\mu_{\mathcal{L}}]$$

is a continuous contracting function which must also have a unique (stable) fixed point. In this case, there exists a unique periodic orbit of type $\mathcal{L}^n\mathcal{R}$ which is the unique attractor in $(0,\mu_{\mathcal{L}}]$.

Finally, if S.3 holds, replacing n by $n-1$ and arguing as in S.1, one has that a stable periodic orbit of type $\mathcal{L}^n\mathcal{R}$ coexists with a stable $\mathcal{L}^{n+1}\mathcal{R}$-periodic orbit. ∎

REMARK 53. *In contrast to all periodic orbits of type $\mathcal{L}^n\mathcal{R}$ with $n \geq 2$, the periodic orbit $\mathcal{LR}$ exists not only for $\mu_{\mathcal{R}} > 0$, but also for $\mu_{\mathcal{R}} \leq 0$. In that case, it coexists with the fixed point $\mathcal{R}$ ($\mathcal{L}^0\mathcal{R}$) (see Figure* 2.3*).*

REMARK 54. *Note that the transitions between cases* S.1*,* S.2*, and* S.3 *are given by border collision bifurcations where the respective periodic orbits are created or de-*

stroyed when they collide with the boundary $x = 0$. This defines the border collision bifurcation curves shown in Figure 2.3.

REMARK 55. *As is known, invariant objects of piecewise-smooth systems do not necessarily have to be separated by another invariant object. In this case, the coexistence of stable periodic objects may also be separated by the discontinuity (and its preimages).*

We focus finally on the bifurcation scenario shown in Figures 2.3–2.4 when the parameter λ of the parametrization (2.7) is varied.

Clearly, the successions a_n and b_n are continuous functions of the parameter γ. Hence, the transitions between S.1, S.2, and S.3 are as described in the proof of Lemma 52. That is, assume that for some γ S.1 holds; then two periodic orbits of types $\mathcal{L}^n\mathcal{R}$ and $\mathcal{L}^{n-1}\mathcal{R}$ coexist. Due to conditions H.1–H.3, when decreasing γ, $\mu_{\mathcal{L}}$ monotonically decreases to zero, whereas $\mu_{\mathcal{R}}$ increases toward some bounded value. Hence, a_{n-1} monotonically decreases to zero and, hence, as $m([0, \mu_{\mathcal{L}}]) < m([a_n, a_{n-1}])$, there exists some value of γ for which $f_{\mathcal{R}}([0, \mu_{\mathcal{L}}]) \subset (a_n, a_{n-1})$ and S.2 holds. Thus, the $\mathcal{L}^{n-1}\mathcal{R}$-periodic orbit bifurcates and only a $\mathcal{L}^n\mathcal{R}$-periodic orbit exists. Arguing similarly, by further decreasing γ, S.3 holds and an $\mathcal{L}^{n+1}\mathcal{R}$-periodic orbit bifurcates and coexists with the $\mathcal{L}^n\mathcal{R}$-periodic orbit.

As this occurs for all n, this argument proves the bifurcation scenario described in section 2.3.

5. Some Remarks on Piecewise-Smooth Expanding Maps. Frequently, both in applications and in theoretical studies, the contracting conditions required in the previous sections become too restrictive and one needs to deal with discontinuous maps exhibiting expansivenesses. However, such maps are shown to undergo similar bifurcations as those described in section 2. Examples can be found in the study of homoclinic bifurcations, such as the Lorenz system [75, 122, 113, 68, 70, 82] or in multiscale dynamics [99, 41], but also in power electronics [76, 30, 33, 116, 102, 87, 138, 19], biology [89, 106, 117], or economics [129], among others. Although the results summarized in Theorem 13 cannot be applied when the map lacks contractiveness, many of the results presented in sections 3 and 4 are still valid under the assumption of weak enough expansion. In this section we review possible scenarios involving the loss of contractiveness; that is, we focus on maps as in (2.1) satisfying

h′.1. $f_{\mathcal{L}}(0) = f_{\mathcal{R}}(0) = 0$,
h′.2. $0 < (f_{\mathcal{L}}(x))'$, $x \in (-\infty, 0)$,
h′.3. $0 < |(f_{\mathcal{R}}(x))'|$, $x \in (0, \infty)$,

where $f_{\mathcal{L}}$ and $f_{\mathcal{R}}$ may be expanding in all or part of their domains.

As before, we now distinguish between the orientable ($(f_{\mathcal{R}}(x))' > 0$) and nonorientable ($(f_{\mathcal{R}}(x))' < 0$) cases.

5.1. Orientable Case. Let us assume that conditions h′.1–h′.3 hold with $(f_{\mathcal{R}}(x))' > 0$. We focus on the case $\mu_{\mathcal{L}}, \mu_{\mathcal{R}} > 0$. We first note that, as long as

$$f_{\mathcal{L}}(-\mu_{\mathcal{R}}) \geq f_{\mathcal{R}}(\mu_{\mathcal{L}}), \tag{5.1}$$

the piecewise-smooth map f is still invertible. Hence, as in the contractive case, it can be reduced to a circle map of type (3.2) satisfying conditions C.1–C.4 by means of the smooth change of variables (3.1). Therefore, all the results in section 3 requiring only that the lift of the map is strictly increasing (which is given by conditions C.1–C.4) also hold as long as (5.1) is fulfilled. That is, recalling that λ parametrizes the curves in (2.7), we find that, for any $\lambda \in [0, 1]$ such that (5.1) is satisfied, we have that

(i) the rotation number (ρ) given in Definition 26 is well defined, unique, and increasing as a function of λ, and
(ii) if $\rho = p/q$, with p, q coprime, then f possesses a p, q-ordered periodic orbit whose symbolic sequence belongs to the Farey tree of symbolic sequences.

Note that (ii) is a consequence of Proposition 28, which requires only conditions C.1–C.4. However, as noted in Remark 34, when the maps $f_{\mathcal{L}}$ and $f_{\mathcal{R}}$ exhibit expansiveness, this periodic orbit might be not only repelling, but also nonunique. However, even in this case, all existing periodic orbits are p, q-ordered, as Proposition 38 still holds, and therefore they all must have the same symbolic dynamics.

Regarding the dynamics for $\rho \in \mathbb{R}\backslash\mathbb{Q}$, Proposition 39 does not hold if $f_{\mathcal{L}}$ or $f_{\mathcal{R}}$ are expanding. The main obstacle is due to the fact that Corollary 3.3 of [133] cannot be applied to show that $\omega(f)$ is a Cantor set (see the proof of Proposition 39). As a consequence, one needs additional conditions to determine whether $\omega(f)$ is a Cantor set or the whole circle.

In contrast to the purely contractive case, when $f_{\mathcal{L}}$ or $f_{\mathcal{R}}$ are expanding, the rotation number no longer necessaily follows a devil's staircase. Without the contracting assumption Theorem 49 does not hold and hence the set of values of λ for which the piecewise-smooth map does not possess any periodic orbit (the rotation number of the associated circle map is irrational) does not necessarily have zero measure. However, $\rho(\lambda)$ is still a nondecreasing continuous function.

As stated above, the crucial property that keeps most of the results shown in section 3 valid even when the map is expansive is the invertibility condition (5.1). When this is lost, the corresponding lift exhibits negative gaps and is not an increasing map. As a consequence, the rotation number becomes nonunique. Instead, one needs to deal with rotation intervals, coexistence of periodic orbits with different rotation numbers and symbolic dynamics, and positive entropy. Although there exist many results in the literature (see, for example, [2, 4, 3, 1, 5, 6, 86]), a precise description of the bifurcation scenarios becomes difficult under general assumptions that can be difficult to state.

5.2. Nonorientable Case. Let us now consider a class of maps as in (2.1) satisfying

h″.1. $f_{\mathcal{L}}(0) = f_{\mathcal{R}}(0) = 0$,
h″.2. $0 < (f_{\mathcal{L}}(x))'$, $x \in (-\infty, 0)$,
h″.3. $0 > |(f_{\mathcal{R}}(x))'|$, $x \in (0, \infty)$,

where $f_{\mathcal{L}}$ and $f_{\mathcal{R}}$ may be expanding in all or part of their domains.

Unlike in the orientable case, such a map fulfilling conditions h″.1–h″.3 is always invertible for $\mu_{\mathcal{L}}, \mu_{\mathcal{R}} > 0$. However, even in the linear case, when the map $f_{\mathcal{L}}$ or $f_{\mathcal{R}}$ is expanding, the bifurcation scenario may change significantly (see, for example, [15]). On one hand, one may lose pairwise uniqueness of periodic orbits, as this relies on Brower's fixed point theorem needing contractiveness. Hence, expansiveness may lead to the absence of periodic orbits or to the existence of several unstable orbits. On the other hand, whenever they exist, symbolic sequences associated with periodic orbits may be very different. Obviously, provided that $\mu_{\mathcal{R}} > 0$, $f_{\mathcal{R}}(x) \leq 0$ if $x \geq 0$ and hence no symbolic sequence can contain two consecutive $\mathcal{R}$'s. Then, symbolic sequences may contain blocks of the form $\mathcal{L}^n\mathcal{R}\mathcal{L}^m$, with $n \neq m$. Numerical studies have also shown evidence of the existence of chaotic attractors, whose associated symbolic dynamics are similar [12, 13, 14].

However, if $f_{\mathcal{R}}$ is expansive but $f_{\mathcal{L}}$ is not, it may happen that, for $\mu_{\mathcal{L}} > 0$ smaller than a certain quantity (which may depend on $\mu_{\mathcal{R}}$), the number of iterations

performed in the negative domain might be large enough to compensate for the expanding dynamics of $f_{\mathcal{R}}$. This is because the smaller $\mu_{\mathcal{L}} > 0$, the larger the number of iterations needed to return to the right domain. Hence, when this occurs, a period incrementing bifurcation takes place but only involves periodic orbits of type $\mathcal{L}^n\mathcal{R}$ and $\mathcal{L}^{n+1}\mathcal{R}$ with n large enough, which are attracting despite $f_{\mathcal{R}}$ being expanding.

6. Maximin Itineraries and Piecewise-Smooth Maps in $\mathbb{R}^n$.

6.1. Introduction. Often, due to the complexity of real applications, one-dimensional maps are not enough and one needs to consider maps in higher dimensions. Examples of two- (or higher-) dimensional piecewise-smooth maps are found as Poincaré (or stroboscopic) maps in nonautonomous mechanical systems [37, 109, 44], but they are also found in power electronics [45, 29, 114, 67, 138, 7], control theory [46, 135, 137, 51], mathematical neuroscience or biology [126, 127, 57, 103, 125, 117]. Piecewise-smooth maps in higher dimensions are also obtained when studying Filippov flows in $\mathbb{R}^n$ ($n \geq 3$) [49]; they appear as half-return Poincaré maps and become discontinuous close to grazing and Hopf bifurcations [56, 108, 94, 112, 39, 38].

As occurs with homoclinic bifurcations for smooth flows (see sections 1, 2.2, and 7.1.1 for references), symbolic dynamics of piecewise-smooth discontinuous maps in $\mathbb{R}^n$ may help us to determine the number of loops performed by periodic orbits in different zones of the state space [108, 38]. There exist some general results for piecewise-smooth continuous maps on the plane [120, 119, 55] (see [118] for a recent survey). Unfortunately, although some efforts have been made to exhaustively investigate specific systems [42, 69, 29, 93, 48, 54, 57, 7] there exist very few items of literature providing general results on piecewise-smooth discontinuous maps in higher dimensions.

6.2. Maximin/Minimax Properties of Symbolic Sequences. We continue at the symbolic level by defining the *maximin/minimax* properties of symbolic sequences in $W_{p,q}$.

DEFINITION 56. *We say that a symbolic sequence* $\mathbf{x} \in W_{p,q}$ *is*

- *maximin if*

$$\min_{0\leq k\leq q}\left(\sigma^k(\mathbf{x})\right) = \max_{\mathbf{y}\in W_{p,q}}\left(\min_{0\leq k\leq q}\left(\sigma^k(\mathbf{y})\right)\right),$$

- *minimax if*

$$\max_{0\leq k\leq q}\left(\sigma^k(\mathbf{x})\right) = \min_{\mathbf{y}\in W_{p,q}}\left(\max_{0\leq k\leq q}\left(\sigma^k(\mathbf{y})\right)\right).$$

As was proven in [32, 61] using different techniques, the maximin and minimax properties are equivalent; that is, one has the following theorem.

THEOREM 57 (see [32, 61]). *Let* $\mathbf{x} \in W_{p,q}$. *Then* $\mathbf{x}$ *is maximin if and only if it is minimax.*

EXAMPLE 58. *Let* $\eta = 2/5$. *Up to cyclic permutations, there exist only two periodic sequences in* $W_{2,5}$, *which are represented by the minimal and maximal blocks*

$$\mathcal{L}^3\mathcal{R}^2 = \min_{0\leq k\leq q}\left(\sigma\left(\mathcal{L}^3\mathcal{R}^2\right)\right),$$
$$\mathcal{R}^2\mathcal{L}^3 = \sigma^2(\mathcal{L}^3\mathcal{R}^2) = \max_{0\leq k\leq q}\left(\sigma\left(\mathcal{L}^3\mathcal{R}^2\right)\right)$$

and

$$\mathcal{L}^2\mathcal{R}\mathcal{L}\mathcal{R} = \min_{0\leq k\leq q}\left(\sigma\left(\mathcal{L}^2\mathcal{R}\mathcal{L}\mathcal{R}\right)\right),$$
$$\mathcal{R}\mathcal{L}\mathcal{R}\mathcal{L}^2 = \sigma^2(\mathcal{L}^2\mathcal{R}\mathcal{L}\mathcal{R}) = \max_{0\leq k\leq q}\left(\sigma\left(\mathcal{L}^2\mathcal{R}\mathcal{L}\mathcal{R}\right)\right).$$

Then, as

$$\mathcal{L}^2\mathcal{R}\mathcal{L}\mathcal{R} > \mathcal{L}^3\mathcal{R}^2,$$
$$\mathcal{R}\mathcal{L}\mathcal{R}\mathcal{L}^2 < \mathcal{R}^2\mathcal{L}^3,$$

the sequence $\mathcal{L}^2\mathcal{R}\mathcal{L}\mathcal{R}$ is minimax and maximin.

The following result tells us that all the sequences shown in the Farey tree of symbolic sequences (see Figure 3.1(b)) (given by consecutive concatenation) are maximin (minimax).

PROPOSITION 59 (see [59, Proposition II.2.4-3]). *Let $p/q < p'/q'$ be the irreducible form of two Farey neighbors, and let $\mathbf{x}^\infty \in W_{p,q}$ and $\mathbf{y}^\infty \in W_{p',q'}$ be two maximin sequences, with $\mathbf{x} \in \{\mathcal{L},\mathcal{R}\}^q$ and $\mathbf{y} \in \{\mathcal{L},\mathcal{R}\}^{q'}$ minimal blocks. Then, the sequences given by the concatenation of these two blocks $(\mathbf{xy})^\infty \in W_{(p+p')/(q+q')}$ is maximin.*

We provide a sketch of the proof given in [59].

Proof. One first sees that $\mathbf{x}$ and $\mathbf{y}$ belong to the same domain of some deflation, i.e., a map which collapses blocks contained in sequences as follows:

$$\pi = \begin{cases} \mathcal{L}^{n+1}\mathcal{R} \longrightarrow \mathcal{R}, \\ \mathcal{L}^n\mathcal{R} \longrightarrow \mathcal{L}. \end{cases}$$

Then one proceeds by induction using that $\pi(\mathbf{x})$ and $\pi(\mathbf{y})$ are maximin, as is $\pi^{-1}(\mathbf{xy})$. See [59] for more details. ∎

The following result tells us that maximin symbolic sequences are also well-ordered sequences (see Definition 43).

THEOREM 60 (see [61]). *Let $\mathbf{x} \in W_{p,q}$. Then $\mathbf{x}$ is maximin if and only if it is p,q-ordered.*

The previous result was also proven in [32] for the one-dimensional case using endomorphisms of the circle. Moreover, note that for the one-dimensional case we also already have such a result using the Farey tree of symbolic sequences and Ptoposition 47. However, the previous theorem was proven using only symbolic properties.

6.3. Quasi-contractions and Piecewise-Smooth Maps in $\mathbb{R}^n$. In this section we review some results for piecewise-smooth maps in $\mathbb{R}^n$ regarding their symbolic properties.

We consider maps defined in some suitable open set $U \subset \mathbb{R}^n$,

$$f : U \longrightarrow U,$$

of the following form. Let

$$h : \mathbb{R}^n \longrightarrow \mathbb{R}$$

be some differentiable function. We then consider a switching manifold $\Sigma \subset U$ as

$$\Sigma = h^{-1}(0) \cap U,$$

which splits U into two subsets

$$E_{\mathcal{L}} = \{x \in U \,|\, h(x) < 0\} \quad \text{and} \quad E_{\mathcal{R}} = \{x \in U \,|\, h(x) > 0\}.$$

Then we write such maps as

$$f : E_{\mathcal{L}} \cup E_{\mathcal{R}} \longrightarrow U,$$

defined as

$$f(x) = \begin{cases} f_{\mathcal{L}}(x) & \text{if } x \in E_{\mathcal{L}}, \\ f_{\mathcal{R}}(x) & \text{if } x \in E_{\mathcal{R}}, \end{cases} \tag{6.1}$$

where

$$f_{\mathcal{L}} : \mathbb{R}^n \longrightarrow \mathbb{R}^n \quad \text{and} \quad f_{\mathcal{R}} : \mathbb{R}^n \longrightarrow \mathbb{R}^n$$

are two smooth maps.

Note that (6.1) does not define f in Σ. Similarly, as for the one-dimensional case, we consider that f is two-valued for $x \in \Sigma$:

$$f(\Sigma) = f_{\mathcal{L}}(\Sigma) \cup f_{\mathcal{R}}(\Sigma).$$

Given $x \in U$ one can also define its symbolic itinerary by f as in (2.2) by considering the encoding

$$a(x) = \begin{cases} \mathcal{R} & \text{if } x \in E_{\mathcal{R}}, \\ \mathcal{L} & \text{if } x \in E_{\mathcal{L}}. \end{cases} \tag{6.2}$$

Note that if $\mathbf{x}$ is the symbolic sequence associated with a periodic orbit of a map of type (6.1), then it still makes sense to consider its η-number, $\eta(\mathbf{x})$, as defined in (2.6). However, we will not provide a definition of the rotation number for such maps, although the classical definition through the lift for the one-dimensional case (see Definition 26) could be extended by considering f as a map onto an n-dimensional cylinder (see section 8 for a discussion).

Below we will assume that f is a contraction (or that f contracts), which means that there will exist some $0 < k < 1$ such that, for any $P, Q \in U$, we have

$$\|f(P) - f(Q)\| < k\|P - Q\|. \tag{6.3}$$

We then recover the result presented by Gambaudo and Tresser in [63], which states the possible number of periodic orbits and their possible symbolic properties.

THEOREM 61 (see [63]). *Let f be a piecewise-smooth map as defined above satisfying*

1. *$f^n(\Sigma) \cap \Sigma = \emptyset$ for all $n > 0$,*
2. *f contracts.*

Then

(i) *f admits 0, 1, or 2 periodic orbits;*
(ii) *any periodic orbit of f has an itinerary which is maximin; and*
(iii) *if f has two periodic orbits, then their itineraries belong to $W_{p,q}$ and $W_{p',q'}$ and p/q and p'/q' are Farey neighbors.*

Before discussing it, we remark that the theorem above was indeed stated for a more general type of piecewise-defined map called a *quasi-contraction*. For completeness we provide such a definition in its original form.

DEFINITION 62 (quasi-contraction). *Let (E_0, d_0) and (E_1, d_1) be two metric spaces and $F_0 \in E_0$ and $F_1 \in E_1$ two points. Then a map*

$$f : E_0 \cup E_1 \longrightarrow E_0 \cup E_1 \tag{6.4}$$

is a quasi-contraction if there exists $0 \leq k \leq 1$ such that for any $(i,j) \in \{0,1\}^2$, $\forall P, Q \in f^{-1}(E_j) \cap E_i$, $\forall R \in f^{-1}(E_{1-j}) \cap E_i$, one has
(i) *$d_j\left(f(P), f(Q)\right) \leq k d_i\left(P, Q\right)$,*
(ii) *$d_j\left(f(P), F_j\right) + d_{1-j}\left(f(R), F_{1-j}\right) \leq k d_i(P, R)$.*

Despite the arbitrary dimension of the metric spaces E_i, Theorem 61 was stated while bearing in mind the one-dimensional case. This is why the two points F_i were considered instead of manifolds. If considering $E_0 = (-\infty, 0]$ and $E_1 = [0, \infty)$, F_i would be chosen to coincide with the boundary: $F_0 = F_1 = 0$ and we would recover the type of one-dimensional map considered in (2.1).

Theorem 61 was proved in [60] (Theorem A) for f a quasi-contraction with constant k satisfying $0 \leq k \leq 1/2$. The version given in [63] not only extends to the case of quasi-contractions with $0 \leq k \leq 1$, but it also provides more information; we give here a mutilated version which is sufficient for our purposes. It can be easily seen that both proofs also hold when one replaces the points F_i by closed sets whose iterates are all kept connected. This is why we required condition 1 in Theorem 61 instead of considering general quasi-contractions. Finally, note that if f is a contraction in terms of (6.3), then it is automatically a quasi-contraction when choosing $E_0 = E_{\mathcal{L}}$, $E_1 = E_{\mathcal{R}}$, and the switching manifold Σ instead of the points F_i and using

$$d(f(P), \Sigma) = \min_{x \in \Sigma} d\left(x, f(P)\right)$$

(similarly for $f(Q)$). Hence, conditions 1 and 2 in Theorem 61 replace the quasi-contracting condition for the particular case of the type of piecewise-smooth map that we are considering here.

Note that, obviously, Theorem 61 also holds when considering f a quasi-contraction for some $F_0 = F_1 \in \Sigma$. However, this becomes much more restrictive than conditions 1 and 2.

We now analyze Theorem 61 analogously with the results summarized in section 2 for the one-dimensional case.

We first note that the case in which only a periodic orbit exists is analogous to the orientation preserving case for one-dimensional maps. Although this is not stated in the result itself, it comes from the proof provided in [60, 63]. By Proposition 59, such a periodic orbit must have a symbolic sequence which belongs to the Farey tree of symbolic sequences (see Figure 3.1(b)).

As also occurs for the one-dimensional case, when the map is nonorientable one finds the possibility of coexistence between two periodic orbits. As before, this comes from the proof provided in [60, 63]. Let β and Δ be the symbolic sequences of those

periodic orbits. From (iii) $(\beta)^\infty \in W_{p,q}$ and $(\Delta)^\infty \in W_{p',q'}$ with p/q and p'/q' Farey neighbors in some Farey sequence $\mathcal{F}_n$ (see Definition 15). Assume that $q' > q$; then they are neighbors at the Farey sequence of order q' and p/q is a Farey parent of p'/q'. Then, if $p/q > p'/q'$, by Proposition 47 we know that $\Delta = \alpha\beta$, where α is the Farey sequence of the other Farey parent of p'/q'. Then, by going down through the Farey tree of symbolic sequence, we find two sequences, σ and γ, such that $\beta = \sigma^n\gamma$ and $\Delta = \sigma^{n+1}\gamma$ for some $n \geq 0$.

Then, by considering the iterates of the maps $f_{\mathcal{L}}$ and $f_{\mathcal{R}}$ given by the sequences σ and γ (see the example below), the periodic orbits of the original map collapse to periodic orbits of the form $\mathcal{L}^{n+1}\mathcal{R}$ and $\mathcal{L}^n\mathcal{R}$ (or $\mathcal{L}\mathcal{R}^{n+1}$ and $\mathcal{L}\mathcal{R}^n$) for the composite map, which corresponds to the coexistence of periodic orbits given at the period incrementing structure.

EXAMPLE 63. *Assume that we are in the situation described in Theorem* 61(iii) *with two periodic orbits with symbolic sequences in* $W_{3,8}$ *and* $W_{2,5}$ *coexisting. From section* 3.4 *we know that, with the notation above, these symbolic sequences are* $\Delta = \left(\mathcal{L}^2\mathcal{R}\right)^2\mathcal{L}\mathcal{R}$ *and* $\beta = \mathcal{L}^2\mathcal{R}\mathcal{L}\mathcal{R}$. *By going down through the tree, we find* $\alpha = \sigma = \mathcal{L}^2\mathcal{R}$ *and* $\gamma = \mathcal{L}\mathcal{R}$. *Then, for two properly chosen sets* $\tilde{E}_{\mathcal{L}}$ *and* $\tilde{E}_{\mathcal{R}}$ *(see below for more details), the map*

$$\tilde{f}(x) = \begin{cases} \tilde{f}_{\mathcal{L}}(x) := f_{\mathcal{L}}^2 \circ f_{\mathcal{R}}(x) & \text{if } x \in \tilde{E}_{\mathcal{L}}, \\ \tilde{f}_{\mathcal{R}}(x) := f_{\mathcal{L}} \circ f_{\mathcal{R}}(x) & \text{if } x \in \tilde{E}_{\mathcal{R}} \end{cases}$$

possesses two periodic orbits with symbolic sequences $\mathcal{L}^2\mathcal{R}$ *and* $\mathcal{L}\mathcal{R}$, *which correspond to those predicted by the period incrementing bifurcation structure.*

Note that the sets $\tilde{E}_{\mathcal{L}}$ *and* $\tilde{E}_{\mathcal{R}}$ *need to be properly found. This can be done by noting that the iterates by* $\tilde{f}_{\mathcal{L}}$ *or* $\tilde{f}_{\mathcal{R}}$ *provide the boundaries of the domains of attraction between the points of the periodic orbits. See* [26] *and* [25] *for explicit examples.*

Finally, the third case for which f has no periodic orbit corresponds to quasi-periodic dynamics. In this case f possesses an attracting Cantor set (see [63]).

REMARK 64. *Theorem* 61 *does not provide any information about the bifurcation structures that may appear when adding parameters to* f. *As will be discussed in section* 8, *similar structures to the period adding structure may appear, although it is not guaranteed that all periodic orbits in the tree may exist for some parameter.*

6.4. Maximin Approach for the One-Dimensional Case. In this section we present an alternative path to proving the period adding structure for one-dimensional piecewise-smooth maps. More precisely, we show that one can use Theorem 61 after Gambaudo et al. to identify sequences in the Farey tree of symbolic sequences with the itineraries of one-dimensional orientation preserving circle maps. By using the concept of maximin sequences instead of p, q-ordered sequences (see Definition 43), this approach provides stronger results than the one presented in section 3.4, as they give more information about the symbolic sequences. In particular, given the rotation number, p/q, the maximin property enables us to obtain the proper symbolic itinerary of a periodic orbit without constructing the whole Farey tree of symbolic sequences up to level q. Instead, one needs to find the symbolic sequence in $W_{p,q}$ that verifies the maximin/minimax condition (see Definition 56).

However, a downside to these advantages is the requirement for contraction, since, as was remarked in section 5, many of the results gained through circle maps (see sections 3.3 and 3.4) also hold for expansive maps. Moreover, the proof of Theorem 61,

especially for $1/2 \leq k \leq 1$ (see [63]), is significantly more difficult than those in section 3.4.

This alternative proof is as follows. From Proposition 28 we obtain that, under conditions C.1–C.4, if the rotation number is rational, p/q, then a periodic orbit exists. When adding the assumption of contraction, Theorem 61 holds and, due to uniqueness of the rotation number, it tells us that a unique periodic orbit must exist; moreover, its symbolic itinerary is maximin. Then, from Proposition 59, we get that its symbolic sequence belongs to the Farey tree of symbolic sequences. Once we find that the symbolic itineraries of orientation preserving circle maps belong to the Farey tree of symbolic sequences, we proceed as in section 3.4 to study the bifurcation structure when the parameters c or λ are varied, in order to prove (i) in Theorem 13.

7. Applications. In section 7.1 we present examples for which Theorem 13 provides a full description of their dynamics.

In the first example (section 7.1.1), we will focus on the codimension-two bifurcation given by the simultaneous collision of two periodic orbits of a one-dimensional discontinuous map with the boundary. By applying Theorem 13 we generalize the results obtained in [61, 60] by providing a precise description of the bifurcation scenario.

In the second example (section 7.1.2) we deal with a system of control theory. We consider a first order system with a stable equilibrium point. In order to stabilize this system at another value, we perform a nonsmooth control action based on relays, which is a well-known technique in engineering control, known as *sliding-mode* control. Theorem 13 holds and describes the dynamics of this system.

In section 7.1.3 we consider a generic *integrate-and-fire* system subject to a periodic forcing. Such a system consists of a hybrid model widely used in neuroscience. We show how Theorem 13 can be applied to describe not only its dynamics, but also relevant biological properties such as the *firing-rate* under parameter variation. There exist in the literature other examples of neuron models from which one derives a piecewise-smooth discontinuous map such that Theorem 13 (ii) holds; see, for example, [84, 127].

Section 7.2 is devoted to illustrating the results revisited in section 6 for higher-dimensional piecewise-smooth maps. We first consider a higher order system controlled with relays (section 7.2.1). This represents an extension of the example shown in section 7.1.2.

In section 7.2.2 we consider a ZAD-controlled DC-DC boost converter. We show how symbolic dynamics given by the maximin periodic orbits describe how the saturation of a pulse width modulation process is distributed along periodic cycles.

7.1. One-Dimensional Examples.

7.1.1. Codimension-Two Border Collision Bifurcations. Our first example consists of a generic dynamical system given by a piecewise-smooth map for which, under variation of two parameters, two periodic orbits transversally collide with the boundary. In two-dimensional parameter space, this is given by the crossing of two border collision bifurcation curves and is hence a codimension-two bifurcation point. Below we will show that the map (2.1) is a normal form for such a bifurcation, and hence the dynamics are given by Theorem 13.

This bifurcation codimension-two bifurcation was described as a *gluing bifurcation* [61, 60] when studying *figure of eight* or *butterfly* homoclinic bifurcations for three-dimensional flows. Assuming the existence of a strong stable direction it is

possible to reduce the dynamics near a homoclinic bifurcation to a two-dimensional system. Then, one considers a first-return Poincaré map, which turns out to be a one-dimensional discontinuous map of the form given in (2.1) (see [11, 122] for more details). Depending on the orientability of the stable and unstable manifolds, this map exhibits different configurations with respect to its monotonicity near the discontinuity (see [66, 80]), leading to the cases (i)–(iv) of Theorem 16 and Remark 14.

Later, in the context of simulations of piecewise-smooth dynamical systems, this codimension-two bifurcation was rediscovered and called a *big bang* bifurcation [22] as, depending on the monotonicity properties of the map, it may involve the emergence of an infinite number of bifurcation curves from the codimension-two bifurcation point in the parameter space. Such points organize the dynamics around them and have been frequently reported in simulations of piecewise-smooth maps [20, 21, 23, 24, 17, 27, 28, 65, 78].

From the piecewise-smooth perspective, the bifurcation scenarios that appear around such a codimension-two bifurcation point have been recently reconsidered in [64]. There, the authors distinguish between cases (i) and (ii) of Theorem 13. For the period adding structure (case (i)) the authors use renormalization arguments to demonstrate the existence of periodic orbits nested between regions in the parameter space. However, the proof is not complete, as it is not shown that this occurs only for regions containing periodic orbits with Farey neighbors rotation numbers, which is the main result. Regarding period incrementing (case (ii)), the authors of [64] repeat the proof provided in [18] and in section 4.

We now start with the example. We will show that, under nondegeneracy conditions, after collapsing the colliding periodic orbits to fixed points and performing a reparametrization, such a bifurcation can be reduced to the study of a map of the form of (2.1) under variation of the parameters $\mu_{\mathcal{L}}$ and $\mu_{\mathcal{R}}$.

Assume that we have a dynamical system given by

$$x_{n+1} = f(x_n), \tag{7.1}$$

with

$$f(x) = \begin{cases} f_{\mathcal{L}}(x; a, b) & \text{if } x < 0, \\ f_{\mathcal{R}}(x; a, b) & \text{if } x > 0, \end{cases} \tag{7.2}$$

where $a, b \in \mathbb{R}$ are two parameters.

Assume that system (7.1) possesses two periodic orbits $(x_0, \dots, x_{n-1})$ and $(y_0, \dots, y_{m-1})$, $x_i, y_i \in \mathbb{R}$, satisfying

$$\begin{aligned} f(x_i) &= x_{i+1},\ 0 \le i < n-1, \\ f(x_{n-1}) &= x_0 \end{aligned}$$

and

$$\begin{aligned} f(y_i) &= y_{i+1},\ 0 \le i < m-1, \\ f(y_{m-1}) &= y_0. \end{aligned}$$

Note that the periodic orbits are indexed by dynamical and not spatial order, which implies that we do not necessarily have $x_i < x_{i+1}$ and $y_i < y_{i+1}$.

Assume that these periodic orbits undergo right and left border collision bifurcations at two curves, $b = \xi_x(a)$ and $b = \xi_y(a)$, in the parameter space (a, b), respectively; i.e., there exist unique integers $k_x \in \{0, \dots, n-1\}$ and $k_y \in \{0, \dots, m-1\}$

such that, for any $a \in \mathbb{R}$,

$$\lim_{b \to \xi_x(a)^+} x_{k_x} = 0^-,$$
$$\lim_{b \to \xi_y(a)^-} y_{k_y} = 0^+.$$

Assume that these two curves intersect transversally at some point (a^*, b^*). In order to write the map (7.2) in the form of (2.1) for parameter values near (a^*, b^*) we first need to consider a higher iterate of f so that these periodic orbits become fixed points. To this end, let $\mathbf{x} = (\mathbf{x}_1, \ldots, \mathbf{x}_n) \in \{\mathcal{L}, \mathcal{R}\}^n$ and $\mathbf{y} = (\mathbf{y}_1, \ldots, \mathbf{y}_m) \in \{\mathcal{L}, \mathcal{R}\}^m$ be symbolic sequences such that

$$I_f(x_{k_x}) = \mathbf{x}^\infty,$$
$$I_f(y_{k_y}) = \mathbf{y}^\infty.$$

Next, consider the iterates

$$\bar{f}_{\mathcal{L}} = f_{\mathbf{x}_1} \circ f_{\mathbf{x}_2} \circ \cdots \circ f_{\mathbf{x}_n}(x),$$
$$\bar{f}_{\mathcal{R}} = f_{\mathbf{y}_1} \circ f_{\mathbf{y}_2} \circ \cdots \circ f_{\mathbf{y}_m}(x)$$

and the map

$$\bar{f}(x; a, b) = \begin{cases} \bar{f}_{\mathcal{L}}(x; a, b) & \text{if } x < 0, \\ \bar{f}_{\mathcal{R}}(x; a, b) & \text{if } x > 0. \end{cases}$$

Note that one can always find proper shifts of the sequences $\mathbf{x}$ and $\mathbf{y}$ such that the domains of $\bar{f}_{\mathcal{L}}$ and $\bar{f}_{\mathcal{R}}$ become $x < 0$ and $x > 0$, respectively. Indeed, this occurs when the sequences $\mathbf{x}$ and $\mathbf{y}$ start with the points x_{k_x} and y_{k_y}, respectively. See [26] and [25] for explicit examples.

These compositions collapse the periodic orbits of the maps $f_{\mathcal{L}}$ and $f_{\mathcal{R}}$ to fixed points of $\bar{f}_{\mathcal{L}}$ and $\bar{f}_{\mathcal{R}}$, respectively. There then exists a neighborhood $(a^*, b^*) \in \mathcal{U} \subset \mathbb{R}^2$ which is split into four subsets in which $\bar{f}$ has two fixed points, a unique positive fixed point, a unique negative fixed point, and no fixed points, respectively. These fixed points undergo simultaneous border collision bifurcations at $(a, b) = (a^*, b^*)$ in such a way that the map $\bar{f}$ becomes continuous at $x = 0$ for these parameter values.

We now perform a reparametrization along the curves ξ_x and ξ_y. The nondegeneracy conditions given by their transversal intersection tell us that, to first order, the new parameters will be equivalent to the offset parameters $\mu_{\mathcal{L}}$ and $\mu_{\mathcal{R}}$ of the general map given in (2.1). This reparametrization is given by

$$\begin{array}{rccc} \phi: & \mathbb{R}^2 & \longrightarrow & \mathbb{R}^2, \\ & (\mu_{\mathcal{L}}, \mu_{\mathcal{R}}) & \longmapsto & (a^* + \mu_{\mathcal{L}} + \mu_{\mathcal{R}}, \xi_x(a^* + \mu_{\mathcal{L}}) + \xi_y(a^* + \mu_{\mathcal{R}})), \end{array}$$

which maps the axes $\mu_{\mathcal{L}} = 0$ and $\mu_{\mathcal{R}} = 0$ to the bifurcation curves $(a, \xi_x(a))$ and $(a, \xi_y(a))$, respectively. Expanding in powers of x, $\mu_{\mathcal{L}}$, and $\mu_{\mathcal{R}}$ around $(x, \mu_{\mathcal{L}}, \mu_{\mathcal{R}}) = (0, 0, 0)$, we obtain

$$\begin{aligned} \bar{f}_{\mathcal{L}}(x; \phi(\mu_{\mathcal{L}}, \mu_{\mathcal{R}})) = \bar{f}_{\mathcal{L}}(x; \phi(0, 0)) \\ + D_{\mu_{\mathcal{L}}, \mu_{\mathcal{R}}} \bar{f}_{\mathcal{L}}(x; \phi(\mu_{\mathcal{L}}, \mu_{\mathcal{R}}))\Big|_{\substack{x=0 \\ \mu_{\mathcal{L}}=0 \\ \mu_{\mathcal{R}}=0}} \cdot \begin{pmatrix} \mu_{\mathcal{L}} \\ \mu_{\mathcal{R}} \end{pmatrix} \\ + O(\mu_{\mathcal{L}} x, \mu_{\mathcal{R}} x, , \mu_{\mathcal{L}} \mu_{\mathcal{R}}, x^2, \mu_{\mathcal{L}}^2, \mu_{\mathcal{R}}^2), \end{aligned}$$

$$D_{\mu_{\mathcal{L}},\mu_{\mathcal{R}}}\left(\bar{f}_{\mathcal{L}}(x;\phi(\mu_{\mathcal{L}},\mu_{\mathcal{R}}))\right)\Big|_{\substack{x=0\\ \mu_{\mathcal{L}}=0\\ \mu_{\mathcal{R}}=0}} = D_{\mu_{\mathcal{L}},\mu_{\mathcal{R}}}\left(f(0;\phi(\mu_{\mathcal{L}},\mu_{\mathcal{R}}))\right)\Big|_{\substack{\mu_{\mathcal{L}}=0\\ \mu_{\mathcal{R}}=0}}$$
$$= \left(\frac{\partial}{\partial\mu_{\mathcal{L}}}\bar{f}_{\mathcal{L}}(0;\phi(\mu_{\mathcal{L}},\mu_{\mathcal{R}})),\ \frac{\partial}{\partial\mu_{\mathcal{R}}}\bar{f}_{\mathcal{L}}(0;\phi(\mu_{\mathcal{L}},\mu_{\mathcal{R}}))\right)\Big|_{\substack{\mu_{\mathcal{L}}=0\\ \mu_{\mathcal{R}}=0}},$$

$$\frac{\partial}{\partial\mu_{\mathcal{L}}}\bar{f}(0;\phi(\mu_{\mathcal{L}},\mu_{\mathcal{R}}))\Big|_{\substack{\mu_{\mathcal{L}}=0\\ \mu_{\mathcal{R}}=0}} = \frac{\partial}{\partial\mu_{\mathcal{L}}}\bar{f}_{\mathcal{L}}(0;\phi(\mu_{\mathcal{L}},0))_{\mu_{\mathcal{L}}=0}\cdot\mu_{\mathcal{L}} + O(\mu_{\mathcal{L}}^2,\mu_{\mathcal{R}}^2,\mu_{\mathcal{L}}\mu_{\mathcal{R}}),$$

$$\frac{\partial}{\partial\mu_{\mathcal{R}}}\bar{f}(0;\phi(\mu_{\mathcal{L}},\mu_{\mathcal{R}}))\Big|_{\substack{\mu_{\mathcal{L}}=0\\ \mu_{\mathcal{R}}=0}} = \left(\frac{\partial}{\partial\mu_{\mathcal{R}}}\underbrace{\bar{f}_{\mathcal{L}}(0;\phi(0,\mu_{\mathcal{R}}))}_{=0}\right)_{|\mu_{\mathcal{R}}=0}\cdot\mu_{\mathcal{R}} + O(\mu_{\mathcal{L}}^2,\mu_{\mathcal{R}}^2,\mu_{\mathcal{L}}\mu_{\mathcal{R}}).$$

Proceeding similarly for $\bar{f}_{\mathcal{R}}$ we find that there exist constants $\delta_{\mathcal{L}},\delta_{\mathcal{R}}\in\mathbb{R}$ such that the map $\bar{f}$ can be written, close to $(x,\mu_{\mathcal{L}},\mu_{\mathcal{R}})=(0,0,0)$, as

$$\bar{f}(x;\mu_{\mathcal{L}},\mu_{\mathcal{R}}) = \begin{cases} \delta_{\mathcal{L}}\mu_{\mathcal{L}} + \bar{f}_{\mathcal{L}}(x;a^*,b^*) + h.o.t., \\ \delta_{\mathcal{R}}\mu_{\mathcal{R}} + \bar{f}_{\mathcal{R}}(x;a^*,b^*) + h.o.t., \end{cases} \tag{7.3}$$

where $h.o.t. = O(\mu_{\mathcal{L}}x,\mu_{\mathcal{R}}x,\mu_{\mathcal{L}}\mu_{\mathcal{R}},\mu_{\mathcal{L}}^2,\mu_{\mathcal{R}}^2)$. Hence, taking $\delta_{\mathcal{L}}\mu_{\mathcal{L}}$ and $\delta_{\mathcal{R}}\mu_{\mathcal{R}}$ as new parameters, the first order terms of the map $\bar{f}$ given in (7.3) are of the form given in map (2.1) and satisfy condition h.1.

Finally, if the two periodic orbits $(x_0,\dots,x_{n-1})$ and $(y_0,\dots,y_{m-1})$ are attracting, the maps $\bar{f}_{\mathcal{L}}$ and $\bar{f}_{\mathcal{R}}$ become contracting near $x=0$. This implies that conditions H.1–H.3 are satisfied and Theorem 13 can be applied to system (7.3) for $\delta_{\mathcal{L}}\mu_L L$ and $\delta_{\mathcal{R}}\mu_{\mathcal{R}}$ small. Hence, depending on the signs of $(\bar{f}_{\mathcal{L}})'(0^-;a^*,b^*)$ and $(\bar{f}_{\mathcal{R}})'(0^+;a^*,b^*)$, we will obtain situations (i)–(iv) of Theorem 13 and Remark 14.

The periodic orbits of the original map f given in (7.2) are obtained from those of $\bar{f}$ given by Theorem 13 by replacing each point x_i with

$$\begin{aligned} x_i &\longrightarrow (x_i, f_{\mathbf{x}_1}(x_i), f_{\mathbf{x}_2}\circ f_{\mathbf{x}_1}(x_i),\dots, f_{\mathbf{x}_n}\circ\cdots\circ f_{\mathbf{x}_1}(x_i)) && \text{if } x_i<0,\\ x_i &\longrightarrow (x_i, f_{\mathbf{y}_1}(x_i), f_{\mathbf{y}_2}\circ f_{\mathbf{y}_1}(x_i),\dots, f_{\mathbf{y}_m}\circ\cdots\circ f_{\mathbf{y}_1}(x_i)) && \text{if } x_i>0. \end{aligned}$$

The corresponding symbolic dynamics for each periodic orbit of the map f sequence will be obtained by replacing

$$\begin{aligned} \mathcal{L} &\longrightarrow \mathbf{x},\\ \mathcal{R} &\longrightarrow \mathbf{y}. \end{aligned}$$

7.1.2. First Order Sliding-Mode Controlled System with Relays. In our next example we consider a first order one-dimensional system,[2]

$$\dot{y} = f(y), \tag{7.4}$$

[2]In this section we abuse notation and use f to refer to a field rather than a map.

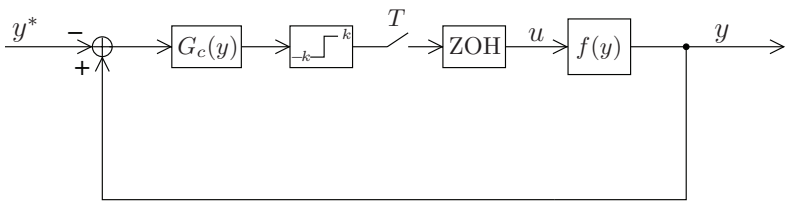

Fig. 7.1 *Schematic representation of the control strategy based on sliding and relays.*

such that f is monotonically decreasing and has a simple zero at the origin, $f(0) = 0$, which is a stable equilibrium point of system (7.4). We generalize the results presented in [50] for a linear system and in [51] for second order linear system.

We wish to stabilize system (7.4) at a new equilibrium point y^* by performing a *control* action $u(t, y)$:

$$\dot{y} = f(y) + u(t, y). \tag{7.5}$$

Obviously, as f is monotonically decreasing, one can always choose u constant (*open loop* control) such that $f(y^*)+u = 0$. However, if u is chosen to depend on the current value of the system, y (*closed loop* control), then such a control action will be robust to small perturbations and inaccuracies of the modeling. The type of control that we will consider is based on the *sliding-mode*. This consists of performing a particular action when $y > y^*$ and another action otherwise, so that solutions are "pushed" toward y^*. In a hardware setting this is implemented by means of relays. The term *sliding* comes from the generalization to higher dimensions, $y \in \mathbb{R}^n$. In this case, one defines a surface $\sigma(y) = 0$ and the desired behavior consists of a sliding motion along this surface. To achieve this, one acts similarly depending on whether $\sigma(y) > 0$ or $\sigma(y) < 0$.

In addition, we will also assume that u depends on t, as we will perform a periodic sampling in order to discretize the system and use a digital control.

Altogether, we will show that the dynamics of such a system are given by a piecewise-smooth map of the form (2.1) satisfying h.1–h.3. Hence, Theorem 13 can be applied to accurately describe the dynamics of system (7.5).

We now describe how the control action u is defined and how we derive the piecewise-smooth map.

The control is schematically illustrated in Figure 7.1. As one can see, this is a closed loop system, whose input is the desired new equilibrium y^*. The error $y - y^*$ becomes the input of a controller represented by the module G_c. In this work we will assume a proportional control only. Indeed, there will be no loss of generality if we set its gain equal to 1 (it does not perform any action), provided that the next module, the relay, will also have some tunable gain.

The output of the controller is pushed to a relay of gain k. This means that, depending on the sign of its input, the relay will set its output to k or $-k$ depending on whether $y - y^* > 0$ or $y - y^*$, respectively.

The parameter T is the sampling period, which digitalizes the system. At every time T the switch closes and provides a new sample to the ZOH (zero order hold) block. This block holds the received value until it is changed at the next sampling.

The input of the module $f(y)$ thus becomes a piecewise-constant function:

$$u(t) = \begin{cases} -k & \text{if } y(nT) - y^* < 0, \\ k & \text{if } y(nT) - y^* > 0 \end{cases} \tag{7.6}$$

for $t \in [nT, (n+1)T)$.

In order to obtain stable sliding motion we require $f(y^*)+k < 0$ and $f(y^*)-k > 0$; that is, we require the field (7.5) to point toward y^*. Note that by imposing the opposite requirement one obtains unstable sliding, as both fields point in the opposite direction to y^* This condition can be generalized to higher dimensions in terms of the so-called *equivalent control* and Lie derivatives (see [131] for details). In our case, this implies that necessarily $k < 0$, although note that this is not a sufficient condition.

The fact that the variable y is periodically sampled suggests that the dynamics of system (7.5) with u given by (7.6) can be better represented by a map

$$y_{n+1} = P(y_n),$$

where $y_k = y(nT)$ is the value of y at the nth sample, and P is the stroboscopic (time-T return map) of system (7.5), (7.6). It becomes the piecewise-smooth map

$$P(y) = \begin{cases} P_{\mathcal{L}}(y) := \varphi(T; y; -k) & \text{if } y < y^*, \\ P_{\mathcal{R}}(y) := \varphi(T; y; k) & \text{if } y > y^*, \end{cases}$$

where $\varphi(t; y; k)$, satisfying $\varphi(0; y; k) = y$, is the flow associated with the system $\dot{y} = f(y)+k$. Note that $P(y)$ is a smooth map as regular as the flow φ if $y > y^*$ or $y < y^*$, and it is discontinuous at $y = y^*$ if $k \neq 0$.

Due to the monotonicity of f the maps $P_{\mathcal{L}}$ and $P_{\mathcal{R}}$ are contracting for $y \in \mathbb{R}$. Moreover, they are both increasing (they preserve orientation), as they are given by integration of an autonomous differential equation. Finally, if $k < 0$ is such that the sliding condition is satisfied, we find that $P_{\mathcal{L}}(y^*) > y^*$ and $P_{\mathcal{R}}(y^*) < y^*$, and P undergoes a negative gap at $y = y^*$. Due to the monotonicity of f, this will occur for any $k < 0$ such that $|k|$ is large enough. Let us now fix $k < 0$ and study the dynamics of the system under variation of the parameter y^*, the desired output. If $|k|$ is large enough such that the sliding condition is satisfied, then the attracting fixed points $y_{\mathcal{L}}$ and $y_{\mathcal{R}}$ of $P_{\mathcal{L}}$ and $P_{\mathcal{R}}$, respectively, are virtual:

$$y_{\mathcal{R}} < y^* < y_{\mathcal{L}}.$$

Therefore, when y^* is varied, these fixed points may undergo border collision bifurcations when

$$y_{\mathcal{R}}(k_{\mathcal{R}}) = y^*,$$
$$y_{\mathcal{L}}(k_{\mathcal{L}}) = y^*.$$

After applying the change of variables $z \longmapsto y - y^*$, the one-parameter family of maps $\tilde{P}_{y^*}(z) := P(z + y^*) - y^*$ is in the class of maps given by applying the reparametrization (2.7) to the piecewise-smooth map (2.1) satisfying (i) of Theorem 13. Hence, when varying y^* from $y_{\mathcal{R}}$ to $y_{\mathcal{L}}$, one observes periodic orbits following the period adding structure.

As this occurs for any $k < 0$, if y^* is close enough to the equilibrium point of system (7.4), $y = 0$, the origin of the parameter space (y^*, k) represents a codimension-two bifurcation point. This is shown in Figure 7.2 for the linear system

$$f(y) = ay$$

with $a < 0$. The bifurcation curves shown in Figure 7.2(a) are straight lines due to the linearity of the system.

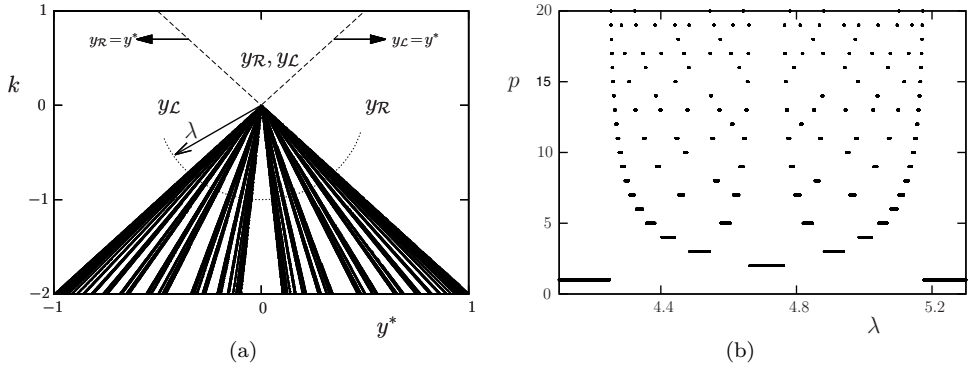

Fig. 7.2 (a) *Codimension-two bifurcation point of the adding type for the system* $f(y) = -0.2y$ *and* $T = 0.1$. *The fixed points* y_i *are labeled in the regions where they are feasible, and, as dashed lines, the curves where they undergo border collision bifurcation. In* (b) *we show the periods* p *of the periodic orbits found along the pointed curve in* (a), *which is parametrized by the angle* λ.

The parameter region where one finds the period adding structure is the one for which the system performs the proper tracking. Its asymptotic dynamics consists of periodic orbits bouncing around the desired equilibrium point whose amplitude can be made arbitrarily small by choosing T small enough. For any chosen y^*, there exists a maximal value of k for which the system performs tracking. However, although for larger values of k the system oscillates between the desired values y^*, not only the amplitude of the periodic motion grows, but also its symbolic dynamics, which can be modified by properly tuning k such that a certain behavior is achieved (or avoided). For example, one may wish to minimize the time for which the system's output exceeds y^*, and hence one may choose symbolic sequences with low rotation number.

7.1.3. Hybrid Systems in Biology. In this example we consider a generalization of an integrate-and-fire system, a widely used neuron model. It consists of a hybrid system given by[3]

$$\dot{x} = f(x), \tag{7.7}$$

$f \in C^\infty(\mathbb{R})$, subject to the reset condition

$$x = \theta \longrightarrow x = 0; \tag{7.8}$$

that is, whenever the variable x reaches a certain threshold θ, it is reset to a certain

[3] As in section 7.1.2, in this section we abuse notation and use f to refer to a field rather than a map.

value, which we assume to be $x = 0$. This emulates a *spike* of a neuron (action potential).

Typically, the dynamics of system (7.7)–(7.8) are studied by means of the so-called *firing* map [89], which is a Poincaré map onto the threshold $x = \theta$. However, when system (7.7) is periodically forced, this map is not optimal for obtaining general results, as one has to explicitly compute the time when spikes occur.

In this example we present the results reported in [74], where it was shown that, when a periodic forcing is considered, it is more convenient to study the system by means of the stroboscopic map (time-T return map, with T the period of the forcing).

Following [74], in this example we periodically force system (7.7) by means of a square wave function, which models a pulsatile stimulus of a neuron. That is, we consider the system

$$\dot{x} = f(x) + I(t), \quad x \in \mathbb{R}, \tag{7.9}$$

with $f(x) \in C^\infty(\mathbb{R})$ and $I(t)$ the T-periodic function

$$I(t) = \begin{cases} A & \text{if } t \in (nT, nT + dT], \\ 0 & \text{if } t \in (nT + dT, (n+1)T], \end{cases} \tag{7.10}$$

where $A > 0$ and $0 \leq d \leq 1$ is the so-called *duty* cycle. We are interested in the bifurcation structure in the parameter space given by the amplitude of the pulse, A, and its duty cycle, d. We refer the reader to [73] for the study of the bifurcation structures in this parameter space under frequency variation of the input, $1/T$.

Let us assume that system (7.7) satisfies the following conditions:

A.1. It possesses an attracting equilibrium point

$$0 < \bar{x} < \theta.$$

A.2. $f(x)$ is a monotonic decreasing function in $[0, \theta]$:

$$f'(x) < 0, \ x \in [0, \theta].$$

Note that conditions A.1–A.2 guarantee that spikes can only occur when the pulse is active ($I = A$) with A large enough; otherwise, when the pulse is off, trajectories are attracted by the equilibrium point $\bar{x}$.

As mentioned above, in contrast to typical approaches using the firing map, we use the stroboscopic map

$$\begin{array}{rccc} \mathfrak{s}: & [0,\theta) & \longrightarrow & [0,\theta), \\ & x_0 & \longmapsto & \phi(T; x_0), \end{array} \tag{7.11}$$

where $\phi(t; x_0)$ is the solution of system (7.8)–(7.10) with initial condition $\phi(0; x_0) = x_0$. Note that the flow ϕ is well defined, although it is discontinuous when spikes occur. The stroboscopic map $\mathfrak{s}$ is a piecewise-smooth map. To see this, we define the sets

$$\begin{aligned} S_n = \Big\{ & x_0 \in [0,\theta) \text{ s.t. } \phi(t; x_0) \text{ reaches the threshold } \{x = \theta\} \\ & n \text{ times for } 0 \leq t \leq T \Big\}, \ n \geq 0. \end{aligned} \tag{7.12}$$

When restricted to S_n, the map $\mathfrak{s}$ becomes a concatenation of maps consisting of integrating the system $\dot{x} = f(x) + A$ and performing resets for $t \in [0, dT]$, and then integrating the system $\dot{x} = f(x)$ for $t \in (dT, T]$. Recall that, as mentioned above,

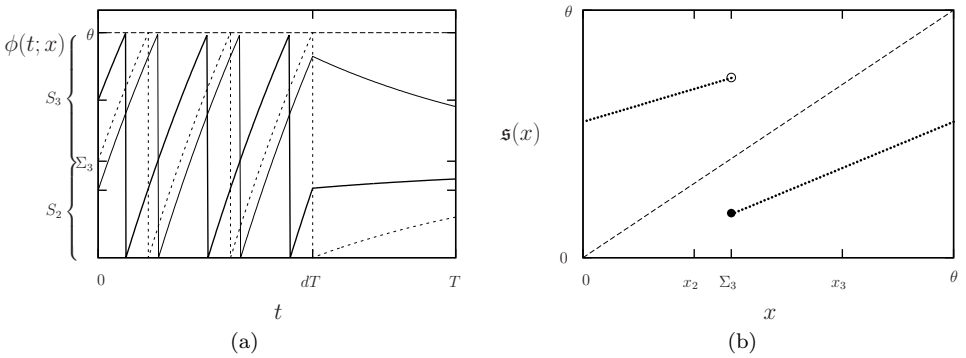

Fig. 7.3 (a) *The trajectories of system* (7.8)–(7.10). *Dashed line: trajectory with* Σ_3 *as initial condition. Thick line: trajectory with* $x_3 > \Sigma_3$ *as initial condition, which spikes three times. Normal line: trajectory with* $x_2 < \Sigma_3$ *as initial condition, which spikes two times.* (b) *The stroboscopic map, continuity at* $x = \Sigma_3$.

no resets can occur for $t \in (dT, T)$. Hence, $\mathfrak{s}$ is smooth in the interior of S_n, as it is given by a certain composition of smooth maps; however, $\mathfrak{s}$ is discontinuous at the boundaries of S_n, because of the following fact. Let us define $\Sigma_n \in S_n$ as the initial condition that leads to a trajectory exhibiting its nth spike precisely when the pulse is deactivated:

$$\phi(dT; \Sigma_n) = \theta.$$

Note that, as the flow $\phi(t; x_0)$ of system (7.8)–(7.10) is well defined if it exists, such an initial condition is unique and can only exist for certain n. Notice also that, if there exists $\Sigma_n \in (0, \theta)$, then points above Σ_n exhibit n spikes, whereas points below exhibit $n-1$ spikes (see Figure 7.3).

As a consequence, the map $\mathfrak{s}$ undergoes at most one discontinuity, at $x = \Sigma_n$, and points to its left and right exhibit $n-1$ and n spikes, respectively, for $t \in [0, dT]$. As shown in [74], for any n the discontinuity Σ_n satisfies

$$\frac{d\Sigma_n}{dA} < 0, \tag{7.13}$$

and hence it decreases monotonically with A. By increasing this parameter, the discontinuity Σ_n collides with $x = 0$, disappears, and a new discontinuity, Σ_{n+1}, appears at $x = \theta$. At this moment, the system changes from exhibiting $n-1$ and n spikes to exhibiting n and $n+1$ spikes (see [74] for more details).

If we compute the lateral images of $\mathfrak{s}$ at these values, they are given by

$$\mathfrak{s}(\Sigma_n^-) = \varphi(T - dT; \theta; 0),$$
$$\mathfrak{s}(\Sigma_n^+) = \varphi(T - dT; 0; 0),$$

where $\varphi(t; x_0; A)$ is the flow associated with the system $\dot{x} = f(x) + A$, with initial condition $\varphi(0; x_0; A) = x_0$. Note that $\mathfrak{s}(\Sigma_n^-) > \mathfrak{s}(\Sigma_n^+)$ and hence $\mathfrak{s}$ undergoes a negative gap at $x = \Sigma_n$ (see Figure 7.3). Clearly, as the reset action and the integration of the flow provide orientation preserving maps, $\mathfrak{s}$ is an increasing map.

The stroboscopic map $\mathfrak{s}$ is always contracting in $[0, \Sigma_n)$. However, it is contractive in $[\Sigma_n, \theta)$ only if n is large enough (see [74, Lemma 3.4]).

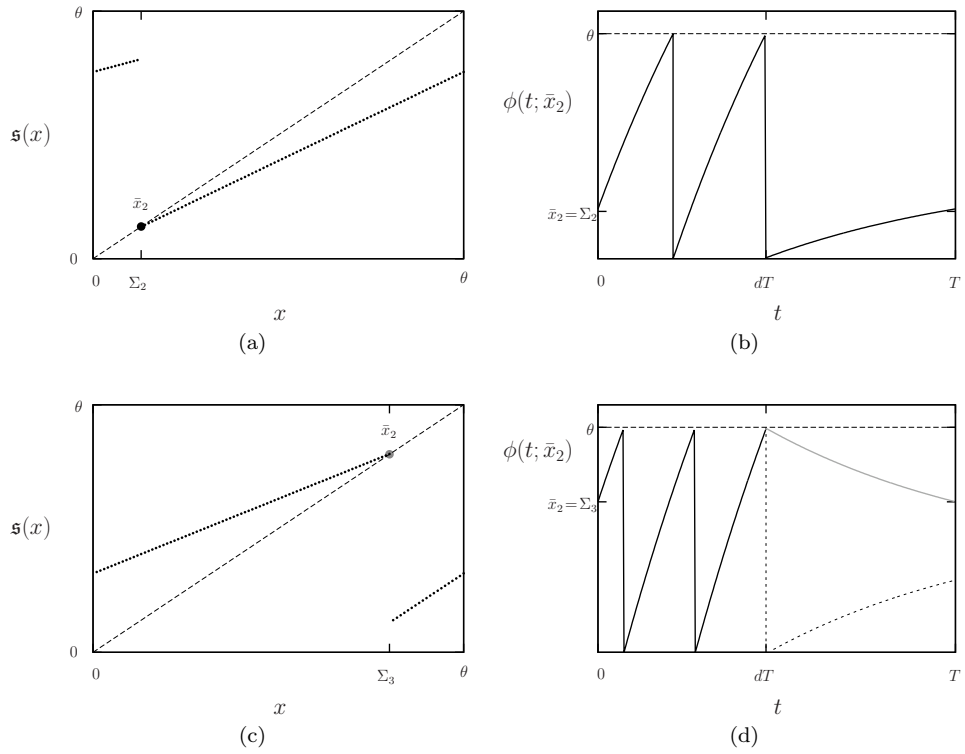

Fig. 7.4 (a) *Fixed point $\bar{x}_2$ colliding with the boundary Σ_2 for $A = A_2^{\mathcal{R}}$.* (b) *T-periodic orbit for $A = A_2^{\mathcal{R}}$.* (c) *Fixed point $\bar{x}_2$ colliding with the boundary Σ_3 for $A = A_3^{\mathcal{L}}$.* (d) *T-periodic orbit for $A = A_3^{\mathcal{L}}$. Note that the periodic orbit in* (d) *should exhibit a reset at $t = dT$; this is why it is plotted in gray.*

One can see [74] that, for any $n \geq 0$ and $d \in (0,1)$, there exists a range of values of A, $(A_n^{\mathcal{R}}, A_n^{\mathcal{L}})$, for which $\mathfrak{s}$ possesses a unique fixed point, $\bar{x}_n \in S_n \subset (0,\theta)$. These fixed points undergo border collision bifurcations at $A = A_n^{\mathcal{R}}$ and $A = A_n^{\mathcal{L}}$ when colliding with the boundaries Σ_n and Σ_{n-1}, respectively:

$$A \longrightarrow A_n^{\mathcal{L}}(d) \Longrightarrow \bar{x}_n \longrightarrow (\Sigma_n)^-, \ n \geq 0,$$
$$A \longrightarrow A_n^{\mathcal{R}}(d) \Longrightarrow \bar{x}_n \longrightarrow (\Sigma_{n-1})^+, \ n \geq 1$$

(see Figure 7.4 for $n = 2$).

As given in (7.13), Σ_n monotonically decreases with A. Hence, for any $n \geq 0$, one can apply a reparametrization such that $\mathfrak{s}$ can be written as in (2.1) and A becomes equivalent to the parameter λ in (2.7). Therefore, if n is large enough such that $\mathfrak{s}$ is contracting, conditions H.1–H.3 and (i) of Theorem 13 are satisfied, and $\mathfrak{s}$ exhibits a period adding bifurcation structure under variation of $A \in [A_n^{\mathcal{L}}, A_{n+1}^{\mathcal{R}}]$ (see [74, Proposition 3.4]). As this occurs for any $d \in (0,1)$, the parameter space $(d, 1/A)$ possesses an infinite number of period adding structures. These are shown in Figure 7.5 for a linear system for $f(x)$. The black regions shown in Figure 7.5(a) correspond to fixed points; for example, for parameter values at points B, C, D, and E there exist the fixed points $\bar{x}_0 \in S_0$, $\bar{x}_1 \in S_1$, $\bar{x}_2 \in S_2$, and $\bar{x}_3 \in S_3$, respectively. As one can see from the periods of the periodic orbits shown in Figure 7.5(b), there

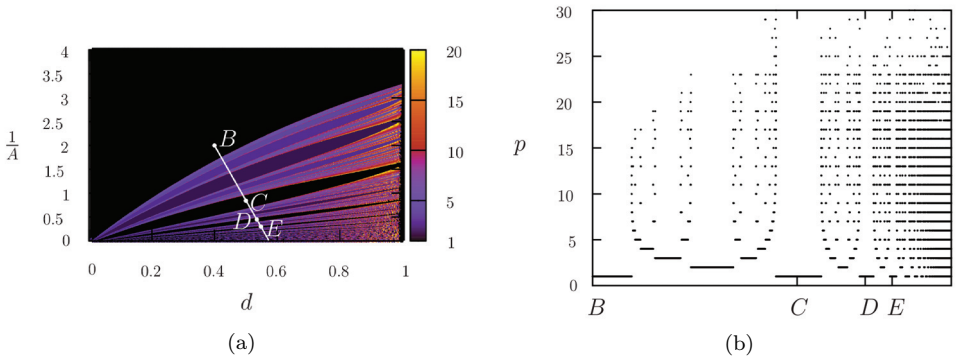

Fig. 7.5 (a) *Bifurcation scenario in the* $(d, 1/A)$ *parameter space for the map* $\mathfrak{s}$ *with* $f(x) = -0.5x + 0.2$, $\theta = 1$, *and* $T = 1.9$. *The colors refer to the periods of the periodic orbits found by simulating the system.* (b) *Period of the periodic orbits found along the the line shown in* (a).

exist period adding structures nested between the regions of existence of fixed points, as predicted by Theorem 13. Note, however, that the adding structure between B and C (involving the discontinuity Σ_1) is not complete. This is due to the fact that $n = 1$ is not large enough to guarantee the contractiveness of $\mathfrak{s}$ on the interval $[\Sigma_1, \theta)$. As the map $\mathfrak{s}$ (after proper reparametrization and change of variables) satisfies conditions C.1–C.4, Proposition 28 can be used to provide the existence of a periodic orbit. However, due to the expansiveness, periodic orbits may be unstable and not unique, and hence they are not easy to detect by direct simulation.

One of the most interesting properties that one can derive from the period adding structures comes from the symbolic dynamics and the rotation numbers associated with these periodic orbits. Specifically, consider parameter values such that $\Sigma_n \in (0, \theta)$ and suppose that the stroboscopic map has a periodic orbit. As explained above, on each iteration of the stroboscopic map the flow can perform $n - 1$ or n spikes. We assign a symbolic sequence to this periodic orbit by setting its kth symbol to be $\mathcal{L}$ if this number is $n - 1$ and $\mathcal{R}$ if it is n. Hence, when divided by the period of the periodic orbit, this becomes the so-called *firing number*, which is the average number of spikes per iteration of the stroboscopic map. Therefore, after recalling Definition 11 and Corollary 46, it is easy to see that the rotation number (ρ) and the firing number (η) satisfy the relationship

$$\eta = n + \rho,$$

where n is such that the periodic orbit steps around the discontinuity Σ_{n+1}, $n \geq 0$. Therefore, by Theorem 13, under parameter variation, the firing number follows a devil's staircase growing from 0 to infinity (see Figure 7.6). When divided by T (period of the periodic forcing $I(t)$), the firing number becomes the so-called *firing rate*, which is the asymptotic average number of spikes per unit time. Hence, it also follows a devil's staircase when varying parameters A and d along lines such as the one shown in Figure 7.5(a). However, as most of the bifurcation structures shown in Figure 7.5(a) do not qualitatively depend on T, when this parameter is varied the firing rate follows a devil's staircase with pieces of hyperbolas as steps. This is shown in Figure 7.6(b), and more details on this frequency analysis can be found in [73].

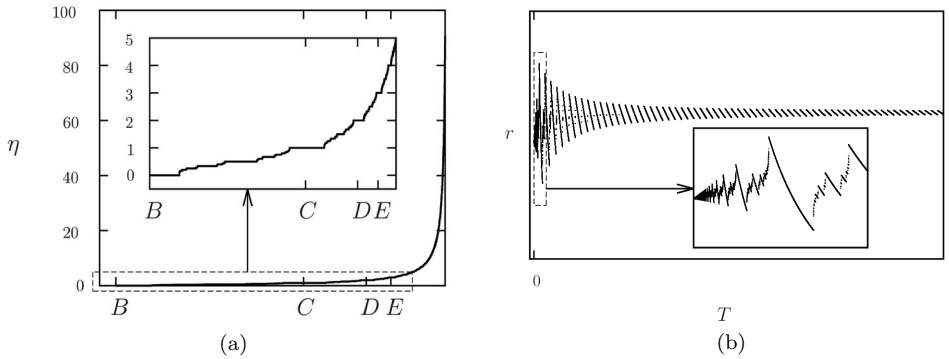

Fig. 7.6 (a) *Firing number along the line shown in Figure* 7.5(a)*, for the same system.* (b) *Firing rate under variation of* T.

7.2. Examples in Higher Dimensions.

7.2.1. Higher Order Sliding-Mode Controlled System with Relays. In this example we recover the results presented in [51], which extend the example shown in section 7.1.2 to higher order linear systems.

Assume that system (7.4) is a linear system of order n with an equilibrium point at the origin. In this case, due to the linearity, the block representing the open loop system in Figure 7.1 can be replaced by its Laplace transform

$$G_s(s) = \frac{b}{U(s)},$$

where $U(s)$ is a polynomial of the form

$$U(s) = s^n + a_{n-1}s^{n-1} + \cdots + a_0, \tag{7.14}$$

which we assume to have real negative roots only.

The system can be written in terms of a differential equation as

$$y^{n)} + a_{n-1}y^{n-1)} + \cdots + a_0 y = bu(t), \tag{7.15}$$

with $y(t), a_i, b \in \mathbb{R}$, $y^{i)} = d^i y/dt^i$, and where $u(t) \in \mathbb{R}$ is the input of the system. We wish to design a control such that the output of the system, $y(t) \in \mathbb{R}$, is stabilized around a new equilibrium point y^*; that is, $y(t) \simeq y^*$ and $y^{i)} \simeq 0$ for $1 \leq i \leq n$. To achieve this, we consider a two-step control. A first action is taken by a classic controller given by the block $G_c(s)$, which we assume to be of the form

$$G_c(s) = 1 + c_1 s + \cdots + c_{n-1}s^{n-1}.$$

The second part will be given by a relay of gain k. Then the desired motion becomes

$$y - y^* + c_1 y^{1)} + \cdots + c_{n-1}y^{n-1)} = 0.$$

Equivalently, system (7.15) can be written as a first order n-dimensional system as

$$\dot{\bar{y}} = A\bar{y} + Bu, \tag{7.16}$$

where

$$\bar{y} = (y, y^{1)}, \ldots, y^{n-1)}) \in \mathbb{R}^n,$$

and A and B become

$$A = \begin{pmatrix} 0 & 1 & 0 & \ldots & & 0 \\ 0 & 0 & 1 & & & 0 \\ \vdots & \vdots & & \ddots & & \\ 0 & 0 & \ldots & 0 & 1 & 0 \\ -a_0 & -a_1 & \ldots & & -a_{n-2} & -a_{n-1} \end{pmatrix}, \qquad B = \begin{pmatrix} 0 \\ \vdots \\ 0 \\ b \end{pmatrix};$$

we wish to stabilize the system around the point

$$\bar{y} = \begin{pmatrix} y^* \\ 0 \\ \vdots \\ 0 \end{pmatrix}.$$

After the T-periodic sampling, the input u becomes constant on the intervals $t \in [iT, (i+1)T)$:

$$u = \begin{cases} -k & \text{if } \sigma(\bar{y}) < 0, \\ k & \text{if } \sigma(\bar{y}) > 0, \end{cases} \tag{7.17}$$

where

$$\sigma(\bar{y}) = y - y^* + c_1 y^{1)} + \cdots + c_{n-1} y^{n-1)}. \tag{7.18}$$

We wish to stabilize the system close to the switching surface

$$\sigma(\bar{y}) = 0.$$

The fact that the polynomial $U(s)$ possesses real negative roots only ensures us that, for $k = 0$, system (7.16) possesses an attracting node at the origin. In order to find proper values of k such that there exists dynamics satisfying $\sigma(\bar{y}(t)) = 0$, we impose (stable) sliding motion on the surface given by $\sigma = 0$, which occurs when the vector fields $F^{\pm} = A\bar{y} \pm Bk$, obtained by replacing $u = \pm k$, both point to the surface σ. As in section 7.1.2, if one imposes that both fields point toward opposite directions, one obtains unstable sliding. Since $F^{\pm}$ are smooth everywhere, sliding motion occurs if

$$(\mathcal{L}_{F^+}\sigma)\,(\mathcal{L}_{F^-}\sigma) < 0, \tag{7.19}$$

where $\mathcal{L}_F\sigma$ is the Lie derivative of σ along the field X.

Let us define $u_{eq} = -\frac{(\nabla\sigma)A\bar{y}}{c_{n-1}b}$. Then the previous inequality holds in the subset of σ defined by

$$-|k| < u_{eq} < |k| \tag{7.20}$$

(see [131] for details), which also provides stable sliding. In turn, this result can be read as *for k properly selected (both in sign and in absolute value), there is stable sliding motion on σ.*

After the discretization performed by the T-periodic sampling, the system is better understood by the time-T return (stroboscopic) map

$$P(y) = \begin{cases} P_{\mathcal{L}}(\bar{y}) := \rho\bar{y} + \mu_{\mathcal{L}} & \text{if } \sigma(\bar{y}) < 0, \\ P_{\mathcal{R}}(\bar{y}) := \rho\bar{y} + \mu_{\mathcal{R}} & \text{if } \sigma(\bar{y}) > 0, \end{cases} \tag{7.21}$$

where ρ, $\mu_{\mathcal{L}}$, and $\mu_{\mathcal{R}}$ are the matrices

$$\rho = e^{AT}, \quad \mu_{\mathcal{R}} = k(\rho - Id)(A^{-1}B), \quad \mu_{\mathcal{L}} = -k(\rho - Id)(A^{-1}B).$$

The maps $P_{\mathcal{L}}$ and $P_{\mathcal{R}}$ are the time-T return maps (stroboscopic) maps associated with the fields F^+ and F^-, respectively.

Using the facts that system (7.16) is linear and that, for $k = 0$, it possesses an attracting node, the matrix ρ possesses real positive eigenvalues with modulus less than 1 only.

Each branch, P_r and $P_{\mathcal{L}}$, of the map (7.21) has a fixed point

$$\bar{y}_{\mathcal{R}} = -(\rho - Id)^{-1}\mu_{\mathcal{R}}, \quad \bar{y}_{\mathcal{L}} = -(\rho - Id)^{-1}\mu_{\mathcal{L}}, \tag{7.22}$$

which may be *feasible* or *virtual* depending on whether or not they belong to the domain of their respective map. When feasible, these fixed points become attracting nodes, and they undergo border collision bifurcations when they collide with boundary $\sigma(\bar{y}) = 0$.

Regarding the possible dynamics, we distinguish between three different situations.

If both fixed points are feasible ($\sigma(\bar{y}_{\mathcal{R}}) > 0$ and $\sigma(\bar{y}_{\mathcal{L}}) < 0$), they also become attracting fixed points of the map (7.21). Their domains of attraction are formed by the values of $\bar{y} \in \mathbb{R}^n$ such that $\sigma(\bar{y}) > 0$ and $\sigma(\bar{y}) < 0$, respectively.

If only one of the fixed points is feasible ($\sigma(\bar{y}_{\mathcal{R}}) < 0$ and $\sigma(\bar{y}_{\mathcal{L}}) < 0$ or vice versa), then it becomes the unique fixed point of the map (7.21). As it is attracting, all trajectories tend toward it, and now its domain of attraction becomes $\mathbb{R}^n$.

Note that, in these two cases, the control specification is not fulfilled since $\sigma(\bar{y}) = 0$ is not flow invariant by the vector fields $F^{\pm}$.

The third situation occurs when both fixed points are virtual ($\sigma(\bar{y}_{\mathcal{R}}) < 0$ and $\sigma(\bar{y}_{\mathcal{L}}) > 0$). This occurs when the sliding condition (7.19) is fulfilled, guaranteeing that the original time-continuous system possesses sliding motion on $\sigma(\bar{y}) = 0$. Provided that the fixed points are attracting, the map (7.21) satisfies condition 2 of Theorem 61. Letting

$$\Sigma = \{\bar{y} \in \mathbb{R}^n \mid \sigma(\bar{y}) = 0\} \cap U,$$

condition 1 is also satisfied by taking the set U small enough while still containing both virtual fixed points. As a consequence and noting that both $P_{\mathcal{L}}$ and $P_{\mathcal{R}}$ preserve orientation as they are obtained from the integration of a flow, the map P admits zero or one periodic orbit. When it exists, such a periodic orbit must have a symbolic itinerary contained in the Farey tree of symbolic sequences shown in Figure 3.1(b).

As noted in Remark 64, the results given in section 6 do not provide information about bifurcation structures. In Figure 7.7 we show the bifurcation structure obtained for the planar case when the parameters k and y^* are varied. As one can see in Figure 7.7(b), the structure obtained resembles the period adding described in section 2.2 for the one-dimensional case, although it is not known whether for the

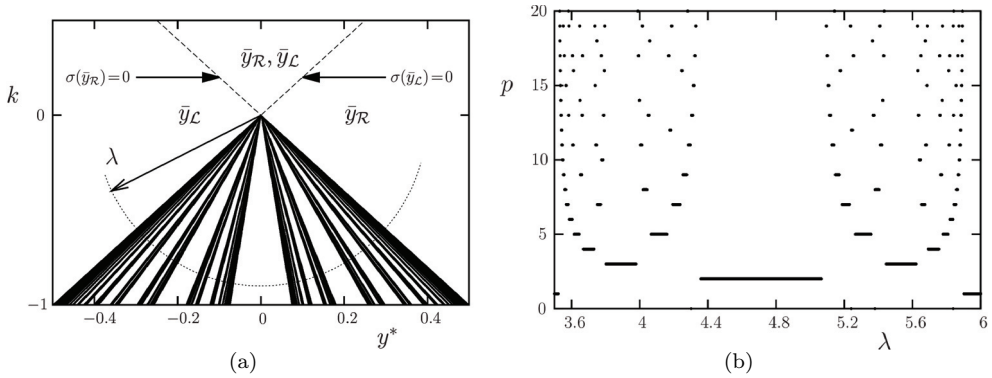

Fig. 7.7 *Bifurcation scenario in the (y^*, k)-parameter space for the planar case, $n = 2$. The rest of the parameters are fixed to $a_0 = -2$, $a_1 = -5$, $b = 1$, $c_1 = 1.5$, and $T = 0.1$. In* (a) *we show the border collision bifurcation curves separating existence regions of periodic orbits. In* (b) *is shown the periods of the periodic orbits found along the pointed curve in* (a) *parametrized by λ.*

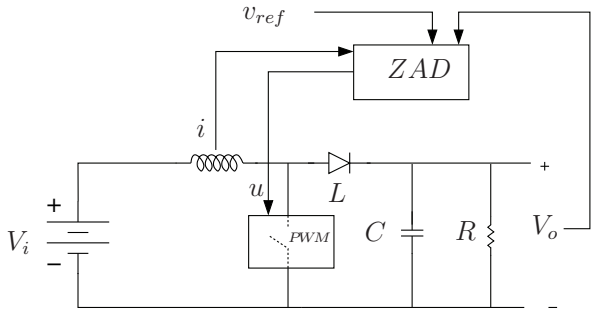

Fig. 7.8 *Schematic representation of a ZAD-controlled boost converter.*

planar case the gluing of orbits is also fractal. A similar physical interpretation of the bifurcation structure as in the first order case (section 7.1.2) also holds in this case.

7.2.2. ZAD-Controlled DC-DC Boost Converter. In this applied example we recover the results shown in [7] and state them in terms of the quasi-contractions of section 6. We consider a DC-DC boost converter, which converts a given constant DC voltage, v_i, into a desired lower one, v_o. Its circuit is shown schematically in Figure 7.8. To achieve this conversion in a robust way (to guarantee a certain stability of v_o under possible fluctuations of v_i), the transistor shown in Figure 7.8 needs to be properly controlled. There exist different approaches to designing such a control; in this example we consider the so-called zero average dynamics (ZAD) strategy, which is well-used in the community [52, 8, 9, 10, 53, 16, 7].

Letting v be the voltage at the capacitor, i the current through the solenoid, setting

$$x = \frac{v}{v_i}, \quad y = \sqrt{\frac{L}{C}}\frac{i}{v_i},$$

and rescaling time by a factor of $\sqrt{LC}$, the nondimensional equations that model the system become

$$\begin{aligned} \dot{x} &= -\gamma x + y(1-u), \\ \dot{y} &= -x(1-u) + 1, \end{aligned} \tag{7.23}$$

with $\gamma = \sqrt{\frac{L}{R^2 C}}$. The function u takes the values 0 or 1 depending on whether the transistor is opened or closed, respectively. It is given by the output of a pulse width modulation (PWM) process and can be written as

$$u(t) = \begin{cases} 1 & \text{if } kT \le t < kT + 1/2Td_k, \\ 0 & \text{if } kT + 1/2Td_k \le t < (k+1)T - 1/2Td_k, \\ 1 & \text{if } (k+1)T - 1/2Td_k \le t < (k+1)T, \end{cases}$$

where $d_k \in [0,1]$ is the so-called duty cycle. It is computed at each sampling moment, $t_k = kT$, and is kept constant until the next sampling period, t_{k+1}. Note that if $d_k = 1$ or $d_k = 0$, then u becomes constant in the time interval $[kT, (k+1)T)$, equal to 1 or 0, respectively.

The ZAD strategy consists of computing the value of the duty cycle at each T-time interval, d_k, by imposing

$$\int_{kT}^{(k+1)T} s(t)dt = 0 \quad \forall k \in \mathbb{Z}, \tag{7.24}$$

where $s(t)$ is the error surface

$$s(x(t), y(t)) = k_1 \left(x(t) - x_{ref}\right) + k_2 \left(y(t) - y_{ref}\right),$$

with

$$x_{ref} = \frac{v_{ref}}{v_i}, \quad y_{ref} = \left(x_{ref}\right)^2 \gamma,$$

and k_1 and k_2 two control constants.

Equation (7.24) becomes transcendental in d_k. However, if the solution of system (7.23) is approximated by piecewise-linear functions, the duty cycle can be approximated by the closed expression

$$d_k = \frac{2s_0 + T\dot{s}_2}{\dot{s}_2 - \dot{s}_1}, \tag{7.25}$$

where

$$\begin{aligned} \dot{s}_1 &= -\gamma k_1 x(kT) + k_2, \\ \dot{s}_2 &= k_1 \left(-\gamma x(kT) + y(kT)\right) + k_2 \left(1 - x(kT)\right), \\ s_0 &= k_1 \left(x(kT) - x_{ref}\right) + k_2 \left(y(kT) - y_{ref}\right) \end{aligned}$$

(see [7] for more details). Provided that the duty cycle lies in the interval $[0,1]$, it is set to 1 or 0 depending on whether the result of expression (7.25) is greater than 1 or less than 0, respectively. That is, one imposes the saturation condition

$$d_k = \begin{cases} 1 & \text{if } \dfrac{2s_0 + T\dot{s}_2}{\dot{s}_2 - \dot{s}_2} \ge 1, \\ 0 & \text{if } \dfrac{2s_0 + T\dot{s}_2}{\dot{s}_2 - \dot{s}_2} \le 0. \end{cases} \tag{7.26}$$

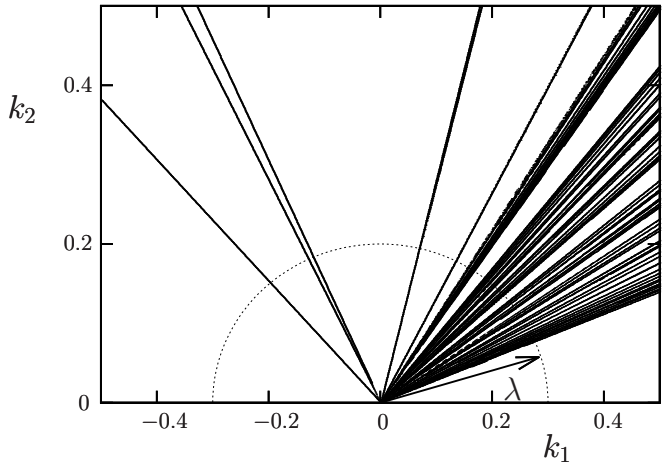

Fig. 7.9 *Bifurcation curves in the $k_1 \times k_2$ parameter space.*

Let us now consider the time-T return (stroboscopic) map of system (7.23). It becomes the composition of three stroboscopic maps consisting of flowing system (7.23) for the time intervals $[kT, kT + 1/2Td_k)$, $[kT + 1/2Td_k, (k+1)T - 1/2Td_k)$, and $[(k+1)T - 1/2Td_k, (k+1)T)$ setting $u = 1$, $u = 0$, and $u = 1$, respectively (see [7] for more details). As these three maps are smooth maps, their composition is also a smooth map, as long as d_k given by (7.25) lies in the interval $(0, 1)$. However, due to the saturation condition (7.26), the stroboscopic map indeed becomes a piecewise-defined map with two switching manifolds,

$$\Sigma_1 = \{(x, y) \mid d_k(x, y) = 1\},$$
$$\Sigma_0 = \{(x, y) \mid d_k(x, y) = 0\}.$$

Hence, the stroboscopic map is indeed defined in three different partitions.

In Figures 7.9 and 7.10 we show the numerical results obtained by direct simulation of the stroboscopic map, when fixing the initial conditions to $(x_0, y_0) = (2.5, (2.5)^2\gamma)$ and varying the parameters k_1 and k_2. In Figure 7.9 we show the bifurcation curves in the parameter space (k_1, k_2). Due to the linearity of the system, these become straight lines. In Figure 7.10 we show the results obtained along the curve labeled in Figure 7.9 and parametrized by the angle λ. As shown in Figure 7.10(a), for $\lambda \in (0, 0.27)$, $\lambda \in (0.95, 1.2)$, and $\lambda \in (2.5, 3)$ (approximately), the stroboscopic map possesses a fixed point. For the first and third intervals, the duty cycle associated with the fixed points is saturated to 0, whereas for the second one the duty cycle lies in the interval $(0, 1)$. As one can see in Figure 7.10(a), there exists a period–adding-like structure between the first two intervals. The periodic orbits that one finds there possess points in the partitions where the duty cycles are saturated to 1 and to 0. As a consequence, associated to each periodic orbit there exists a sequence of 0's and 1's, which are distributed such that the sequence is maximin (see Definition 56), or, equivalently, they belong to the Farey tree of symbolic sequences shown in Figure 3.1(b). For example, for the two 5-periodic orbits found one obtains the sequences of duty cycles $(0, 0, 0, 0, 1)$ and $(0, 0, 1, 0, 1)$, which are maximin. Note that, when d_k is saturated to 1, the transistor remains closed for a whole sampling

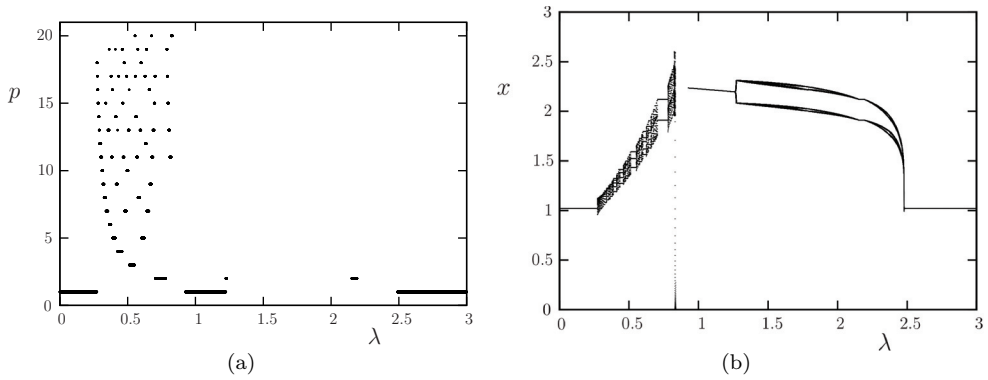

Fig. 7.10 *Bifurcation scenario found around the curves labeled in Figure* 7.9 *and parametrized by* λ*, for parameter values* $\gamma = 0.35$*,* $x_{ref} = 2.5$*,* $T = 0.18$*. In* (a) *we show the periods of the periodic orbits found when varying* λ*. In* (b) *we show the bifurcation diagram corresponding to* x*.*

period and more energy is drained from the source. Therefore, periodic orbits with high rotation number may not be desired, as they possess a larger number of saturated cycles, leading to a less efficient conversion.

Although a more accurate study of the properties of the stroboscopic map is needed, provided that the map contracts, there is evidence that the stroboscopic map is a quasi-contraction, at least for those values of λ corresponding to the period–adding-like structure.

Finally, note that for values of λ in (1.2), (2.5), trajectories with the initial condition used converge toward a chaotic attractor or are aperiodic.

8. Conclusions and Future Directions. In recent years, piecewise-smooth maps, both in $\mathbb{R}$ and in $\mathbb{R}^n$, have been widely investigated and very interesting bifurcation phenomena (border collisions, big bangs, period adding, period incrementing, etc.) have been reported by many authors. This has included works by both more applied communities, such as power electronics [8, 30, 116], control theory [46, 51, 137], biology [57, 106], neuroscience [74, 88, 121], or economics [128] (see sections 1, 6, and 7 for more references), but also researchers with a more theoretical and/or computational perspective on nonsmooth systems [22, 65, 78]. It is well known that some of these bifurcations resemble phenomena observed and well-studied in other contexts, especially in the theory for circle maps developed in the 1980s and early 1990s [2, 34, 40, 60, 61, 115, 133] and in homoclinic bifurcations [80, 113, 122, 130] (see sections 1, 5, and 6 for more references).

In this survey article we have considered a general setting for piecewise-smooth contracting maps with a discontinuity at the origin and exhibiting a codimension-two border collision bifurcation. It is well known that, depending on the sign of the slopes of the map near the discontinuity, one generally finds two different bifurcation scenarios: period adding (for the increasing-increasing case) and period incrementing (when the slopes have different sign). In this survey article we have revisited the latter and have shown a path through the literature providing a rigorous proof for the former. Moreover, we have discussed the extent o which these results can be applied to piecewise-smooth expanding maps and to higher dimensions. Finally, we have shown how they can be used to provide a rigorous basis to applied examples.

8.1. Period Adding for Contracting One-Dimensional Piecewise-Smooth Maps. The main contribution of this review article is its revisiting of the literature in order to provide sufficient conditions for the occurrence of this bifurcation scenario (described in section 2.2), which occurs when the map preserves orientation near the discontinuity at the origin (is of the increasing-increasing type); the proof is summarized in section 3.2. The key step is to link such maps with maps in the circle. Although the resulting circle map is also discontinuous, the fact that the map is contracting guarantees that its lift is a strictly increasing map, which is a sufficient condition for the main properties of the rotation number of a map to hold: existence, uniqueness, and continuity and monotonicity with respect to parameters. By using the concept of "well-ordered" cycles, periodic orbits are linked with the symbolic sequences given in the Farey tree of symbolic sequences. When parameters are varied, the theory for expanding circle maps is applied to its inverse to show that the rotation number follows a devil's staircase and, when the rotation number is irrational (which occurs in a Cantor set of zero measure), the omega limit of the map becomes instead the whole circle or a Cantor set. The latter occurs when the circle map obtained is discontinuous; the former may occur otherwise.

8.2. Period Incrementing for One-Dimensional Piecewise-Smooth Maps. The period incrementing scenario occurs when the piecewise-smooth map has different monotonicity at both sides of the discontinuity at the origin. We revisit results in the literature that provide sufficient conditions for the contracting case. The bifurcation scenario leads to the existence of stable periodic orbits of the type $\mathcal{L}^n\mathcal{R}$ or $\mathcal{L}\mathcal{R}^n$, depending on whether the map is increasing-decreasing or decreasing-increasing, respectively. Moreover, such a periodic orbit may coexist with another periodic orbit of the type $\mathcal{L}^{n+1}\mathcal{R}$ (or $\mathcal{L}\mathcal{R}^{n+1}$). In this case, both periodic orbits are stable and their domains of attraction are separated by the origin (the discontinuity).

8.3. Period Adding and Incrementing Bifurcations in Piecewise-Smooth Expanding Maps. Most of the results about the orientable case (increasing-increasing) shown in this review rely on the fact that the lift of the corresponding circle map is a monotonically increasing map, and indeed they do not require the map to be contracting. A necessary condition is then the reversibility of the map, which is guaranteed when it contracts near the discontinuity. However, such a reversibility condition also holds when the map is not too expanding. In particular, if it holds, the map possesses the same types of periodic orbits as in the contracting case, although they may not be unique or stable. In contrast to the contracting case, the set of parameters for which one finds dynamics associated with irrational rotation numbers is of nonzero measure.

When the map becomes sufficiently expanding that the reversibility condition no longer holds, one loses the uniqueness of the rotation number and needs to deal with rotation intervals instead. Although there is a large body of theory and literature on this [1, 2, 4, 5, 68, 70, 134], more work is needed in order to provide general sufficient conditions leading to a precise and concrete description of the possible bifurcation scenarios.

The results for the nonorientable case (period incrementing bifurcation) are based on topological arguments for maps on the interval. This type of periodic orbit performs a number of steps (reinjection number) on the domain of the increasing branch and only one step on the decreasing one. The smaller the gap at the origin of the increasing branch compared to the gap of the decreasing one, the larger the reinjection number is. Therefore, when the decreasing branch is expanding, some of the techniques can

also be used when this reinjection number is large enough to compensate for the expansiveness of the decreasing branch. This results in the existence of the same types of bifurcations for periodic orbits of large enough length (reinjection number). Although the same types of period orbits with shorter period may also exist even when the decreasing branch is expanding, they may be unstable and coexist with more than one periodic orbit of the type $\mathcal{L}^n\mathcal{R}$.

In the case where both branches of the map are expanding, the map may possess positive topological entropy and might hence be chaotic, even when the lift is continuous [105, 92, 91].

8.4. Maps in Higher Dimensions. The jump from dimension one to dimension two represents a really challenging problem when it comes to providing general conditions for the occurrence of a concrete type of bifurcation. This is magnified when they are piecewise-smooth discontinuous maps. However, as we have shown in this review article (see section 6), some results already existing in the literature might significantly help in achieving such a goal. Of special interest is the concept of quasi-contractions developed in the 1980s by Gambaudo et al. [59, 60, 63]. Although such results provide a very precise description of the type of symbolic sequences associated with periodic orbits for such maps, the results rely heavily on contraction conditions. Numerical evidence (see references in section 6.1) shows that one may find similar symbolic properties under more relaxed conditions, as occurs for the one-dimensional case.

Unfortunately, the rotation theory shown in sections 3.3 and 3.4 cannot be exported straightforwardly for maps in higher dimensions. However, as for the one-dimensional case, one may convert such maps into discontinuous maps in higher-dimensional cylinders by identifying the images of the switching manifolds from both sides in order to introduce a rotating behavior. Under more restrictive conditions than in the one-dimensional case, proceeding similarly as in [36] for a particular example, this allows one to define the lift of a map, its rotation number, and obtain some theoretical results based on rotation theory.

REFERENCES

[1] Ll. Alsedà and A. Falcó, *On the topological dynamics and phase-locking renormalization of Lorenz-like maps*, Ann. Inst. Fourier (Grenoble), 53 (2003), pp. 859–883. (Cited on pp. 261, 285)

[2] Ll. Alsedà and J. Llibre, *Kneading theory of Lorenz maps*, in Dynamical Systems and Ergodic Theory, Banach Center Publ. 23, PWN, Warsaw, 1989, pp. 83–89. (Cited on pp. 261, 284, 285)

[3] Ll. Alsedà, J. Llibre, and M. Misiurevicz, *Combinatorial Dynamics and Entropy in Dimension One*, World Scientific, Singapore, 2000. (Cited on pp. 242, 243, 244, 245, 247, 261)

[4] Ll. Alsedà, J. Llibre, M. Misiurewicz, and C. Tresser, *Periods and entropy for Lorenz-like maps*, Ann. Inst. Fourier (Grenoble), 39 (1989), pp. 929–952. (Cited on pp. 261, 285)

[5] Ll. Alsedà and F. Mañosas, *Kneading theory and rotation intervals for a class of circle maps of degree one*, Nonlinearity, 3 (1990), pp. 413–452. (Cited on pp. 261, 285)

[6] Ll. Alsedà and F. Mañosas, *Kneading theory for a family of circle maps with one discontinuity*, Acta Math. Univ. Comenianae, 65 (1996), pp. 11–22. (Cited on p. 261)

[7] A. Amador, S. Casanova, H. A. Granada, G. Olivar, and J. Hurtado, *Codimension-two big-bang bifurcation in a ZAD-controlled boost DC-DC converter*, Internat. J. Bifur. Chaos Appl. Sci. Engrg., 24 (2014), 1450150. (Cited on pp. 228, 262, 281, 282, 283)

[8] F. Angulo, E. Fossas, and G. Olivar, *Transition from periodicity to chaos in a PWM-controlled buck converter with ZAD strategy*, Internat. J. Bifur. Chaos Appl. Sci. Engrg., 15 (2005), pp. 3245–3264. (Cited on pp. 281, 284)

[9] F. Angulo, G. Olivar, and M. di Bernardo, *Two-parameter discontinuity-induced bifurcation curves in a ZAD-strategy-controlled DC-DC buck converter*, IEEE Trans. Circuits Syst. I, 55 (2008), pp. 2392–2401. (Cited on p. 281)

[10] F. Angulo, G. Olivar, and A. Taborda, *Continuation of periodic orbits in a ZAD-strategy controlled buck converter*, Chaos Solitons Fractals, 38 (2008), pp. 348–363. (Cited on p. 281)

[11] A. Arneodo, P. Coullet, and C. Tresser, *A possible new mechanism for the onset of turbulence*, Phys. Lett., 81 (1981), pp. 197–201. (Cited on p. 268)

[12] V. Avrutin, B. Eckstein, and M. Schanz, *The bandcount increment scenario.* I: *Basic structures*, Proc. R. Soc. Lond. Ser. A Math. Phys. Eng. Sci., 464 (2008), pp. 1867–1883. (Cited on p. 261)

[13] V. Avrutin, B. Eckstein, and M. Schanz, *The bandcount increment scenario.* II: *Interior structures*, Proc. R. Soc. Lond. Ser. A Math. Phys. Eng. Sci., 464 (2008), pp. 2247–2263. (Cited on p. 261)

[14] V. Avrutin, B. Eckstein, and M. Schanz, *The bandcount increment scenario.* III: *Deformed structures*, Proc. R. Soc. Lond. Ser. A Math. Phys. Eng. Sci., 465 (2009), pp. 41–57. (Cited on p. 261)

[15] V. Avrutin, B. Eckstein, M. Schanz, and B. Schenke, *Bandcount incrementing scenario revisited and floating regions within robust chaos*, Math. Comput. Simulation, 95 (2014), pp. 23–38. (Cited on p. 261)

[16] V. Avrutin, E. Fossas, A. Granados, and M. Schanz, *Virtual orbits and two-parameter bifurcation analysis in ZAD-controlled buck-converter*, Nonlinear Dynam., 63 (2011), pp. 19–33. (Cited on pp. 226, 281)

[17] V. Avrutin, B. Futter, and M. Schanz, *The discontinuous flat top tent map and the nested period incrementing bifurcation structure*, Chaos Solitons Fractals, 45 (2012), pp. 465–482. (Cited on p. 268)

[18] V. Avrutin, A. Granados, and M. Schanz, *Sufficient conditions for a period increment big bang bifurcation in one-dimensional maps*, Nonlinearity, 24 (2011), pp. 2575–2598. (Cited on pp. 227, 228, 234, 257, 258, 259, 268)

[19] V. Avrutin, E. Mosekilde, Z. T. Zhusubaliyev, and L. Gardini, *Onset of chaos in a single-phase power electronic inverter*, Chaos, 25 (2015), p. 043114. (Cited on p. 260)

[20] V. Avrutin and M. Schanz, *Border-collision period-doubling scenario*, Phys. Rev. E, 70 (2004), 026222. (Cited on p. 268)

[21] V. Avrutin and M. Schanz, *Period doubling scenario without flip bifurcations in a one-dimensional map*, Internat. J. Bifur. Chaos Appl. Sci. Engrg., 15 (2005), pp. 1267–1284. (Cited on p. 268)

[22] V. Avrutin and M. Schanz, *On multi-parametric bifurcations in a scalar piecewise-linear map*, Nonlinearity, 19 (2006), pp. 531–552. (Cited on pp. 228, 234, 268, 284)

[23] V. Avrutin, M. Schanz, and S. Banerjee, *Multi-parametric bifurcations in a piecewise-linear discontinuous map*, Nonlinearity, 19 (2006), pp. 1875–1906. (Cited on p. 268)

[24] V. Avrutin, M. Schanz, and S. Banerjee, *Codimension-3 bifurcations: Explanation of the complex* 1*-,* 2*- and* 3*D bifurcation structures in nonsmooth maps*, Phys. Rev. E, 75 (2007), 066205. (Cited on p. 268)

[25] V. Avrutin, M. Schanz, and L. Gardini, *Calculation of bifurcation curves by map replacement*, Internat. J. Bifur. Chaos Appl. Sci. Engrg., 20 (2010), pp. 3105–3135. (Cited on pp. 266, 269)

[26] V. Avrutin, M. Schanz, and L. Gardini, *Self-similarity of the bandcount adding structures: Calculation by map replacement*, Regul. Chaotic Dyn., 15 (2010), pp. 685–703. (Cited on pp. 266, 269)

[27] V. Avrutin, M. Schanz, and B. Schenke, *On a bifurcation structure mimicking period adding*, Proc. R. Soc. Lond. Ser. A Math. Phys. Eng. Sci., 467 (2011), pp. 1503–1518. (Cited on p. 268)

[28] V. Avrutin and I. Sushko, *A gallery of bifurcation scenarios in piecewise smooth* 1*D maps*, in Global Analysis of Dynamic Models in Economics, Finance and the Social Sciences, G.-I. Bischi, C. Chiarella, and I. Sushko, eds., Springer, New York, 2013, pp. 269–395. (Cited on p. 268)

[29] S. Banerjee and C. Grebogi, *Border collision bifurcation in two-dimensional piecewise smooth maps*, Phys. Rev. E, 59 (1999), pp. 4052–4061. (Cited on pp. 228, 262)

[30] S. Banerjee, M. S. Karthik, G. Yuan, and J. A. Yorke, *Bifurcations in one-dimensional piecewise smooth maps—theory and applications in switching circuits*, IEEE Trans. Circuits Syst. I Regul. Pap., 47 (2000), pp. 389–394. (Cited on pp. 260, 284)

[31] S. Banerjee and G. C. Verghese, *Nonlinear Phenomena in Power Electronics: Attractors, Bifurcations, Chaos, and Nonlinear Control*, IEEE Press, Piscataway, NJ, 2001. (Cited on p. 226)

[32] C. Bernhardt, *Rotation intervals of a class of endomorphisms of the circle*, Proc. London Math. Soc. (3), 45 (1982), pp. 258–280. (Cited on pp. 262, 263)

[33] F. Bizzarri, M. Storace, and L. Gardini, *Bifurcation analysis of a circuit-related generalization of the shipmap*, Internat. J. Bifur. Chaos Appl. Sci. Engrg., 16 (2006), pp. 2435–2452. (Cited on p. 260)

[34] C. Boyd, *On the structure of family of cherry fields on the torus*, Ergodic Theory Dynam. Systems, 5 (1985), pp. 27–46. (Cited on pp. 250, 255, 284)

[35] R. Brette, *Dynamics of one-dimensional spiking neuron model*, J. Math. Biol., 48 (2004), pp. 38–56. (Cited on p. 226)

[36] H. Broer, C. Simó, and J. C. Tatjer, *Towards global models near homoclinic tangencies of dissipative diffeomorphisms*, Nonlinearity, 11 (1998), pp. 667–770. (Cited on p. 286)

[37] B. Brogliato, *Nonsmooth Mechanics*, Springer, London, 1999. (Cited on p. 262)

[38] V. Carmona, S. Fernández-García, F. Fernández-Sánchez, E. García-Medina, and A. Teruel, *Noose bifurcation and crossing tangency in reversible piecewise linear systems*, Nonlinearity, 27 (2014), pp. 585–606. (Cited on p. 262)

[39] V. Carmona, S. Ferndández-García, F. Fernández-Sánchez, E. García-Medina, and A. E. Teruel, *Reversible periodic orbits in a class of* $3D$ *continuous piecewise linear systems of differential equations*, Nonlinear Anal., 75 (2012), pp. 5866–5883. (Cited on p. 262)

[40] P. C. Coullet, J.-M. Gambaudo, and C. Tresser, *Une nouvelle bifurcation de codimension* 2: *Le colage de cycles*, C. R. Acad. Sci. Paris Sér. I Math., 299 (1984), pp. 253–256. (Cited on pp. 234, 284)

[41] M. Desroches, J. Guckenhiemer, B. Krauskopf, C. Kuehn, H. M. Osinga, and M. Wechselberger, *Mixed-mode oscillations with multiple time scales*, SIAM Rev., 54 (2012), pp. 211–288, https://doi.org/10.1137/100791233. (Cited on p. 260)

[42] R. L. Devaney, *A piecewise linear model for the zones of instability of an area preserving map*, Phys. D, 10 (1984), pp. 387–393. (Cited on p. 262)

[43] M. di Bernardo, C. J. Budd, and A. R. Champneys, *Grazing, skipping and sliding: Analysis of the nonsmooth dynamics of the DC/DC buck converter*, Nonlinearity, 11 (1998), pp. 858–890. (Cited on p. 226)

[44] M. di Bernardo, C. J. Budd, A. R. Champneys, and P. Kowalczyk, *Piecewise-smooth Dynamical Systems: Theory and Applications*, Appl. Math. Sci. 163, Springer, New York, 2008. (Cited on p. 262)

[45] M. di Bernardo, F. Garofalo, L. Glielmo, and F. Vasca, *Switchings, bifurcations and chaos in DC/DC converters*, Fundam. Theory Appl., 45 (1998), pp. 133–141. (Cited on pp. 228, 262)

[46] M. di Bernardo, F. Garofalo, L. Iannelli, and F. Vasca, *Bifurcations in piecewise-smooth feedback systems*, Internat. J. Control, 75 (2002), pp. 1243–1259. (Cited on pp. 228, 262, 284)

[47] M. di Bernardo, P. Kowalczyk, and A. Nordmark, *Sliding Bifurcations: A Novel Mechanism for the Sudden Onset of Chaos in Dry-Friction Oscillators*, Preprint 2003.16, Bristol Centre for Applied Nonlinear Mathematics, Bristol, UK, 2003. (Cited on p. 226)

[48] P. Dutta, B. Routroy, S. Banerjee, and S. Alam, *On the existence of low-period orbits in n-dimensional piecewise linear discontinuous maps*, Nonlinear Dynam., 53 (2008), pp. 369–380. (Cited on p. 262)

[49] A. F. Filippov, *Differential Equations with Discontinuous Righthand Sides*, Math. Appl. (Soviet Ser.) 18, Kluwer Academic, Dordrecht, 1988. (Cited on p. 262)

[50] E. Fossas and A. Granados, *Big bang bifurcations in a first order systems with a relay*, in Proceedings of the 11th Conference on Dynamical Systems Theory and Applications, P. Olejnik J. Mrozowski. J. Awrejcewicz, and M. Kaźmierczak, eds., 2011, pp. 147–152. (Cited on pp. 228, 271)

[51] E. Fossas and A. Granados, *Occurrence of big bang bifurcations in discretized sliding-mode control systems*, Diff. Equ. Dyn. Syst., 21 (2013), pp. 35–43, https://doi.org/10.1007/s12591-012-0121-y. (Cited on pp. 228, 262, 271, 278, 284)

[52] E. Fossas, R. Griñó, and D. Biel, *Quasi-sliding control based on pulse width modulation, zero averaged dynamics and the* L_2 *norm*, in Advances in Variable Structure Systems: Analysis, Integration and Applications, World Scientific, Singapore, 2001, pp. 335–344. (Cited on pp. 226, 281)

[53] E. Fossas, S. J. Hogan, and T. M. Seara, *Two-parameter bifurcation curves in power electronic converters*, Internat. J. Bifur. Chaos Appl. Sci. Engrg., 19 (2009), pp. 341–357. (Cited on pp. 226, 281)

[54] D. Fournier-Prunaret, P. Chargé, and L. Gardini, *Border collision bifurcations and chaotic sets in a two-dimensional piecewise linear map*, Commun. Nonlinear Sci. Numer. Simul., 16 (2010), pp. 916–927. (Cited on p. 262)

[55] A. M. Fox and J. D. Meiss, *Greene's residue criterion for the breakup of invariant tori of volume-preserving maps*, Phys. D, 243 (2013), pp. 45–63. (Cited on p. 262)

[56] E. Freire, E. Ponce, and J. Ros, *The focus-center-limit cycle bifurcation in symmetric 3D piecewise linear systems*, SIAM J. Appl. Math, 65 (2005), pp. 1933–1951, https://doi.org/10.1137/040606107. (Cited on p. 262)

[57] J. G. Freire and J. A. C. Gallas, *Stern-Brocot trees in the periodicity of mixed-mode oscillations*, Phys. Chem. Chem. Phys., 13 (2011), pp. 12191–12198. (Cited on pp. 228, 237, 262, 284)

[58] Z. Galias and X. Yu, *Study of periodic solutions of discretized two-dimensional sliding mode control systems*, IEEE Trans. Circuits Systems II Express Briefs, 58 (2011), pp. 381–385. (Cited on p. 228)

[59] J.-M. Gambaudo, *Ordre, désordre, et frontiére des systèmes Morse-Smale*, Ph.D. thesis, Université de Nice, France, 1987. (Cited on pp. 242, 251, 263, 286)

[60] J.-M. Gambaudo, P. Glendinning, and C. Tresser, *The gluing bifurcation: Symbolic dynamics of the closed curves*, Nonlinearity, 1 (1988), pp. 203–214. (Cited on pp. 227, 232, 234, 265, 267, 284, 286)

[61] J.-M. Gambaudo, O. E. Lanford III, and C. Tresser, *Dynamique symbolique des rotations*, C. R. Acad. Sci. Paris Sér. I Math., 299 (1984), pp. 823–826. (Cited on pp. 227, 262, 263, 267, 284)

[62] J.-M. Gambaudo, I. Procaccia, S. Thomae, and C. Tresser, *New universal scenarios for the onset of chaos in Lorenz-type flows*, Phys. Rev. Lett, 57 (1986), pp. 925–928. (Cited on pp. 227, 234)

[63] J.-M. Gambaudo and C. Tresser, *On the dynamics of quasi-contractions*, Bol. Soc. Brasil. Mat., 19 (1988), pp. 61–114. (Cited on pp. 227, 232, 234, 264, 265, 266, 267, 286)

[64] L. Gardini, V. Avrutin, and I. Sushko, *Codimension-2 border collision, bifurcations in one-dimensional, discontinuous piecewise smooth maps*, Internat. J. Bifur. Chaos Appl. Sci. Engrg., 24 (2014), 1450024. (Cited on p. 268)

[65] L. Gardini and F. Tramontana, *Border collision bifurcations in 1D PWL map with one discontinuity and negative jump. Use of the first return map*, Internat. J. Bifur. Chaos Appl. Sci. Engrg., 20 (2010), pp. 3529–3547. (Cited on pp. 268, 284)

[66] R. Ghrist and P. J. Holmes, *Knotting within the gluing bifurcation*, in IUTAM Symposium on Nonlinearity and Chaos in the Engineering Dynamics, J. Thompson and S. Bishop, eds., John Wiley, New York, 1994, pp. 299–315. (Cited on pp. 227, 234, 268)

[67] D. Giaouris, S. Banerjee, O. Imrayed, K. Mandal, B. Zahawi, and V. Pickert, *Complex interaction between tori and onset of three-frequency quasi-periodicity in a current mode controlled boost converter*, IEEE Trans. Circuits Syst. I, 59 (2012), pp. 207–214. (Cited on pp. 228, 262)

[68] P. Glendinning, *Topological conjugation of Lorenz maps to β-transformations*, Math. Proc. Cambridge Philos. Soc., 107 (1990), pp. 401–413. (Cited on pp. 227, 260, 285)

[69] P. Glendinning, *Milnor attractors and topological attractors of a piecewise linear map*, Nonlinearity, 14 (2001), pp. 239–257. (Cited on p. 262)

[70] P. Glendinning and C. Sparrow, *Prime and renormalisable kneading invariants and the dynamics of expanding Lorenz maps*, in Proceedings of a NATO Advanced Research Workshop held at the Centre for Nonlinear Phenomena and Complex Systems on Homoclinic Chaos, Elsevier North-Holland, Amsterdam, The Netherlands, 1993, pp. 22–50. (Cited on pp. 260, 285)

[71] A. Granados, S. J. Hogan, and T. M. Seara, *The Melnikov method and subharmonic orbits in a piecewise-smooth system*, SIAM J. Appl. Dyn. Syst., 11 (2012), pp. 801–830, https://doi.org/10.1137/110850359. (Cited on p. 226)

[72] A. Granados, S. J. Hogan, and T. M. Seara, *The scattering map in two coupled piecewise-smooth systems, with numerical application to rocking blocks*, Phys. D, 269 (2014), pp. 1–20. (Cited on p. 226)

[73] A. Granados and M. Krupa, *Firing-rate, symbolic dynamics and frequency dependence in periodically driven spiking models: A piecewise-smooth approach*, Nonlinearity, 28 (2015), pp. 1163–1192. (Cited on pp. 274, 277)

[74] A. Granados, M. Krupa, and F. Clément, *Border collision bifurcations of stroboscopic maps in periodically driven spiking models*, SIAM J. Appl. Dyn. Syst., 13 (2014), pp. 1387–1416, https://doi.org/10.1137/13094637X. (Cited on pp. 226, 228, 274, 275, 276, 284)

[75] J. Guckenheimer and R. F. Williams, *Structural stability of Lorenz attractors*, Inst. Hautes Études Sci. Publ. Math., 50 (1979), pp. 59–72. (Cited on p. 260)

[76] D. C. Hamill, J. H. B. Deane, and D. J. Jefferies, *Modeling of chaotic DC–DC converters by iterated nonlinear mappings*, IEEE Trans. Power Electron., 7 (1992), pp. 25–36. (Cited on p. 260)

[77] G. H. Hardy and E. M. Wright, *An Introduction to the Theory of Numbers*, 4th ed., Oxford University Press, London, 1960. (Cited on p. 236)

[78] S. J. Hogan, L. Higham, and T. C. L. Griffin, *Dynamics of a piecewise linear map with a gap*, Proc. R. Soc. Lond. Ser. A Math. Phys. Eng. Sci., 463 (2007), pp. 49–65. (Cited on pp. 268, 284)

[79] S. J. Hogan, *On the dynamics of rigid block motion under harmonic forcing*, Proc. Roy. Soc. London Ser. A, 425 (1989), pp. 441–476. (Cited on p. 226)

[80] A. J. Homburg, *Global aspects of homoclinic bifurcations of vector fields*, Mem. Amer. Math. Soc., 578 (1996). (Cited on pp. 227, 234, 257, 259, 268, 284)

[81] A. J. Homburg, *Piecewise smooth interval maps with non-vanishing derivative*, Ergodic Theory Dynam. Systems, 20 (2000), pp. 749–773. (Cited on p. 227)

[82] A. J. Homburg and B. Krauskopf, *Resonant homoclinic flip bifurcations*, J. Dynam. Differential Equations, 12 (2000), pp. 807–850. (Cited on p. 260)

[83] E. M. Izhikevich, *Dynamical Systems in Neuroscience: The Geometry of Excitability and Bursting*, MIT Press, Cambridge, MA, 2007. (Cited on p. 226)

[84] N. D. Jimenez, S. Mihalas, R. Brown, E. Niebur, and J. Rubin, *Locally contractive dynamics in generalized integrate-and-fire neurons*, SIAM J. Appl. Dyn. Syst., 12 (2013), pp. 1474–1514, https://doi.org/10.1137/120900435. (Cited on pp. 228, 267)

[85] T. Kabe, S. Parui, H. Torikai, S. Banerjee, and T. Saito, *Analysis of piecewise constant models of current mode controlled DC–DC converters*, IEICI Trans. Fundamentals, E90-A (2007), p. 448. (Cited on p. 228)

[86] K. Kaneko, *On the period-adding phenomena at the frequency locking in a one-dimensional mapping*, Progr. Theoret. Phys., 68 (1982), pp. 669–672. (Cited on p. 261)

[87] S. Kapat, S. Banerjee, and A. Patra, *Discontinuous map analysis of a DC-DC converter governed by pulse skipping modulation*, IEEE Trans. Circuits Syst. I Regul. Pap., 57 (2010), pp. 1793–1801. (Cited on p. 260)

[88] J. P. Keener, *Chaotic behavior on piecewise continuous difference equations*, Trans. Amer. Math. Soc., 261 (1980), pp. 589–604. (Cited on pp. 234, 284)

[89] J. P. Keener, F. C. Hoppensteadt, and J. Rinzel, *Integrate-and-fire models of nerve membrane response to oscillatory input*, SIAM J. Appl. Math., 41 (1981), pp. 503–517, https://doi.org/10.1137/0141042. (Cited on pp. 228, 260, 274)

[90] M. P. Kennedy and L. O. Chua, *Van der Pol and chaos*, IEEE Trans. Circuits Syst., CAS-33 (1986), pp. 974–980. (Cited on p. 234)

[91] C. Kopf, *Symbol sequences and entropy for piecewise monotone transformations with discontinuities*, Discrete Contin. Dynam. Systems, 6 (2000), pp. 299–304. (Cited on p. 286)

[92] C. Kopf, *Coding and entropy for piecewise continuous piecewise monotone transformations*, Nonlinear Analysis, 61 (2005), pp. 169–275. (Cited on p. 286)

[93] P. Kowalczyk, *Robust chaos and border-collision bifurcations in non-invertible piecewise-linear maps*, Nonlinearity, 18 (2005), p. 485. (Cited on p. 262)

[94] P. Kowalczyk, M. di Bernardo, A. R. Champneys, S. J. Hogan, M. Homer, Yu. A. Kuznetsov, A. Nordmark, and P. Piiroinen, *Two-parameter discontinuity-induced bifurcations of limit cycles: Classification and open problems*, Internat. J. Bifur. Chaos Appl. Sci. Engrg., 16 (2006), pp. 601–629. (Cited on p. 262)

[95] N. N. Leonov, *On a pointwise mapping of a line into itself*, Radiofisika, 2 (1959), pp. 942–956 (in Russian). (Cited on pp. 227, 234)

[96] N. N. Leonov, *On a discontinuous piecewise-linear pointwise mapping of a line into itself*, Radiofisika, 3 (1960), pp. 496–510 (in Russian). (Cited on p. 234)

[97] N. N. Leonov, *On the theory of a discontinuous mapping of a line into itself*, Radiofisika, 3 (1960), pp. 872–886 (in Russian). (Cited on p. 234)

[98] N. N. Leonov, *On a discontinuous pointwise mapping of a line into itself*, Dokl. Akad. Nauk SSSR, 143 (1962), pp. 1038–1041. (Cited on p. 234)

[99] M. Levi, *A period-adding phenomenon*, SIAM J. Appl. Math., 50 (1990), pp. 943–955, https://doi.org/10.1137/0150058. (Cited on pp. 234, 260)

[100] D. V. Lyubimov, A. S. Pikovsky, and M. A. Zaks, *Universal Scenarios of Transitions to Chaos via Homoclinic Bifurcations*, Math. Phys. Rev. 8, Harwood Academic, London, 1989. Russian version 1986 as a Preprint (192) of Russian Academy of Science, Institute of Mechanics of Solid Matter, Sverdlovsk. (Cited on p. 234)

[101] O. Makarenkov and J. S. W. Lamb, *Dynamics and bifurcations of nonsmooth systems: A survey*, Phys. D, 241 (2012), pp. 1826–1844. (Cited on p. 227)

[102] Y. Matsuoka and T. Saito, *Rotation map with a controlling segment and its application to A/D converters*, IEICI Trans. Fundamentals, E91-A (2008), pp. 1725–1732. (Cited on p. 260)

[103] X. Meng, G. Huguet, and J. Rinzel, *Type* III *excitability, slope sensitivity and coincidence detection*, Discrete Contin. Dynam. Systems, 32 (2012), pp. 2720–2757. (Cited on pp. 226, 228, 262)

[104] C. Mira, *Chaotic Dynamics: From the One-Dimensional Endomorphism to the Two-Dimensional Diffeomorphism*, World Scientific, Singapore, 1987. (Cited on p. 234)

[105] M. Misiurevicz and W. Szlenk, *Entropy of piecewise monotone mappings*, Studia Math., 67 (1980), pp. 45–63. (Cited on p. 286)

[106] O. Mondragón-Palomino, T. Danino, J. Selimkhanov, L. Tsimring, and J. Hasty, *Entrainment of a population of synthetic genetic oscillators*, Science, 333 (2011), pp. 1315–1319. (Cited on pp. 260, 284)

[107] Z. Nitecki, *Differentiable Dynamics: Introduction to the Orbit Structure of Diffeomorphisms*, MIT Press, Cambridge, MA, 1971. (Cited on p. 248)

[108] A. B. Nordmark and P. Kowalczyk, *A codimension-two scenario of sliding solutions in grazing-sliding bifurcations*, Nonlinearity, 19 (2006), pp. 1–26. (Cited on p. 262)

[109] A. B. Nordmark, *Existence of periodic orbits in grazing bifurcations of impacting mechanical oscillators*, Nonlinearity, 14 (2001), pp. 1517–1542. (Cited on p. 262)

[110] P. T. Piiroinen, L. N. Virgin, and A. R. Champneys, *Chaos and period-adding: Experimental and numerical verification of the grazing bifurcation*, J. Nonlinear Sci., 14 (2004), pp. 383–404. (Cited on p. 234)

[111] H. Poincaré, *Mémoire sur les courbes définiés par une équation differentielle*, J. Math., 7 (1981), pp. 375–422. (Cited on p. 242)

[112] E. Ponce, J. Ros, and E. Vela, *Unfolding the fold-Hopf bifurcation in piecewise linear continuous differential systems with symmetry*, Phys. D, 250 (2013), pp. 34–46. (Cited on p. 262)

[113] I. Procaccia, S. Thomae, and C. Tresser, *First-return maps as a unified renormalization scheme for dynamical systems*, Phys. Rev. A, 35 (1987), pp. 1884–1900. (Cited on pp. 227, 234, 260, 284)

[114] B. Rakshit, M. Apratim, and S. Banerjee, *Bifurcation phenomena in two-dimensional piecewise smooth discontinuous maps*, Chaos, 3 (2010), 033101. (Cited on pp. 228, 262)

[115] F. Rhodes and C. L. Thompson, *Rotation numbers for monotone functions on the circle*, J. London Math. Soc., 34 (1986), pp. 360–368. (Cited on pp. 242, 243, 244, 284)

[116] T. Saito, T. Kabe, Y. Ishikawa, Y. Matsuoka, and H. Torikai, *Piecewise constant switched dynamical systems in power electronics*, Internat. J. Bifur. Chaos, 17 (2007), pp. 3373–3386. (Cited on pp. 260, 284)

[117] J. Signereska-Rynkowska, J. Touboul, and A. Vidal, *A Geometric Mechanism for Mixed-Mode Bursting Oscillations in a Hybrid Neuron Model*, preprint, arXiv:1509.08282 [math.DS], 2015. (Cited on pp. 228, 260, 262)

[118] D. J. W. Simpson, *Border-collision bifurcations in* $\mathbb{R}^n$, SIAM Rev., 58 (2016), pp. 177–226, https://doi.org/10.1137/15M1006982. (Cited on p. 262)

[119] D. J. W. Simpson and J. D. Meiss, *Simultaneous border-collision and period-doubling bifurcations*, Chaos, 19 (2009), 033146. (Cited on p. 262)

[120] D. J. W. Simpson and J. D. Meiss, *Neimark–Sacker bifurcations in planar, piecewise-smooth, continuous maps*, SIAM J. Appl. Dyn. Syst., 7 (2008), pp. 795–824, https://doi.org/10.1137/070704241. (Cited on p. 262)

[121] A. C. Skeldon, D.-J. Dijk, and G. Derks, *Mathematical models for sleep-wake dynamics: Comparison of the two-process model and a mutual inhibition neuronal model*, PLoS One, 9 (2014), e103877. (Cited on pp. 228, 284)

[122] C. Sparrow, *The Lorenz Equations: Bifurcations, Chaos, and Strange Attractors*, Springer-Verlag, New York, 1982. (Cited on pp. 227, 234, 260, 268, 284)

[123] G. Swiatek, *Endpoints of rotation intervals for maps of the circle*, Ergodic Theory Dynam. Systems, 9 (1989), pp. 173–190. (Cited on p. 256)

[124] P. H. E. Tiesinga, J.-M. Fellous, and T. J. Sejnowski, *Spike-time reliability of periodically driven integrate-and-fire neurons*, Neurocomputing, 44 (2002), pp. 195–200. (Cited on p. 228)

[125] A. Tonnelier, *Threshold curve for the excitability of bidimensional spiking neurons*, Phys. Rev. E, 90 (2014), 022701. (Cited on pp. 228, 262)

[126] J. Touboul and R. Brette, *Dynamics and bifurcations of the adaptive exponential integrate-and-fire model*, Biol. Cybernet, 99 (2008), pp. 319–334. (Cited on pp. 228, 262)

[127] J. Touboul and R. Brette, *Spiking dynamics of bidimensional integrate-and-fire neurons*, SIAM J. Appl. Dyn. Syst., 8 (2009), pp. 1462–1506, https://doi.org/10.1137/080742762. (Cited on pp. 228, 262, 267)

[128] F. Tramontana, L. Gardini, and F. Westerhoff, *Heterogeneous speculators and asset price dynamics: Further results from a one-dimensional discontinuous piecewise-linear model*, Comput. Economics, 38 (2011), pp. 329–347. (Cited on pp. 228, 284)

[129] F. Tramontana, F. Westerhoff, and L. Gardini, *On the complicated price dynamics of a simple one-dimensional discontinuous financial market model with heterogeneous interacting traders*, J. Econom. Behav. Organ., 74 (2010), pp. 187–205. (Cited on p. 260)

[130] D. V. Turaev and L. P. Shil'nikov, *Bifurcations of a homoclinic "figure eight" saddle with a negative saddle value*, Soviet Math. Dokl., 34 (1987), pp. 397–401. (Cited on pp. 234, 284)

[131] V. I. Utkin, *Variable structure systems with sliding modes*, IEEE Trans. Automat. Control, 22 (1977), pp. 212–222. (Cited on pp. 272, 279)

[132] V. I. Utkin, *Sliding mode control design principles and applications to electric drives*, IEEE Trans. Indust. Electr., 40 (1993), pp. 23–36. (Cited on p. 226)

[133] P. Veerman, *Irrational rotation numbers*, Nonlinearity, 2 (1989), pp. 419–428. (Cited on pp. 248, 256, 261, 284)

[134] M. A. Zaks, *Scaling properties and renormalization invariants for the "homoclinic quasiperiodicity,"* Phys. D, 62 (1993), pp. 300–316. (Cited on pp. 227, 285)

[135] Zh. T. Zhusubaliyev and E. Mosekilde, *Bifurcations and Chaos in Piecewise-Smooth Dynamical Systems*, World Sci. Ser. Nonlinear Sci. Ser. A Monogr. Treatises 44, World Scientific, Singapore, 2003. (Cited on pp. 226, 228, 262)

[136] Zh. T. Zhusubaliyev, E. Mosekilde, S. De, and S. Banerjee, *Transitions from phase-locked dynamics to chaos in a piecewise-linear map*, Phys. Rev. E, 77 (2008), pp. 1–11. (Cited on p. 228)

[137] Zh. T. Zhusubaliyev, E. A. Soukhoterin, V. N. Rudakov, Y. V. Kolokolov, and E. Mosekilde, *Bifurcations and chaotic oscillations in an automatic control relay system with hysteresis*, Internat. J. Bifur. Chaos, 11 (2001), pp. 1193–1231. (Cited on pp. 228, 262, 284)

[138] Zh. T. Zhusubaliyev, E. Mosekilde, A. I. Andriyanov, and G. Y. Mikhal'chenko, *High-feedback operation of power electronic converters*, electronics, 2 (2013), pp. 113–167. (Cited on pp. 228, 260, 262)